Catalysis Today xxx (xxxx) xxx–xxx

Contents lists available at ScienceDirect

Catalysis Today

journal homepage: www.elsevier.com/locate/cattod

Conversion of CO_2 to C_1 chemicals: Catalyst design, kinetics and mechanism aspects of the reactions

Ashok Jangam, Sonali Das, Nikita Dewangan, Plaifa Hongmanorom, Wai Ming Hui, Sibudjing Kawi*

Department of Chemical & Biomolecular Engineering, National University of Singapore, 117585, Singapore

ARTICLE INFO

Keywords:
CO_2 conversion
Dry reforming of methane
RWGS
CO_2 hydrogenation
Kinetics and mechanism

ABSTRACT

The conversion of carbon dioxide, an abundant and inexpensive feedstock to valuable chemicals is a contemporary challenge with multiple facets. There is a need to elucidate the process of utilizing CO_2 to gain a fundamental understanding to overcome the challenges. This review focuses on the reactions converting CO_2 to C_1 valuable chemicals via reforming and hydrogenation reactions to produce syngas, methane, and methanol. Prior art and recent trends in the development of novel catalysts are highlighted with regards to kinetic and mechanistic aspects of the reactions. Several highly emerging characterization techniques such as *operando* XAS and FTIR and DFT simulation are used to study state of catalyst surface and reaction intermediates involved in the reactions. Furthermore, parameters affecting the selectivity towards desired products and methods to improve the performance are explained in greater details. The technical challenges of CO_2 conversion into useful fuels/chemicals are summarized comprehensively. Finally, the future outlook and direction for the development of catalyst are provided to overcome the limitations and achieve higher utilization of CO_2 to eradicate the problems associated with global warming.

1. Introduction

Utilization of carbon-rich fossil fuels such as coal, oil and natural gas for urbanization, industrialization and technological advancements has led to a continuous rise in atmospheric CO_2 levels. The concentration of carbon dioxide in the atmosphere has increased from 280 ppm before the industrial revolution to 405 ppm in 2017. The increased atmospheric CO_2 concentration is arguably one of the primary causes of accelerated climate change and global warming. Hence, in recent years, there has been wide amount of global interest in finding sustainable ways to reverse the increasing CO_2 concentration in the atmosphere. Globally, treaties such as the Kyoto Protocol and the Paris Agreement identify reduction in carbon emissions as vital in preventing the potentially disastrous effects of further global warming [1].

Reducing CO_2 concentration in the atmosphere while meeting the energy demands of an increasing population is a formidable task and requires long term planning and implementation of CO_2 mitigation strategies. Reduction of CO_2 production by shifting from fossil to renewable fuels, CO_2 capture and storage, and CO_2 capture and utilization are the possible areas for systematic control and reduction of atmospheric CO_2. Carbon Capture and Utilization (CCU) is one of the key areas that can achieve CO_2 emission targets while simultaneously contributing to the production of energy, fuels and chemicals to support the increasing demands. In CCU concept, carbon dioxide is captured and separated from emission gases and then converted into valuable products. Currently, the mature technologies of using CO_2 as a feedstock are production of urea, salicylic acid, organic carbonates etc., which form a limited market and cannot contribute to a significant consumption compared to the large scales of CO_2 production. Conversion of CO_2 into fuel or commodity chemicals like methanol etc. provide a much more wider-scale route for CO_2 utilization. However, conversion of CO_2 into fuels or methanol is technologically challenging because of the high stability of the CO_2 molecule compared to the intended products and availability of renewable hydrogen source for CO_2 hydrogenation processes. The hydrogen required for the CO_2 hydrogenation reaction can be generated from renewable resources, such as biomass gasification, wind power, or solar water-splitting. There are significant technological advancements has been reported for H_2 production from renewable sources. For instance, though biomass is a cheap and renewable source, separation of H_2 from reformate gas mixture of biomass gasification makes the whole process expensive. Researchers are trying various options to make this whole process

* Corresponding author.
E-mail address: chekawis@nus.edu.sg (S. Kawi).

https://doi.org/10.1016/j.cattod.2019.08.049
Received 1 April 2019; Received in revised form 30 July 2019; Accepted 27 August 2019

cheaper such as enriching O_2 in air by using selective membrane [2,3], using catalyst to promote steam reforming of tar [4] and WGS reaction [5] for enriching H_2 gas and integrating WGS reaction with Pd-coated membrane for selective H_2 separation [6]. These studies seem to be possible in lab-scale but application in large scale is challenging. In the solar energy to hydrogen process, the photo-voltaic (PV) energy splits the water molecule into hydrogen and oxygen. Another possible route is via geothermal energy where the heat and electricity can be applied to generate hydrogen by hybrid cycles or electrolysis process. For the process, wind to hydrogen (WTH) via water electrolysis produces surplus electricity in the form of hydrogen which can be transformed back to electricity again when there is a low wind potential.

Significant research work is being done to develop new catalysts to increase activity and selectivity for the conversion of CO_2 into fuels and chemicals. There are two possible routes of thermo-catalytically converting CO_2 and integrating it into the fuel chain: 1. direct synthesis of higher hydrocarbons and oxygenates like methanol, olefins, formic acid, dimethyl carbonate etc. by the hydrogenation of CO_2 (direct route), 2. conversion of CO_2 into synthesis gas (CO and H_2) and Fischer-Tropsch synthesis of hydrocarbons from syn-gas (indirect route) [7–9]. In this review, we will focus on the technologies for the reduction of CO_2 into C_1 molecules that are the fundamental building blocks of the fuel and chemical industry, namely methane, methanol and syn-gas. Technologies covered are CO_2 hydrogenation to methane, syngas, methanol, and methane reforming to syngas production.

Due to the rapid progress in research activity in the CO_2 conversion reactions, there has been several reviews in the recent past focusing on the technical challenges and the recent progress in catalysis, process innovations, novel trends and lifecycle assessments in these areas [10–14]. Thenert et al. did a comprehensive review on different CO_2 technologies including catalysis, challenges and current status of technology and life-cycle assessments [12]. Song et al. reviewed a progress in heterogeneous catalysts for the production of hydrocarbons including methane, methanol, olefins and higher hydrocarbons by hydrogenation of CO_2 [10]. Several recent reviews also focus on challenges and recent progress in catalyst development for CO_2 reforming of hydrocarbons [15,16]. However, there is no recent review focusing on the kinetics and mechanism of the thermo-catalytic conversion of CO_2 to C_1. Fundamental mechanistic studies are crucial to understand the underlying pathways and controlling steps in a reaction and provide essential guidance for the development and optimization of better catalysts and reaction conditions. Kinetic studies are effective methods to identify suitable mechanisms based on correlation with experimental data and are essential for the modeling and design of a suitable reactor system. Although the conversion of CO_2 to C_1 molecules involve relatively simple reactants like H_2 and CH_4, there is significant disagreement over the reaction mechanisms, main reaction intermediate and rate controlling steps for these reactions. A major reason for the varied observations is the strong dependence of the reaction mechanism on the catalytic system used, the active sites and the relative stability of surface-bound intermediates on different catalyst surfaces. Hence, the understanding of new catalyst development in an area is incomplete without the knowledge of how the reaction mechanism is affected by the catalyst design and structure and what may be done to further improve the system. This review shall cover the recent advances in catalyst development in CO_2 hydrogenation and reforming reactions with a focus on the different proposed mechanistic models and kinetic equations over different catalytic configurations.

2. CO_2 conversion to syngas

2.1. CO_2-methane reforming to syngas

Dry reforming of methane (DRM) using CO_2 as a soft oxidant is one of the primary areas being researched for the transformation of CO_2 into higher chemicals through syn-gas (CO + H_2) as an intermediate. By principle, it is similar to steam reforming of methane, which is an established and widely used technology for H_2 or syngas production, but DRM uses CO_2 as an oxidizing agent instead of steam, which makes it more attractive for CO_2 mitigation and a carbon-neutral economy. DRM consumes two major greenhouse gases, CO_2 and CH_4, and converts them to syn-gas which can then be converted into higher chemicals through Fischer-Tropsch synthesis or used as a source of H_2. The H_2/CO ratio in the product syn-gas is 1, which is lower than that achieved by steam reforming, and is suitable for subsequent usage in Fischer-Tropsch synthesis of long-chain hydrocarbons.

$$CH_4 + CO_2 \rightarrow 2CO + 2H_2;\ \Delta H_{298K} = 248\ kJ.mol^{-1} \quad (1)$$

Dry reforming of methane (Eq. 1) is a highly endothermic reaction, and high temperatures (> 800 °C) are required to achieve good conversion of methane and carbon dioxide to syn-gas. The ideal H_2/CO ratio of syngas produced by DRM is 1 but this is influenced by the simultaneous occurrence of Reverse Water Gas Shift (RWGS) reaction (Eq. 2) which lowers the H_2/CO ratio to < 1 by producing water. Apart from RWGS, other significant side-reactions in DRM are methane decomposition (Eq. 3) and the CO disproportionation (Boudouard reaction) (Eq. 4). Both these reactions result in the formation of solid carbon that can cover the catalytically active sites and cause rapid deactivation.

$$CO_2 + H_2 \leftrightarrow CO + H_2O;\ \Delta H_{298K} = 41.2\ kJ.mol^{-1} \quad (2)$$

$$CH_4 \rightarrow C + 2H_2;\ \Delta H_{298K} = 75\ kJ.mol^{-1} \quad (3)$$

$$2CO \leftrightarrow C + CO_2;\ \Delta H^{\circ}_{298K} = -172.6\ kJ.mol^{-1} \quad (4)$$

The major technological challenges for the industrial application of DRM are its high endothermicity and rapid deactivation of catalysts under reaction conditions, caused by coking or sintering. For industrial application of DRM, there is a need to develop cost-effective catalysts that can maintain stable performance for extended durations in DRM. In the past decade, there has been a substantial increase in research focus on catalyst development for DRM and tremendous progress has been made in increasing the activity and stability of catalysts.

2.1.1. Catalysts for DRM

Supported metal catalysts such as Pt, Pd, Rh, Ru, Ni, Cu, Co etc. constitute the major class of catalysts that are active for DRM. The activity and stability of a catalyst in dry reforming of methane depends on a myriad of factors such as the nature of the metal and support, metal-support interaction, catalyst structure, metal particle size etc.

2.1.1.1. Type of active metal. Noble metals such at Pt, Ru, Pd etc. show higher resistance to sintering and coke formation in DRM compared to transition metals, but their usage is limited due to high cost. Due to easier availability and low cost, transition metals like Ni, Cu are gaining more interest as DRM catalysts, and tremendous efforts are being made to improve and stabilize these catalysts under DRM conditions.

Both noble metals and transition metals show good activity for DRM. It has been reported that the metals follow a catalytic activity order of Ru > Rh > Ni > Pt > Pd on SiO_2 support, Ru > Rh > Ni > Pd > Pt on a MgO support and Rh > Ni > Pt > Ir > Ru > Co on an Al_2O_3 support [17]. Noble metals tend to have an advantage of higher coke resistance and stability in dry reforming compared to transition metals. Alloying or promoting transition metals with noble metals to form bimetallic systems have been shown to significantly improve the activity and resistance to deactivation by coke formation or sintering [18]. For instance, doping trace amounts of noble metals like Pt, Pd, Rh can increase the reducibility of Ni by a hydrogen spill-over effect, wherein H_2 molecules preferentially dissociate on noble metal atoms to hydrogen atoms, which diffuse to the non-noble metals and enhance their reduction to create more active sites [18–21]. Based on the synthesis conditions,

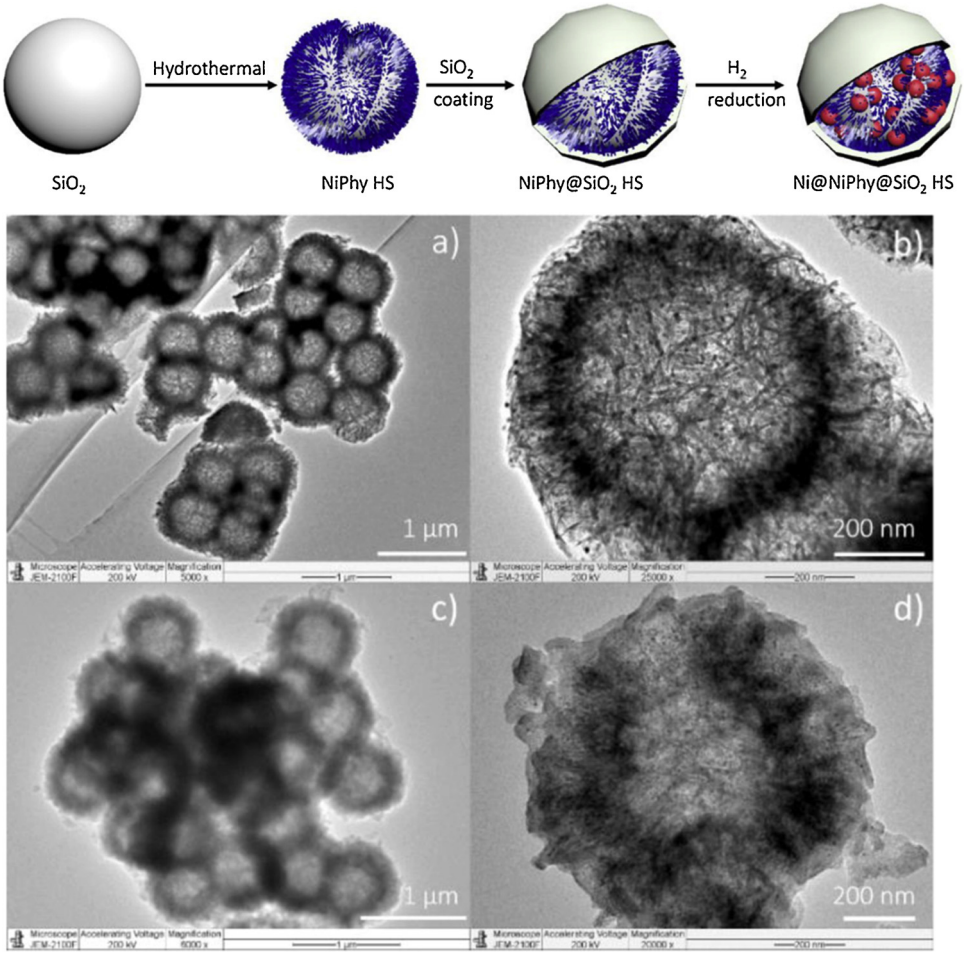

Fig. 1. Schematic of synthesis procedure for Ni@NiPhy@SiO_2 core shell hollow spheres and TEM images of reduced (a,b) NiPhy hollow sphere and (c,d) NiPhy@SiO_2 hollow sphere. The Ni@NiPhy@SiO_2 core shell hollow sphere catalyst showed excellent stability and coke resistance in DRM for 600 h at 700 °C [51].

metals in a bimetallic catalyst may exist in a uniform alloy phase or segregate to form surface enrichment of one metal species, that can affect the catalytic activity [22,23]. Bimetallic systems involving only transition metals such as Ni-Cu, Ni-Fe, Ni-Co have also shown considerable benefits over monometallic catalysts due to a synergistic effect on activity and coke resistance [18,24,25].

The rate of coke formation in DRM has been shown to be a strong function of the metal particle size. Coke formation is favoured on large metal particles, because carbon on smaller metal ensembles are less stable and tend to be gasified more easily. Kim et al. investigated the effect of size of nickel particles supported on alumina aerogel on coke formation in DRM and found that a minimum diameter of about 7 nm is required for the Ni particles to generate filamentous carbon [26,27]. Hence, synthesizing catalysts with high metal dispersion and small particle size is considered an effective strategy to reduce coke formation in DRM.

2.1.1.2. Role of support. Active metal components are usually dispersed on metal oxide supports that provide high surface area for metal dispersion, exposing higher amounts of active sites and preventing metal agglomeration. The nature of support plays an important factor in the activity and stability of catalysts in DRM. Basic supports like MgO, La_2O_3, CaO etc. that can preferentially adsorb and activate CO_2 tend to enhance the DRM activity and reduce the deposition of coke, thereby increasing catalyst stability. Using redox supports like CeO_2 is also a very effective way to reduce coke formation in DRM. Redox oxides like CeO_2, ZrO_2 and perovskite oxides possess highly mobile oxygen species (either as lattice oxygen or surface oxygen species), that can adsorb CO_2 and activate it to accelerate the carbon oxidation process. The oxygen mobility of oxide supports like perovskites can be further enhanced by the introduction of trace amounts of heteroatoms in the oxide structure, that creates structural defects and increases the oxygen mobility [28]. On the other hand, supports like SiO_2 serve primarily as an inert medium to disperse the metal and do not contribute to the reaction mechanism, although some studies have reported the significance of surface hydroxyl groups on silica in DRM [29].

The interaction between the metal and support in the catalyst is instrumental in the catalyst performance. A good metal-support interaction (MSI) reduces the mobility of metal nanoparticles, reducing sintering and maintaining a highly dispersed state during the reaction [30]. Also, MSI can cause chemical modification of the active metal by electronic effects of the support. Numerous studies have elucidated the effect of MSI in enhancing the stability and coke resistance in DRM. However, too strong MSI can retard the reducibility of the metal or cause partial encapsulation and reduce its catalytic activity [31].

Addition of catalyst promoters can also modify the properties of the support. For example, addition of alkali metal and alkaline earth metal oxides such as Na_2O, K_2O, MgO etc. can neutralize the surface acidity of the catalyst, reduce methane dehydrogenation activity, increase CO_2 adsorption, and improve the coke elimination in DRM [16,32].The specific surface area and porosity of the support also plays a key role in dispersing the active metal phase. Ordered mesoporous materials can stabilize small metal nanoparticles within the channels and pores while providing good accessibility to the reactant gas molecules. Silica based ordered mesoporous supports like SBA-15, MCM-41, KIT-6 etc. have been widely used to support metal nanoparticles, and can provide high

metal dispersion, stability and sintering resistance by confining the nanoparticles within the mesopores [33,34].

2.1.1.3. Role of catalyst structure. As mentioned in Section 2.1.1, the selectivity and stability in DRM is highly sensitive to the size of the active metal particles. Significant efforts have hence been made to synthesize catalysts with small well-dispersed metal particles and prevent the sintering of these particles during the DRM reaction. Among different wet chemical synthesis approaches, deposition-precipitation, ion-exchange or strong electrostatic adsorption, sol-gel, micro-emulsion methods etc. are effective in preparing dispersed metal nanoparticles. Impregnation in the presence of complex organic chelating agents like oleic acid/amine, PVP, etc. also lead to self-assembly of metals into small nanoparticles and reduce coke formation in DRM [24,35–41]. Structured catalyst precursors with high metal-support interaction such as phyllosilicates [25,29], perovskites [42], hydrotalcites [43] etc. can also generate supported metal catalysts with lower metal mobility and sintering.

Core-shell structured catalysts are a relatively new and emerging class of nano-materials that have been shown to be highly stable and coke-resistant in DRM [44,45]. A core-shell structured catalyst has the active metal core coated with a porous thermally stable shell such as silica that segregates them and prevents sintering under the harsh reaction conditions of DRM. Additionally, the presence of an encapsulation on the metal provides a steric hindrance for the growth of filamentous carbon during the reforming reaction. Several types of core@shell structured catalysts including multi-core@shell, yolk@shell, multi-core@hollow structures etc. have been reported to show excellent stability and coke-resistance under DRM (Fig. 1) [46–57]. Kawi's group has reported sandwiched multi-core@shell structure catalysts that showed negligible coke formation even under the most severe coking regimes of DRM (low temperature and high CH_4/CO_2 ratio) [48,52]. While SiO_2 remains the most widely used shell material for the ease of controlling the coating process by modifier Stöber process, other material such as CeO_2 [48], ZrO_2 [58] can also provide more coke resistance by aiding in coke removal through CO_2 activation (Table 1).

2.1.2. Reaction mechanism and kinetics

2.1.2.1. DRM mechanism. The mechanism of DRM can vary significantly over different catalyst systems and reaction conditions used, based on the ease of formation of different reaction intermediates. The key steps involved in DRM reaction are – 1. dissociation/activation of CH_4 and CO_2 on the catalyst surface, 2. adsorption of elemental and intermediate C, H and O species formed from CH_4/ CO_2 dissociation on active sites, 3. formation of product species (CO, H_2, H_2O) via surface reaction, 4. desorption of product species. It has been mostly reported that key kinetically significant step in the DRM process is the activation and dissociation of methane on the catalyst surface. However, some studies have also reported various other elementary steps such as the oxidation of active carbon species adsorbed on catalyst by adsorbed CO_2 or by surface $-O$ or $-OH$ groups as the rate determining step.

CH_4 activation requires the presence of metals like Ni, Pt, Ru etc. which can adsorb and dissociate methane either directly or through intermediates like CH_x or formates. Methane activation is believed to happen through intermediate formation at lower temperatures ($< 550\,^{\circ}C$) while direct dissociation is favoured at higher temperatures [65]. Table 2 shows the commonly reported elementary steps for DRM. The decomposition of methane on metal surface has been observed to be a structure sensitive phenomenon, where the properties of the exposed metal crystal facet influences the methane decomposition rate (Ni (110) > Ni (100) > Ni (111) [66]. The indirect activation of methane can occur via oxygenated intermediates like CH_xOH, CH_xO etc. (x = 1–3) formed by the reaction of adsorbed methane with surface oxygen or hydroxyl groups on the catalyst.

It is usually agreed that on catalysts with inert supports like SiO_2, DRM follows a mono-functional pathway where both the CH_4 and CO_2 get activated on the metal surface. On acidic/basic supports like Al_2O_3, MgO, CeO_2 etc., the mechanism is usually bi-functional wherein CH_4 is activated on the metal and CO_2 activates on the acidic/basic support [65]. CO_2 activation occurs through the formation of formates on acidic supports with the surface hydroxyls and through oxy-carbonates/carbonates/bi-carbonates on basic supports. In such catalysts, the catalytic activity becomes a function of the interface area between in the metal and support instead of the metal surface area alone [67]. The mechanism and the rate determining step strongly depend on the catalyst system, and a wide variety of mechanisms and rate determining steps have been reported for different systems [66,68]. Table 2 provides a list of possible elementary reaction steps for dry reforming of methane.

CO_2 adsorption and activation on basic supports may proceed through carbonate or bicarbonate intermediates. For instance, low temperature DRM was studied by Bachiller-Baeza et al. on Ni-CaO/ZrO_2-La_2O_3 catalysts and a bi-functional mechanism was proposed [69]. CH_4 activation and dissociation occurred on Ni surface to form adsorbed carbon (steps i–v, Table 2) and CO_2 was adsorbed on CaO to form $CaCO_3$. The carbonate further reacted with adsorbed -H species on the Ca-Zr-La support to form an adsorbed $-OH$ species and CO (steps xvii, xxii Table 2). The adsorbed $-OH$ on the Ca-Zr-La support then reacts with carbon species on Ni to form CO (step xxiv, Table 2).

On metal/lanthanum oxide catalysts, CO_2 is adsorbed on La_2O_3 to form lanthanum oxycarbonates ($La_2O_2CO_3$) that act as the reaction intermediate. CH_4 excitation and decomposition occurs on the metal particles to generate H_2 and activated carbon intermediate species. CO_2 adsorbs on the La_2O_3 to form reactive $La_2O_2CO_3$ species that reacts with the active carbon on the metal surface to form CO and regenerates the $La_2O_2CO_3$ (steps xix, xxv, Table 2). The activation of CO_2 by lanthanum oxycarbonate formation helps in reducing coke formation in DRM and hence the metal/La_2O_3 interface plays a key role in the coke resistance of the catalyst. Tsipouriari and Verykios utilized SSITKA method to compare the DRM reaction between Ni/Al_2O_3 and Ni/La_2O_3 catalysts and confirmed that the formation of $La_2O_2CO_3$ played an important role in imparting higher stability to Ni/La_2O_3 catalyst [70]. Li et al. studied DRM on two Ni/La_2O_3 catalysts with different morphologies and showed that Ni/La_2O_3 nanorods that had better Ni dispersion and higher Ni-La_2O_3 interface exhibited much lower coke formation because of carbon removal and rapid cycling of $La_2O_2CO_3$ and La_2O_3 at the interface (Fig. 2) [71]. Sutthiumporn et al. showed that doping of alkaline earth metals like Mg, Ca, Sr in Ni/La_2O_3 catalysts can give rise to increased surface oxygen species that adsorb CO_2 to form bidentate oxycarbonate species, that are highly reactive intermediates for oxidation of carbon [32]. Similar oxycarbonate intermediate has also been reported for Co/Sm_2O_3 catalysts in DRM by Cheng et al. [72,73].

A bifunctional redox mechanism is observed on supports like CeO_2 which can reversibly release and adsorb oxygen species. CeO_2 can undergo substantial oxygen stoichiometric changes by switching between Ce^{4+} and Ce^{3+}, which creates a high concentration of highly mobile oxygen vacancies that act as source or sink for oxygen involved in reactions. On Ni/CeO_2 catalysts, active carbon formed on metallic Ni surface from methane decomposition is converted to CO by the mobile oxygen species in ceria at the metal interface. The formed oxygen vacancy O_{x-1} in ceria is then replenished by CO_2 to form another molecule of CO and regenerate the CeO_2 (steps xviii, xxiii, Table 2) [48]. Xie et al. studied DRM mechanism over Pt/CeO_2 and proposed from a kinetic analysis that CH_4 dissociation occurs by an oxygen mediated route using the surface oxygen species on CeO_2 (step xi, Table 2). The concentration of such oxygen species was enhanced in a bimetallic PtCo/CeO_2 compared to Pt/CeO_2 due to increased CO_2 activation, which led to higher activity [74].

2.1.2.2. Kinetic models. Power law models (Eq. 5) are in general too simple to incorporate the nuances of the actual mechanism of DRM but they serve to give a general estimate of the parameters required for reactor modelling and a rough indication of the rate determining step

Table 1
Shows some representative catalysts reported in recent years and their performance in DRM reaction.

Catalyst	Synthesis Method	Reaction Conditions	Catalyst Performance (Activity/ Conversion)	Carbon Resistance	Remarks	Ref.
Supported Catalysts						
Transition metal based						
Ni –La_2O_3/ SiO_2	Wetness impregnation using oleic acid	700 °C CH_4: CO_2 = 1: 1 GHSV = 72 L gcat $^{-1}$ h $^{-1}$	85% CH_4 conversion, 80% CO_2 conversion, 0.8 H_2/CO	100 h TOS, small amount of coke	La_2O_3 promotes performance by increasing metal-support interaction	[27]
Ni/Ce- SBA- 16	Incipient wetness impregnation	700 °C, CO_2: CH_4: He = 1: 1: 1, GHSV = 45 Lgcat $^{-1}$ h^{-1}	72% CH_4 conversion, 77% CO_2 conversion, 0.72 H_2/CO	3.8% after 100 h	Confinement effect of ordered mesoporous SBA-16 and redox nature of Ce increases stability.	[33]
Ni/SiO_2 (OAm)	Incipient wetness impregnation	700 °C GHSV = 72 L gcat $^{-1}$h $^{-1}$	70% CH_4 conversion, 75% CO_2 conversion, 0.95 H_2/CO	17 h & negligible carbon formation on Ni/SiO_2 OAmc	High dispersion of Ni achieved by organic pair assisted impregnation causes better performance.	[37]
Ni/Al-SBA15	Impregnation with ethylene glycol as solvent	700 °C, CO_2: CH_4 = 1: 1, GHSV = 18 Lgcat $^{-1}$h $^{-1}$	73% CH_4 conversion, 80% CO_2 conversion, 0.97 H_2/CO	1.5% after 20 h	High nickel dispersion and confinement inside support prevents deactivation.	[59]
Ni/ZrO_2	Co-precipitation	700 °C, CO_2: CH_4 = 1: 1, GHSV = 24 Lgcat $^{-1}$h $^{-1}$	70% CH_4 conversion, 82.5% CO_2 conversion, 1 H_2/CO	Stable performance over 80 h	Anchoring of Ni in mesoporous ZrO_2 with high Ni-ZrO_2 interface	[60]
Noble metal based						
Pt/xLa_2O_3-Al_2O_3	Incipient Wet Impregnation	600 °C, CO_2: CH_4 = 1: 1, GHSV = 42 Lgcat $^{-1}$h $^{-1}$	36% CH_4 conversion, 80% CO_2 conversion, 1 H_2/CO	Low peak for carbon observed in Raman spectra after 24 h reaction.	Increase in La_2O_3 content from 1 to 6 wt.% gives highly dispersed Pt entities, 12% La_2O_3 gave best performance	[61]
$SrZrRuO_3$	Sol-gel, perovskite precursor	650 °C, CO_2: CH_4 = 1: 1	75% CH_4 conversion, 80% CO_2 conversion, 0.8 H_2/CO	0.0097 g_{coke}/ g_{cat} h, stable performance for 65 h	Effect of preparation method and doping alkaline earth metal (Sr, Ba, Ca) studied.	[62]
Pt, Ru doped TiO_2	Sonochemical synthesis	700 °C, CO_2: CH_4:N_2 = 2:2:96, GHSV = 38,200 h^{-1}	95% CH_4 conversion, 93% CO_2 conversion	0.072 g_{coke}/ g_{cat} after 20 h	High DRM activity observed even at low temperature of 400 °C	[63]
Bimetallic based						
$LaFe_{0.65}Ru_{0.05}Ni_{0.3}O$	Sol-gel, perovskite precursor	800 °C, CO_2: CH_4:He = 45:45:10, GHSV = 22 Lgcat $^{-1}$h $^{-1}$	85% CH_4 conversion, ~20% CO_2 conversion, 0.8 H_2/CO	Negligible after 20h	Partial substitution of iron by ruthenium creates synergistic effect and enhances activity and coke resistance in DRM	[64]
Pt-Ni-Mg/$Ce_{0.6}Zr_{0.4}O_2$	Incipient wetness impregnation	450 °C, CO_2: CH_4:He = 7:7:86, GHSV = 6000 h $^{-1}$	> 10% CH_4 conversion, ~20% CO_2 conversion, 0.32 H_2/CO	Negligible after 100 h	High activity at low temperature due to high dispersion and synergistic effects between platinum and oxide phases.	[20]
Pd-Ni/ mesoporous Al_2O_3	Incipient Impregnation	750 °C, CO_2: CH_4:He = 45:45:10, GHSV = 22.4 Lgcat $^{-1}$h $^{-1}$	88% CH_4 conversion, 92% CO_2 conversion, 1.05 H_2/CO	8% coke after 100 h	Addition of Pd enhances reducibility, activity and coke resistance	[21]
Ni-Co/ SiO_2	Hydrothermal, phyllosilicate precursor	750 °C, CO_2: CH_4:He = 1:1:1, GHSV = 60 Lgcat $^{-1}$h -	85% CH_4 conversion, 90% CO_2 conversion, 0.85 H_2/CO	Negligible coke after 100 h	Addition of small about of Co increases coke removal while too much Co causes Ni oxidation	[25]
Core-shell structured catalysts						
Ni–Yolk@Ni@ SiO_2	Microemulsion method	800 °C, CO_2: CH_4 = 1:1, GHSV = 36 Lgcat $^{-1}$h -	90% CH_4 conversion, 95% CO_2 conversion, 0.81 H_2/CO	Negligible after 90 h	Yolk-shell structure and formation of satellite Ni nanoparticles in the shell imparts high activity	[45]
Ni-Mg phyllosilicate nanotubes@ SiO_2	Hydrothermal	750 °C, CO_2: CH_4 = 1:1, GHSV = 60 Lgcat $^{-1}$h -	86% CH_4 conversion, 90% CO_2 conversion, 0.8 H_2/CO	No coke after 75 h	Silica shell helps retain Ni dispersion and prevent coking.	[56]
NiCo@SiO_2	Microemulsion method	800 °C, CO_2: CH_4 = 1:1, GHSV = 0.3 Lgcat $^{-1}$h -	87.2% CH_4 conversion, 88.9% CO_2 conversion	No coke after 50h	Encapsulation of metal nanoparticles by SiO_2 shell effectively inhibits the agglomeration of active sites	[49]
Ni@yolk-ZrO_2	Reverse Micelle method	750 °C, GHSV = 50.4 Lgcat $^{-1}$h -	90% CH_4 conversion, 0.7 CO selectivity	No coke after 50 h	Effect of porosity of ZrO_2 shell was studied.	[58]
Multi-Ni-Core@Ni Phyllosilicate@CeO_2	Hydrothermal	700 °C, CO_2: CH_4:He = 1:1:1, GHSV = 36 Lgcat $^{-1}$h -	70% CH_4 conversion, 80% CO_2 conversion, 1 H_2/CO	10% coke after 80 h	Confinement effect of core-shell structure on metal sintering and oxygen vacancy of ceria shell increase coke resistance.	[57]

Table 2
List of elementary steps in DRM mechanism.

CH_4 Activation	CO_2 Activation
Direct Decomposition	Direct Decomposition on metal
(i) $CH_4(g) + * \leftrightarrow CH_4*$	(xv) $CO_2(g) + * \leftrightarrow CO_2*$
(ii) $CH_4*+ * \leftrightarrow CH_3* + H*$	(xvi) $CO_2*+ * \leftrightarrow CO* + O*$
(iii) $CH_3*+ * \leftrightarrow CH_2* + H*$	H assisted activation
(iv) $CH_2*+ * \leftrightarrow CH* + H*$	(xvii) $CO_2*+ H* \leftrightarrow COOH*$
(v) $CH*+ * \leftrightarrow C* + H*$	Redox mechanism
Activation by Surface Hydroxyl species	(xviii) $CO_2*+ O_{x-1} \leftrightarrow CO* + O_x$ (O_x, O_{x-1} lattice oxygen and oxygen vacancy in support)
(vi) $CH_3*+ OH* \leftrightarrow CH_3OH*$	Through oxycarbonate formation
(vii) $CH_3OH*+ * \leftrightarrow CH_2 OH* + H*$	(xix) $CO_2 + M_2O_3 \leftrightarrow M_2O_2CO_3$ (M = La, Sm etc.)
(viii) $CH_2OH*+ * \leftrightarrow CHOH* + H*$	**CO and H_2 formation**
(ix) $CHOH*+ * \leftrightarrow COH* + H*$	(xx) $CHO*+ * \leftrightarrow CO* + H*$
(x) $C*+ OH* \leftrightarrow COH*$	(xxi) $C*+ O* \leftrightarrow CO*$
Activation by Surface O species	(xxii) $COOH*+ * \leftrightarrow CO* + OH*$
(xi) $CH_4*+ O* \leftrightarrow CH_3* + OH*$	(xxiii) $C*+ O_x \leftrightarrow CO* + O_{x-1}$
(xii) $CH_3* + O* \leftrightarrow CH_3O*$	(xxiv) $C*+ OH* \leftrightarrow CO* + H*$
(xiii) $CH_3O* + * \leftrightarrow CH_2O* + H*$	(xxv) $M_2O_2CO_3 + C* \leftrightarrow 2\,CO + * + M_2O_3$
(xiv) $CH_2O*+ * \leftrightarrow CHO* + H*$	(xxvi) $CO* \leftrightarrow CO(g) + *$
	(xxvii) $H*+ H* \leftrightarrow H_2* + *$
	(xxviii) $H_2* \leftrightarrow H_2(g) + *$

through the power-law coefficient of the reactant.

$$r = k[CH_4]^m CO_2^n \quad (5)$$

For most studies, the rate law for DRM has been observed to be first order in methane, while the CO_2 reaction order varies from 0 to low positive values (< 0.4) depending on the type of metal and support [66,68,75]. The less than 1 power dependence of CO_2 indicates the presence of an adsorption term of CO_2 or intermediates formed from CO_2 dissociation in the denominator. Wei and Iglesia studied DRM at 600 °C on a Ni catalyst and showed negligible dependence of the rate law on CO_2 concentration [76]. Differences in the kinetic parameters and coefficients in a power law kinetic fitting can sometimes provide valuable insights into the mechanism on a certain catalyst. For instance, Alsabban et al. observed a zero-order dependence on CO_2 for Ni catalysts for DRM but a negative order CO_2 dependence for Co and NiCo catalysts [77]. This indicated the higher affinity of CO_2 chemisorption and activation by Co leading to a higher presence of CO_2 derived species on the catalyst competing with sites for CH_4 activation. Bobrova et al. studied the effect of CH_4 and CO_2 concentrations on a Pt + Ni/PrSmCeZrO/YSZ nanocomposite catalyst and observed a first order dependence on CH_4 in the temperature range of 650 °C to 850 °C and an almost zero order dependence on CO_2 that declines further at increasing temperatures, showing that excess CO_2 acts as an inhibitor or a surface site blocker [78].

To understand and model the mechanistic aspects of DRM, more rigorous models such as the Eley-Rideal (E–R) model or the Langmuir-Hinshelwood-Hougen-Watson (LHHW) models are required. E–R models are based on the reaction between one surface-adsorbed species and one gas phase species. There can be two categories of E–R mechanisms for DRM: (1) where CH_4 is adsorbed on catalyst surface and reacts with CO_2 in gas phase, (2) where CO_2 is adsorbed on the catalyst surface and reacts with CH_4 in the gas phase.

Eley-Rideal Model 1

$$CH_4 + * \leftrightarrow CH_4 - *$$

$$CH_4 - * + CO_2 \leftrightarrow 2\,CO + 2H_2 + *$$

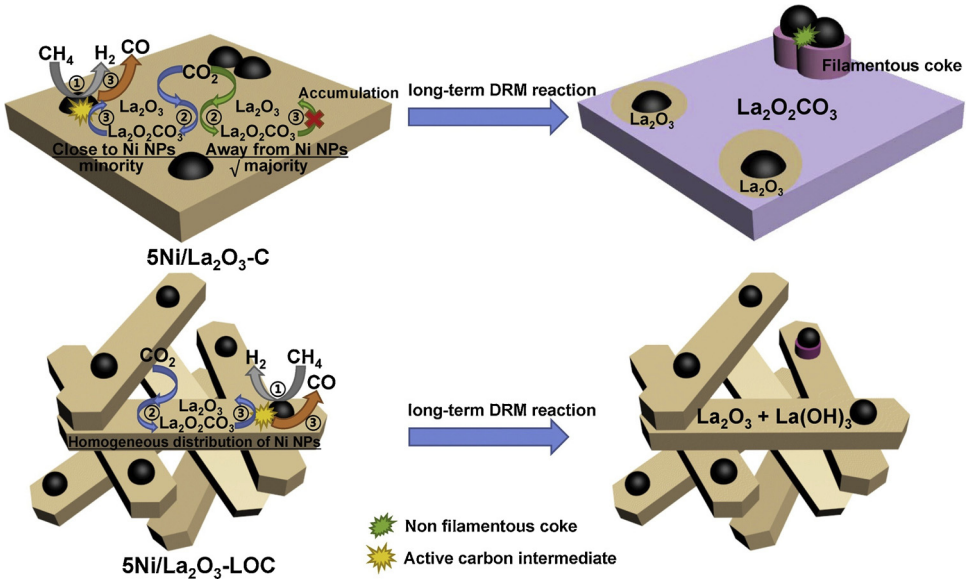

Fig. 2. Schematic of reaction mechanism on different Ni/La_2O_3 morphologies. 5Ni/La_2O_3-LOC with higher metal-support interface shows lower coke formation due to rapid cycling of $La_2O_2CO_3$ and La_2O_3 at the interface [71].

$$r = \frac{k_{ref} K_{CH_4}\left(P_{CO_2}P_{CH_4} - \frac{P_{CO}{}^2 P_{H_2}{}^2}{K_{ref}}\right)}{1 + K_{CH_4}P_{CH_4}}$$

Eley-Rideal Model 2

$CO_2 + * \leftrightarrow CO_2 - *$

$CO_2 - *{+}CH_4 \leftrightarrow 2\,CO + 2H_2 + *$

$$r = \frac{k_{ref} K_{CO_2}\left(P_{CO_2}P_{CH_4} - \frac{P_{CO}{}^2 P_{H_2}{}^2}{K_{ref}}\right)}{1 + K_{CO_2}P_{CO_2}}$$

There are only a few studies that have reported an E–R mechanism for DRM, and mostly the E–R I type of mechanism has been reported. Akpan et al. studied DRM kinetics for a Ni/CeO_2-ZrO_2 catalyst and proposed an E–R redox mechanism where gas-phase CO_2 reacts directly with oxygen vacancies in the support to replenish the oxygen and produce CO. Based on a kinetic fitting of different rate expressions to experimental data, they concluded that methane decomposition is the RDS [79]. The direct reaction of gaseous CO_2 with adsorbed carbon species from methane decomposition was proposed by Singh et al. on Pt-Ru/TiO_2 catalyst [63].

Compared to E–R models, LHHW models have been more extensively reported to explain the mechanism and kinetics in DRM. In a LHHW model, the reaction is assumed to happen between surface adsorbed species and not gas-phase components. Depending on the operating conditions and catalyst system used, there are differing reports on the rate determining step and the overall kinetic expression. The difference in the rate determining step observed often stems from the variation in reaction temperature used in different studies, making direct comparisons difficult. For instance, Cui et al. performed kinetic analysis for DRM on Ni/Al_2O_3 in the temperature range of 550 °C – 750 °C keeping constant reactant partial pressure and observed that the RDS changes from methane decomposition at lower temperatures (550 °C – 575 °C) to surface oxidation of methyl species by CO_2 at higher temperatures (650 °C – 750 °C) [80]. Some of the representative LHHW kinetic expressions along with the corresponding rate determining step are listed in Table 3.

A significant number of mechanism and kinetic studies report LHHW models with CH_4 decomposition as the RDS for both monofunctional and bi-functional DRM mechanisms. The activation energy of CH_4 decomposition varies from catalyst to catalyst and have been reported to be in a range of 10–30 kcal/mol [81]. Iglesia et al. performed isotopic and kinetic assessment of DRM on supported Ni, Pd, Rh catalysts at ≤600 °C and found the reforming of methane with CO_2 and H_2O to be kinetically equivalent with similar turnover rates, first order rate constant and activation energies, suggesting that methane decomposition is the sole kinetically relevant step under the tested conditions [76,82,83].

The oxidation of surface bound carbon species from methane decomposition with surface oxygen or hydroxyl species may also be the kinetically governing step. On a Ce doped Ni-Co/Al_2O_3 catalyst, Foo et al. proposed a dual-site mechanism with a RDS of oxidation of carbon on metal sites by oxygen species on the redox ceria promoted support [84].

$CH_4 + 2X_1 \leftrightarrow CH_3 - X_1 + H - X_1 \ldots\ldots C - X_1 + H - X_1$

$CO_2 + 2X_2 \leftrightarrow CO - X_2 + O - X_2$

$C - X_1 + O - X_2 \rightarrow CO - X_2 + X_1$ (slow step)

$2\,H - X_1 \leftrightarrow H_2 + 2X_1$

$CO - X_2 \leftrightarrow CO + X_2$

$$r = \frac{k_{rxn}\sqrt{P_{CH_4}}\sqrt{P_{CO_2}}}{(1 + \sqrt{K_{CH_4}}\sqrt{P_{CH_4}})(1 + \sqrt{K_{CO_2}}\sqrt{P_{CO_2}})}$$

Several catalytic systems have also been shown to follow kinetic models based on two rate determining elementary steps instead of a single RDS. Ayodele et al. reported that a Co/Pr_2O_3 catalyst followed a bi-functional mechanism with a two-step dual site RDS: CH_4 activation by Co metal and C gasification by adsorbed CO_2 on the support site [85].

$CH_4 - \alpha \leftrightarrow C - \alpha + 2H_2$ (*slow step*)

$CO_2 - \beta + O^{2-} \leftrightarrow + \beta - CO_3^{2-}$ (α = *metal site*, β = *basic support site*)

$\beta - CO_3^{2-} + C - \alpha \leftrightarrow \alpha + \beta + 2CO$ (*slow step*)

$$r = \frac{k_{rxn}P_{CH_4}P_{CO_2}}{K_{CH_4}K_{CO_2}\,k_{CO_2}P_{CH_4}P_{CO_2} + K_{CH_4}k_{CH_4}P_{CH_4} + K_{CO_2}k_{CO_2}P_{CO_2}}$$

Fan et al. also reported a similar kinetic model in a Ni-Co/MgO-ZrO_2 catalyst [86]. Similarly, a two-step dual-site RDS model has been proposed for $SmCoO_3$ perovskite derived catalyst where both methane decomposition and the decomposition of $Sm_2O_2CO_3$ oxycarbonate species formed by CO_2 absorption are slow [72].

Overall, there is significant variation in reports for the mechanism and kinetic modelling for DRM, which may arise from the intrinsic characteristics of the system or from the limited windows of tested conditions and errors arising from inherent catalyst deactivation by coking or sintering. More holistic studies over wide range of operating conditions using transient techniques like SSITKA and TAP analysis and supported by *in-situ* characterization of catalysts and intermediates are required to acquire a more global and cohesive understanding of the mechanism. Complete microkinetic models based on ab initio Density Functional Theory (DFT) analysis can also be conducted in order to obtain a comprehensive database for the various kinetic models.

2.2. CO_2 hydrogenation to CO (Reverse water gas shift reaction)

The reverse water gas shift reaction is the hydrogenation of CO_2 into CO and water and is a pivotal process to produce CO, a building block for the manufacturing of highly valuable chemicals including methanol, hydrocarbons and olefins. RWGS is an intermediate step for the conversion of CO_2 into hydrocarbons or oxygenates via the established Fischer Tropsch process or methanol synthesis processes using syngas (H_2 + CO) as reactants. The advantage of using CO as an intermediate instead of direct hydrogenation of CO_2 to higher hydrocarbons is the higher reactivity of CO compared to CO_2 that makes further conversion processes easier and less thermodynamically challenging. The source of hydrogen for RWGS is critical for the overall CO_2 consumption in the process and it is necessary to develop technologies to harness carbon-free sources of hydrogen like water. The major products of this reaction are CO and water, with methane produced in small quantity as a side product. Apart from industrial application to produce valuable chemicals, RWGS reaction is also of great interest for outer space exploration. For instance, in the high CO_2 containing atmosphere of Mars (95%), it can be used as a platform for conversion to useful commodity chemicals by reaction hydrogen produced from oxygen generation process.

RWGS is an endothermic reaction and thermodynamically favoured at high temperatures (close to 800 °C). The high temperature requirement of the process makes energy efficiency a challenge. In contrast, when the reaction temperature is lowered, the forward water gas shift reaction becomes more prominent. Additionally, the formation of the methane side product increases; thereby, decreasing the selectivity towards of formation of CO.

The RWGS reaction occurs according to Eq. 2 (i.e, $CO_2 + H_2 \leftrightarrow CO + H_2O$). However, several undesired parallel and side reactions (Eqs. 4, 6 and 7) tend to occur as well

$$CO_2 + 4H_2 \rightarrow CH_4 + 2H_2O;\ \Delta H^{\circ}_{298K} = -164\ \text{kJ.mol}^{-1} \quad (6)$$

$$CO + 3H_2 \leftrightarrow CH_4 + H_2O;\ \Delta H^{\circ}_{298K} = -206\ \text{kJ.mol}^{-1} \quad (7)$$

Table 3
Summary of kinetic models for DRM reaction.

Catalyst	Rate model	Temp. range (°C)	Ref.
CH_4 decomposition as RDS			
Pd/ZrO_2	$r = \frac{k_1 P_{CH_4}}{(1+A\sqrt{P_{H_2}})\left(1+\frac{k_1 P_{CH_4}}{(1+A\sqrt{P_{H_2}})}\frac{\frac{B}{D}P_{CO}}{P_{CO_2}+1}\right)^2}$	550	[82]
	RDS: $CH_3-{*}+{*}\rightarrow CH_2-{*}+H-{*}\ldots\ldots\rightarrow C-{*}+H-{*}$		
Ni/Al_2O_3	$r = \frac{k_1 P_{CH_4} {P_{CO_2}}^2}{(a+b{P_{CO_2}}^2+cP_{CH_4})^2}$	500-850	[70]
	RDS: $CH_4-{*}\rightarrow C-{*}+2H_2$		
Carbon oxidation as RDS			
NiCo/Ce doped Al_2O_3	$r = \frac{k_{rxn}\sqrt{P_{CH_4}}\sqrt{P_{CO_2}}}{(1+\sqrt{K_{CH_4}}\sqrt{P_{CH_4}})(1+\sqrt{K_{CO_2}}\sqrt{P_{CO_2}})}$	650- 750	[84]
	RDS: $C-X_1+O-X_2\rightarrow CO-X_2+X_1$		
Ni-Rh/ Al_2O_3	$r = \frac{k_1 K_{CH_4} K_{CO_2}\left(P_{CH_4}P_{CO_2}/P_{H_2}{}^{0.5}-P_{H_2}{}^{1.5}P_{CO}{}^2/K_{ref}\right)}{\left(1+P_{CH_4}/P_{H_2}{}^{0.5}K_{CH_4}+P_{CO_2}K_{CO_2}\right)^2}$	525-625	[87]
	RDS: $CH_x-{*}+CO_2-{*}\rightarrow 2\,CO+2{*}+\frac{x}{2}H_2$		
Reverse Boudouard reaction as RDS			
Ni-Co/Al-Mg-O	$r = \frac{aP_{CH_4}P_{CO_2}}{(bP_{CH_4}+cP_{CO_2}+dP_{CH_4}P_{CO_2})}$	650-750	[88]
	RDS: $CO_2-{*}+C-M\rightarrow 2\,CO+{*}+M$		
2-step dual site RDS			
CH_4 activation by Co metal and C gasification by adsorbed CO_2 on the support			
Co/Pr_2O_3	$r = \frac{k_{rxn}P_{CH_4}P_{CO_2}}{K_{CH_4}K_{CO_2}k_{CO_2}P_{CH_4}P_{CO_2}+K_{CH_4}k_{CH_4}P_{CH_4}+K_{CO_2}k_{CO_2}P_{CO_2}}$	650-750	[85]
	RDS: $CH_4-{*}\rightarrow C-{*}+2H_2$		
	$s-CO_3^{2-}+C-{*}\rightarrow {*}+s+2CO$		
$SmCoO_3$	$r = \frac{K_1k_2K_3k_4P_{CH_4}P_{CO_2}}{K_1k_2K_3P_{CH_4}P_{CO_2}+K_1k_2P_{CH_4}+K_3k_4P_{CO_2}}$	700- 800	[72]
	RDS: $CH_4-{*}\rightarrow C-{*}+2H_2$ (*slow step*)		
	$Sm_2O_2CO_3+C-{*}\rightarrow {*}+Sm_2O_3+2CO$ (*slow step*)		

All of the above reactions occur simultaneously during RWGS producing H_2O, CO, CO_2, H_2, and C in the reaction medium. There are several other studies which compares the RWGS reaction with other processes producing CO. Among the investigated methods, RWGS reaction showed greater potential and higher efficiency when flue gas is the source of CO_2. In the lower temperature region of 600 °C, methanation reaction becomes prominent and only at a temperature higher than 700 °C is required to achieve CO as a significant product.

There are technical challenges associated with RWGS catalyst development such as metal sintering and carbon deposition which causes rapid deactivation of catalysts. Therefore, rational catalyst design is crucial to obtain high activity and selectivity in RWGS to overcome the problems and achieve a promising behavior of the catalyst.

2.2.1. Catalysts for RWGS

Generally, the catalyst is designed to promote dual functionality of active metal/metal oxide sites and sites on the surface of the support. The rational choice for metal/metal oxide and supports promotes better adsorption of reactants, followed by surface intermediate reaction and finally the desorption of reactant. There are mainly three categories of catalyst studied in RWGS, they can be categorized as follows: mixed metal oxide catalyst, supported catalyst and transition metal carbide catalyst. The summary of recently reported catalysts was also presented in Table 4.

2.2.1.1. Mixed metal oxide catalyst. Mixed metal oxides consisting of transition metal oxides such as ZnO, Fe_2O_3, Cr_2O_3 and mixed oxide solid solutions have shown encouraging activity for reverse water gas shift reaction. In the light of this findings, S.-W. Park et al. investigated the ZnO based catalyst. When only ZnO was investigated the activity was lost with time however the stability was significantly improved when mixed with appropriate ratio of Al_2O_3 as it forms spinel phase $ZnAl_2O_4$ at higher temperature. The catalyst was found to be stable at 600 °C for 100 h of operation due to formation of smaller Zn particle in $ZnAl_2O_4$ as compared to ZnO/Al_2O_3 [89]. In the same study, Cr_2O_3 was also used as a support for ZnO. The catalyst showed superb performance and stability with no coke formation. For better comparison Fe_2O_3/Cr_2O_3 was also investigated which showed slight deactivation. The major cause of catalyst deactivation was due to coke deposition. Thus, utilizing high oxygen storage elements such as CeO_2 is another possible way to improve the performance [90]. F. Lin et al., studied the Zn modified ceria nanocrustals for RWGS reaction. This study developed compelling correlation between the structural properties, the oxygen storage capacity and the reaction performance for the RWGS reaction. The catalyst showed higher RWGS activity and stabilitiy at lower temeprature range of 400–600 °C whereas the perforamce rapidly decreases at 800 °C due to metal sintering at this elevated temperature [91]. Co-CeO_2 mixed oxides prepared by co-precipitation method showed excellent performance and lower coke deposition. The presence of well dispersed Co on CeO_2 support suppressed methane formation whereas high loading of cobalt led to increase in the possibility of methanation reaction. Another group of mixed metal oxides extensively applied for RWGS are $Zn_xZr_{1-x}O_{2-x}$ [92], $Ni_xCe_{0.75}Zr_{0.25-x}O_2$ [93], these catalysts offer promising properties

Table 4
Summary of catalysts for RWGS reaction.

Catalyst	Synthesis Method	Reaction Conditions	Catalyst Performance (Activity/ Conversion)	Remarks	Ref.
Mixed oxide catalysts					
ZnO/Al_2O_3	Co-precipitation	400-700 °C H_2/CO_2: 3/1 GHSV = 15,000 ml/gcat h	CO_2 conv. = 70% at 700 °C for Zn:Al = 1:1	Zn and Al ratio effected the CO_2 conversion. The formation $ZnAl_2O_4$ showed promising behavior in stabilizing the catalyst	[82]
Ni/CeO_2- Al_2O_3	Wetness Impregnation	400–750 °C H_2/ CO_2: 4/1 WHSV = 30,000 mL g^{-1} h^{-1}	CO_2 conv. = 70% at 750 °C CO selectivity = 90%	FeOx facilitated the better dispersion of Ni. Due to higher interaction between Ni-Fe the improved CO_2 adsorption, thereby suppressing methane formation.	[83]
Zn modified Ce nanocrystals	Co-precipitation	400-800 °C H_2/ CO_2 :1/1	CO concentration = 1.1 % at 600 °C	Incorporation of Zn increased the oxygen storage capacity of Ce nanocrystals thus improved the stability.	[84]
Zn_xZr_{1-x} O_{2-y} solid solution on m-ZrO2	Wetness impregnation method	500 °C H_2/CO_2:3/1	CO_2 conversion was maximum with Zn wt% of 0.7 : 2.8 mmol $_{CO2}$ g_{cat}^{-1} $^{min-1}$	The formation of solid solution increases the oxygen mobility and reducibility of ZrO_2 thus improved reaction performance was obtained.	[85]
$La_{0.75}Sr_{0.25}Co_{(1-Y)}FeYO_3$	Sol gel method using ethylene glycol	550 °C 10% H_2/He flow rate : 50 mL/min 6.7% CO_2/H_2:48.5 mL/min	CO formation: 0.42 mol/mol perovskite for reduced sample in cycle 1 ;the value decreased to 0.29 after 5 cycles	The low conversion temperature of CO_2 with competitive CO selectivity make for the RWGS-CL process a plausible technology for the formation of C1 feeds.	[87]
Transition /Noble metals supported catalysts					
M(Ni,Co,Cu,Fe,Mn)/ mesoporous CeO_2	KIT-6 as a template or meso-CeO2 and wetness impregnation	260 - 400 °C H_2/CO_2:4/1 WHSV: 60,000 mL/g/h.	The CO_2 conversion was highest for Ni/CeO_2: 69.21% and followed the order of Ni > Co > Fe > Mn > Cu > CeO_2 Fe, Mn and Cu showed 100% CO conversion and Ni and Co showed methane formation.	The formation of solid solution improved the catalytic activity specially for Cu/CeO_2 by improving the CO_2 adsorption	[103]
$Cu/ZnO/Al_2O_3$	Co-precipitation	250 °C & 30 bar H_2/CO_2: 4/1 WHSV:30,000 mL.g_{cat}^{-1}. h^{-1}	CO formation : 450 μmol.$min^{-1.gcat^{-1}}$	H/D substitution during the reaction showed significant effect of RWGS	[97]
Pt/TiO_2	Incipient wetness impregnation	200-500 °C H_2/CO_2 : 1/1	CO_2 conversion: 21% (close to equilibrium) at 400 °C and 1% Pt loading CO selectivity :95% with 1% Pt loading	The product selectivity was dependent on Pt particle size. Large particle led to methane formation and nanoparticle showed higher selectivity for CO.	[106]
Pt-MoO_x/SiO_2	Incipient wetness impregnation	200 °C & P =7.1 bar H_2/CO_2 : 2/1 Total flow rate: 15 mL/min	CO_2 conversion rate: 237 μmol.g^{-1} min^{-1} (dark) and 1640 μmol.g^{-1} $^{min-1}$ (light)	Addition of Mo to Pt decreased the apparent activation energy. Both Mo deposition and visible light during the reaction changed the kinetics.	[109]
K doped Pt/Zeolite	Ion exchange	200-500 °C H_2/CO_2 : 1/1 WHSV: 30,000 mL.g_{cat}^{-1}. h^{-1}.	CO_2 conversion: 28% for K_{80}-Pt/L CO Selectivity: 100% at 500 °C	Cage encapsulation method improved the metal particle dispersion.	[111]
Transition metal carbides					
Au/δ-MoC and Cu/δ-MoC	Depostion of Cu and Au on MoC	500- 600 °C H_2/CO_2 : 9/1 (4.5 atm H_2 and 0.5 atm CO_2	CO molecules produced: 37 *10^{15} molecules. $cm^{-2}.s^{-1}$ for Au/MoC at 550 K. The performance was stable for 15 hour of reaction. CO molecules produced for Cu/MoC > Cu/TiC	DFT calculation revealed that Cu/δ- MoC forms bimetallic type catalyst and the Cu clusters readily dissociate CO_2 into CO and O.	[119]
Cu/β-Mo_2C	TPC procedure	300-600 °C P = 0.1 MPa H_2/CO_2 : 2/1	Rate: 47.7 × 10^{-5} mol_{CO2} /gcat/s and CO_2 conversion : 37.5 % & CO selectivity: 99.2 at 600 °C for 1 wt% Cu/ β-Mo_2C. The stability was tested for 35 h with slight decrease in CO_2 conversion	Higher interaction of Cu–Mo_2C improved the ultrahigh dispersion of Cu.	[120]
Cu-Cs-Mo2C	Co-precipitation and TPC procedure	500 - 750 °C H2:CO2 = 4:1 WHSV: 12,000 ml g^{-1} h^{-1}	CO_2 conversion: 60% CO selectivity: 100% The CO_2 decrease with decreasing H_2/CO_2 ratio.	Due to electropositive character of Cs facilitated the electronic transfer from Cs to Mo and leads to an electronically rich surface which favors the selectivity towards CO.	[121

such as high oxygen storage and reducibility during high temperature reaction condition. In the study including $Zn_xZr_{1-x}O_{2-x}$ as a catalyst for RWGS reaction, under severe reaction conditions, the catalysts undergo deactivation after several cycles. Zn replaces the Zr ions in the lattice forming a surface solid solution. This solid solution increases the reducibility by improving oxygen vacancy which improves the oxygen mobility thereby suppressing carbon formation [85]. In another study, the Ni was incorporated in the $Ce_{0.75}Zr_{0.25-x}O_2$ by co-precipitation and impregnation methods. Higher reducibility of metal oxides and higher metal support interaction of metal with the support led to the enhanced activity.

Perovskite type oxides are widely used for various catalytic applications including reverse water gas shift reaction. Mixed oxide perovskites (ABO_3) consist of A- and B-site ions. This combined with their structural stability allows the variation of composition, oxygen vacancies and oxidation state of metal ions which affect their catalytic activity. Perovskite type oxides have been used in RWGS coupled with chemical looping. Chemical looping has been explored as a technique to break thermodynamic equilibrium limitation and suppress methane formation in RWGS reaction. Perovskite based catalyst possess several possibilities to be modified to achieve desired oxygen vacancy in the structure and thus show huge potential for chemical looping applications. Carbon dioxide is first captured from its emissions source or separated from air and purified. The RWGS–CL operation converts CO_2 and H_2 separately in two steps to form separate streams of CO and water using $La_{0.75}Sr_{0.25}CoO_{3-\delta}$ and $LaFeO_3$ type perovskite catalysts. The CO is combined with additional H_2 for liquid fuel production via FTS or methanol synthesis [94]. These separate product streams eliminate the possibility of methanation as a side reaction because there is no direct interaction between CO_2 and H_2 and aid in avoiding thermodynamic limitations as shown in Fig. 3. A higher CO production was observed during re-oxidation of CO_2 [95]. Ba-Zr-based perovskite catalyst with Zn, Y and Ce doped in the structure was also studied. Among the three doping elements, Zn- and Y-doped BZYZ catalyst showed an outstanding activity for the RWGS reaction at 600 °C whereas Ce doped perovskite showed no positive effect on RWGS reaction [96,97]. Overall, mixed oxides and perovskite type catalysts can be considered as a promising class of catalyst for RWGS reaction as well as chemical looping coupled RWGS.

2.2.1.2. Transition metal /Noble metal based supported catalyst. Different combination of active metal and support result in a varying range of products for CO_2 hydrogenation reaction. An extensive study was done to investigate both noble and transition metals (Ni, Cu, Ag, Rh, Ru, Pt, Pd and Au) supported on ZrO_2 support [98]. It was found that Ag and Cu mostly lead to the production of methanol where Ni and Ru produced methane as the major products. The rest of the metals

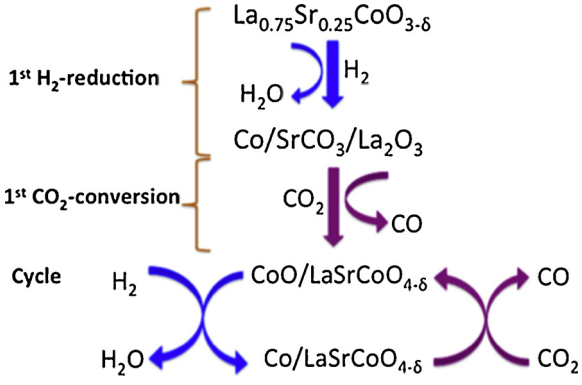

Fig. 3. Schematic representation of CO_2 conversion to CO on the oxygen deficient oxide system. A H_2 treatment reduces the perovskite- type oxides to metallic cobalt and base oxides while producing water. With CO_2 present, the reduced phases re-oxidize producing CO [109].

produced mainly CO, methanol and methane. In another study, Dai et al. studied M (Ni, Cu, Co, Fe, Mn)-mesoporous CeO_2. Among all the metals, Ni and Co showed highest conversion for CO_2 although the selectivity towards CO was lower. On the other hand, metals such as Cu, Fe, Mn showed almost 100% selectivity for CO during RWGS reaction. Nickel catalysts are rarely considered as effective RWGS catalysts because of their excellent hydrogenation behavior making methanation of CO_2 over Ni catalysts more favorable [40,48,99,100]. Catalysts with highly dispersed Ni nanoparticles on supports with large oxygen exchanging capacity are still found to be effective for RWGS reaction [22]. Several modifications such as alloying with Cu [21,101–103], doping with alkali metals [104,105], and enhanced metal-support interaction [106,107] for Ni based catalysts have been reported to improve the selectivity towards desired CO product in RWGS by methane suppression [48,108,109]. An interesting piece of research finding was introduced by H. C. Wu et al. where the authors investigated the effect of metal particle size on the product selectivity. It was shown that the catalyst becomes more favorable for methane formation with increased nickel loading. High CO selectivity of the catalyst with small Ni particles is attributed to enhanced dissociation of formate species [110].

Theoretical and experimental studies performed on various catalysts elucidated the key criteria for designing a good catalyst for RWGS reaction. There are basically two properties of metals to be considered, the electron properties of d-orbital holes of metals and the difference between desorption energy and dissociation barrier of metal carbonyls determined by the adsorption configuration [111]. The availability of incompletely filled d-orbitals facilitates the easy adsorption of reactants forming intermediates. Hence, noble metal based catalysts are highly preferred. In a study by Chen et.al, the Pt/TiO_2 was reported for RWGS reaction. TiO_2 offers several advantages being a reducible support, and the presence of oxygen defects in the structure enhances interfacial sites which changes the reactant adsorption at low and high temperature. Another study investigated the effect of the morphological characteristics of TiO_2 support. From this study, it was found that TiO_2 crystallite size played a crucial role by governing the reducibility of TiO_2 sites [112]. Pt based catalyst was also modified by adding other transition metals such as Ni, Co to enhance the electronic property of Pt. The formation of bimetallic catalysts enhances the CO selectivity as compared to only Pt which leads to the formation of methane [113]. Reducible types oxide supports are more promising than the non-reducible supports due to lower activity of catalysts including non-reducible supports [114,115]. The addition of reducible phase such as MoOx to the parent metals (Pt) decreases the activation energy barrier; thereby, enhancing the RWGS activity. Moreover, reducible oxide as catalyst supportpossess high oxygen mobility in the presence of oxidant CO_2 thus improving the activity [116]. Another strategy to improve metal sintering of noble metal is the addition of alkali metals such as potassium and sodium (Fig. 4) [117,118]. The presence of alkali metal provides a site for formate decomposition, reduces the adsorption strength of CO and shows higher TOF than un-doped Pt.

Single atom catalysts have recently attracted intense research attention and considerable work is being done to understand the properties and wide applications of such materials. Metal particle size plays a unique role in maintaining the stability of catalyst during the CO_2 hydrogenation reaction. Matsubu et al., studied Rh/TiO_2 catalyst and observed that during the reaction conditions, Rh nanoparticles disintegrates to form isolated Rh sites. This change in size controls the reactivity with time on stream. A strong correlation was observed between the reaction mechanism, TOF and number of Rh-isolated sites and methanation reaction [119]. Another investigation revealed the importance of Ru loading on the Al_2O_3. With the loading percentage of less than 0.5% the active metal was mostly atomically dispersed and high selectivity for CO was obtained [120]. Therefore, from all the studies done so far on supported metal catalyst for RWGS reaction, it can be concluded that the metal particle size, type of support (reducible

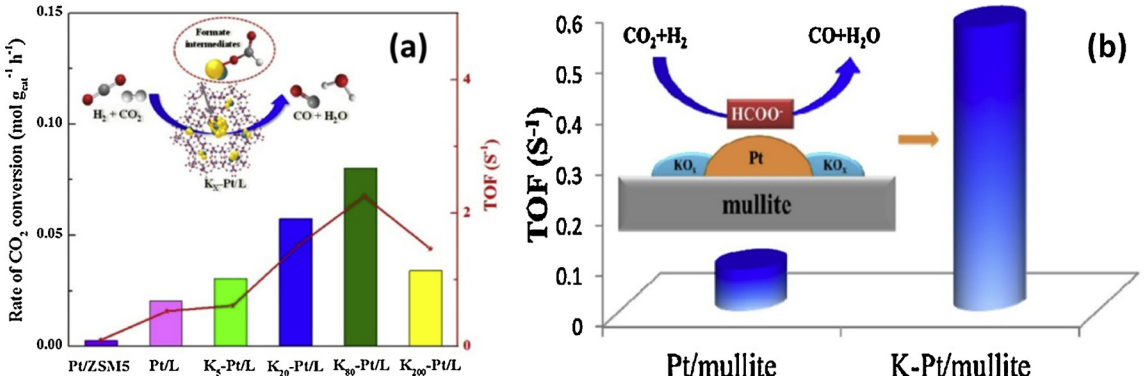

Fig. 4. (a) The effect of addition of alkali metal to Pt/ZSM- 5 on the rate and TOF value [117] (b) The enhanced TOF value obtained after the addition of potassium to Pt/Mullite [118].

and non-reducible), morphology of support, bimetallic nature of catalyst etc. showed distinctive behavior to enhance the activity and stability of catalyst under different reaction conditions.

2.2.1.3. Transition metal carbide (TMC) catalyst: A cheaper and efficient alternative to noble metal based catalyst. Due to the higher price of noble metal catalyst and low regeneration capability, there is a need to search for cheaper alternative catalyst. The low cost of transition metals makes them very attractive, and specifically transition metals in the form of metal carbides are considered as an alternative to noble metal catalysts in RWGS. TMC catalyst are low in cost and easy to synthesize. Levy and coworkers were among the first ones to report the similarity in electronic properties of metal carbide and noble metals such as Pt [121]. However, the surface and bulk properties change with different transition metals. Apart from the cost, TMC have also shown great potential in improving the metal dispersion. TMC can also be used as a catalyst support for the dispersion of active metal sites to form small sized and stable nanoclusters. The enhanced metal dispersion promotes hydrogen dissociation and C═O scissoring, as reported previously for RWGS reaction [122]. Additionally, several studies also reported the activation of CO_2 by β-Mo_2C. Here, the carbide catalyst facilitates the adsorption of CO_2 which binds to Mo_2C in bent configuration, eventually breaking the C═O bond [121,123]. Further, this dissociated CO desorbs while O interacts with Mo_2C to form Mo_2C-O. After this step comes the important role of hydrogen as a reactant which completes the cycle by reducing the Mo_2C-O and releasing a water molecule, thereby completing the reaction cycle [124]. This oxycarbide formed is crucial as it is a descriptor for determining the activity of RWGS reaction [125]. TMC not only acts as a catalyst but also offers favourable property as a support. Zhang et al. studied Cu/Mo_2C prepared using Cu-MoO_3 as a precursor [126]. This catalyst showed excellent performance at higher temperature range of 600 °C and maintained 85% activity for 40 h of operation. The stability was attributed to the strong metal support interaction, enhancing Cu dispersion and preventing Cu agglomeration as shown in Fig. 5. Recently, Q. Zhang et al. reported the effect of adding promoters (Cu and Cs) to Mo_2C. Cu as a promoter added extra sites for the reaction in the form of different oxidation states of Cu (Cu^+ and Cu^0). Addition of Cs generated electronic perturbations on the surface of the catalyst leading to highly enhanced catalytic activity. The robust activity of Cs doped catalyst was due to *in-situ* activation by re-carburization making the catalyst more stable for continuous operation. Also the Cs doped Mo_2C does not require any pretreatment of catalyst prior to reaction making it an advantageous class of catalyst for RWGS reaction [127].

2.2.2. Reaction mechanism and kinetics

Several techniques are used to study the kinetics and mechanism of RWGS reaction. The techniques mainly involve *in-situ* characterizations (XPS, XRD, EXAFS), isotopic tracer method, *operando* DRIFTS and simulation methods such as DFT. There are basically two reaction mechanisms proposed for RWGS reaction as shown below in Table 5.

2.2.2.1. Surface redox mechanism. In the redox mechanism, an instantaneous change occurs on the active sites due to oxidation and reduction step in the presence of CO_2 and H_2. The hydrogen acts an a reducing agent without directly participitating in the intermediate formation. The CO_2 present as another reactant further reoxidizes the partially reduced support even at lowe temperatures forming CO. Wang et al. investigated the redox mechanism using gold metal support on CeO_2 as a catalyst for RWGS. The author used TAP analysis to elucidate the mechanism and to show the interaction of CO_2 with the catalyst [116].

In this study it was found that the surface oxygen can be removed by reaction with H_2 shown in Eq. 8.

$$H_2 + O_{CeO2} \rightarrow H_2O + O_{CeO2} \quad (8)$$

where O_{CeO2} is the oxygen atom and O_{CeO2} oxygen vacancies at the surface of the CeO_2 support

In the second step, CO_2 acts as an oxidant for the partly reduced Au/CeO_2 catalyst surface shown in Eq. 9.

$$CO_2 + O_{CeO2} \rightarrow CO + O_{CeO2} \quad (9)$$

It is shown that it is possible to re-oxidize surface reduced Au/CeO_2 by exposing the catalyst to CO_2 via pulses. During this step,the surface oxygen from CO_2 will be removed. A quantitative relationship between CO uptake and formation of CO_2 is required. Due to high stability of active oxygen species, it was concluded that an active atomic oxygen species was formed. Indeed, these sites were generated in three steps: 1. adsorption, 2. activation and 3. dissociation of CO_2 on the surface oxygen vacancies created after CO reduction step [116]. A recent study by Bobadilla et al., performed transient and steady state *operando* DRIFTs to reveal the mechanism on Au/TiO_2 and Au/Al_2O_3. Au/Al_2O_3 shown to follow formate mechanism whereas Au/TiO_2 follows redox mechanism. The DRIFTs study performed on the catalyst showed the carbonate route was the main pathway to form gaseous CO. CO_2 is first adsorbed on the surface to form carbonates which reacts directly with the oxygen vacancies in the TiO_2 to form CO. Another novel characterization technique used to study the mechanism was *operando* UV–Vis spectroscopy which unraveled the role of TiO_2. The support can be reduced even in the absence of Au; thereby, creating the oxygen vacancy. However, the role of Au is to activate the hydrogen molecule for hydrogen spillover to occurs. The dissociated hydrogen atoms diffuse toTiO_2 support and generate more oxygen vacancies which increase the number of active sites for CO_2 to react, the schematic for the mechanism is shown in Fig. 6 [128].

Apart from noble metals such as Au, redox mechanism study was

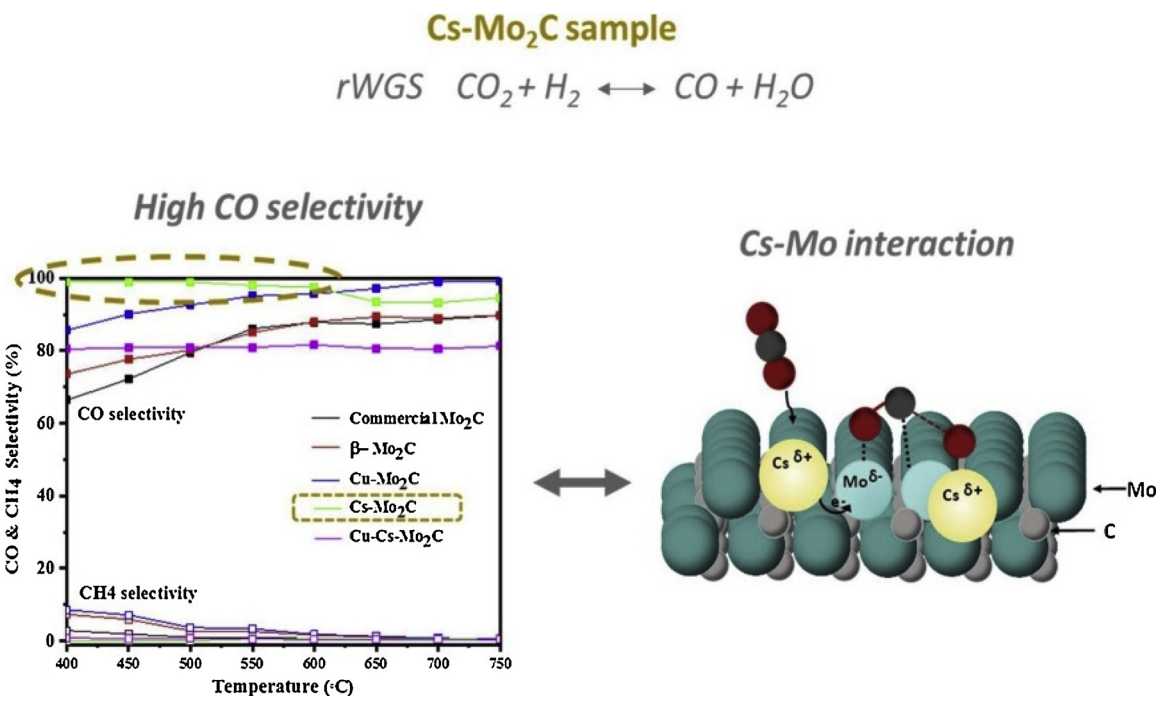

Fig. 5. Schematic showing the metal support interaction with reaction rate. [122].

Table 5
Reaction mechanism for RWGS reaction.

Redox Mechanism	Dissociative Mechanism
$CO_2(g) + * \rightarrow CO_2*$	$CO_2(g) + * \rightarrow CO_2*$
$H_2(g) + 2* \rightarrow 2H*$	$CO_2* + H* \rightarrow$ trans-COOH* + *
$CO_2* + * \rightarrow CO* + O*$	trans-COOH* → cis-COOH*
$O* + H* \rightarrow OH* + *$	cis-COOH* → CO* + OH*
$OH* + * \rightarrow O* + H*$	cis-COOH* → COH* + O*
$OH* + H* \rightarrow H_2O* + *$	$COH* \rightarrow CO* + H*$
$OH* + OH* \rightarrow H_2O* + O*$	$CO* \rightarrow * + CO(g)$
$H_2O* + O* \rightarrow OH* + OH*$	
$CO* \rightarrow * + CO(g)$	
$H_2O* \rightarrow * + H_2O(g)$	

also conducted for copper based catalysts active for reverse water gas shift reaction. In this type of active centers, CO_2 is first dissociated at metallic Cu atoms as an active sites and the reduction of the oxidized Cu catalyst was shown to be faster than the oxidation process [130,131], as shown in Eqs. 10 and 11.

$$CO_{2(g)} + 2Cu^{\circ}_{(s)} \rightarrow CO_{(g)} + Cu_2O_{(s)} \quad (10)$$

$$H_{2(g)} + Cu_2O_{(s)} \rightarrow H_2O_{(g)} + 2Cu^{\circ}_{(s)} \quad (11)$$

Gines et al. studied the role of H_2/CO_2 ratio on $CuO/ZnO/Al_2O_3$ based catalysts. The change in ratio shifts the reaction from first order in H_2 to first order in CO_2 by varying the pressure of the two gases [132]. The authors concluded that surface redox mechanism pathway is due to the presence of subsurface hydrogen trapped on the re-constructed copper surface caused by oxygen over-layer. This serves in making the surface more reactive to CO_2 adsorption [133]. Wang et al. [134] performed a DFT study on the structure sensitivity of reverse

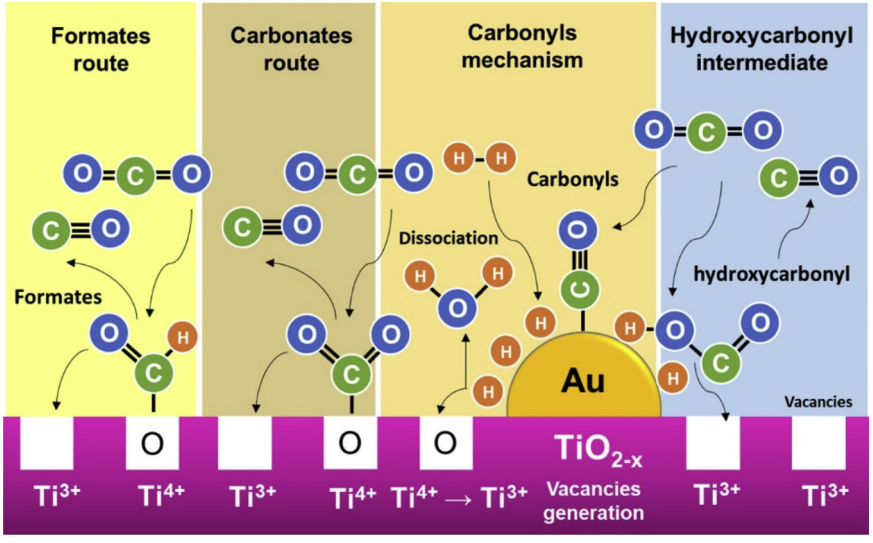

Fig. 6. Redox mechanism of the RWGS on Au/TiO_2 [129].

water gas shift considering Cu as a model for redox mechanism. The deviation for DFT calculation and experimental calculations was negligible which show the reproducibility of the proposed mechanism. From the analysis,it is concluded that the there is a difference between the virtual adsorption energy of atomic oxygen/strongly adsorbed species at the transition level which is important to account for the structure sensitivity reactions. Q. Zhang et al. also observed redox mechanism on Cu and Cs supported β- Mo_2C for RWGS reaction where the CO_2 dissociation occurs at the Cu° active sites and the presence of Cu^{+} stabilizes the intermediate formate species when formate mechanism is more dominant. And the presence of Cu^{+2} leads to the lower CO selectivity.

2.2.2.2. Dissociative mechanism. The dissociative mechanism includes the formation of several intermediates during the reaction, they are, formate, carbonates, and carbonyl. These intermediates are crucial for RWGS reaction. In a study done on Pt/Al_2O_3, a characterization techniques *in-situ* ATR-IRS study showed that RWGS reaction occurs at the sites of oxygen defects present on the thin surface of Al_2O_3 whcih leads to the formation of carbonate like species on the Pt sites. In next step, the CO_2 adsorbs on the oxygen vacancy of Al_2O_3 near the interface of Pt further reacting with H_2 to form CO. The formate mechanism postulates a bidentate formate reaction intermediate produced through the CO reaction with terminal hydroxyl groups over the oxide support. The intermediates formed decomposes to produce H_2 and also a monodentate carbonate was formed. On the other hand, copper based catalysts Cu, the formate species was derived from the association of H_2 and CO_2 which is a key intermediate for CO production. Another technique involving mass spectroscopy and diffuse reflectance Fourier transform infrared spectroscopy (DRIFTS) were used during the steady-state isotopic transient kinetic analysis (SSITKA) experiments to dynamically detect the surface species over Pt/CeO_2 catalyst [135]. By performing pulse-response TAP experiments, 1% CO_2 + 4% H_2 reaction mixtures containing isotopic CO_2 were introduced alternatively in a single reactor. Likewise, other metals such as Pd, Ni and Ru on Al_2O_3 showed the formation of carbonates on alumina support [136]. N. Ishito et al., investigated the mechanism on alumina supported Au catalyst. The DRIFTs analysis revealed that the formate species on Al_2O_3 decomposed to form CO at above 210 °C which suggests that the CO on Au nanoparticles supported on alumina was formed through the formate formation from CO_2 and H_2 [137].

Yet in another study [138], the RWGS mechanism on Pd/Al_2O_3 was studied using DRIFTS. The study showed that the surface species and their evolution patterns are comparable during transient and steady-state experiments. There was also no direct dissociation of observed CO_2, rather, the CO_2 first reacted with surface hydroxyls on the oxide support. The formed bicarbonates react with adsorbed hydrogen which dissociates on Pd particles to produce adsorbed formate species. Formates near the Pd particles rapidly reacts with adsorbed H to produce CO, which then adsorbs on the metallic Pd particles. In this analysis, it is found that there are two types of Pd sites available. The first site has a weak interaction with CO and the second site interacts more strongly with CO, and this site is reactive toward adsorbed H atoms on Pd leading eventually to CH_4 formation, as shown in Fig. 7.

2.2.2.3. Kinetic models. The reaction mechanism for reverse water-gas shift reaction proceeds through the similar mechanism as reported for water gas shift reactions. For this reaction, most of the kinetics study was based on Cu-based catalyst as an active metal sites via surface redox mechansim [130,139,140]. The reaction rate and rate limiting step varied with the reaction parameters. Ernst el al. provided a broad overview on the mechanistic aspects for reverse water gas shift and also developed a kinetic model for comparison between the rates over Cu (110) surface for direct comparison with the dissociative mechanism of CO_2 [141]. The results shows that the kinetics are strongly affected by the surface phase transition due to hydrogen surface coverage. Another study by Gines at al. also showed the similar surface kinetics over $CuO/ZnO/AI_2O_3$ catalyst where the rate limiting step was CO_2 dissociation step [132]. The study found that at high P^0_{H2}/P^0_{CO2} ratios, the rate is limited by the rate of dissociative CO_2 adsorption and with increase in CO_2 concentration, the rate of the reaction increases until it is first order with respect to CO_2. It was found that the hydrogen coverage drops below some critical OH value where the copper surface reconstructs to form less active phase. The rate constant diminishes and the reaction is then limited by the H_2 adsorption, becoming strongly positive order in hydrogen. Chen et al. studied the kinetics on copper nanoparticles supported on SiO_2 prepared by atomic layer epitaxy technique [130]. FTIR study was perfomed which showed that CO binding on the defect sites was not affected by the adsorption of CO_2 on the active sites. Two mechanisms were proposed - redox and formate mechanism. In the formate mechanism it was proposed that the CO was formed by the formate intermediate decompsition and the CO production increased with the increase in the concentration of formate species on copper. On the other hand, in the redox mechanism Cu^0 atoms provided active sites to dissociate CO_2, and the reduction was done by the presence of hydrogen gas as a reducing agent. The rate equation derived from the model is shown in Table 6.

E.L. Fornero et al. performed kinetics study on Cu/ZrO_2 and $Ga_2O_3/Cu/ZrO_2$ and the rate expressions were derived using Langmuir-Hinshelwood-Hougen-Watson formalism [142]. The experimental results were validated and further evaluated to perform the kinetics study. A reaction mechanism featuring the dissociative adsorption of H_2 and CO_2 on the metal sites, which further leads to the reaction of the hydrogen moiety (H-•) and atomic oxygen (O-•) on surface of the catalyst was derived. From this dissociative adsorption model it was found that the direct kinetic isotope effect was observed in the first minute of reaction where the CO evolution in the gas phase is non-linear and the surface reaction between atomic oxygen and hydrogen is considered as rate determining step. On the other hand, when the dissociative adsorption of CO_2 on Cu was rate determining step then the CO evolution in the gas phase followed linear zone. The simplified model correctly predicts that the rate of the RWGS reaction is almost independent of the total pressure. Based on the following step on the metal sites and CO_2 dissociation as the rate determining step, the kinetic model was derived as shown in Table 6.

$$CO_2 + 2^{\bullet} \leftrightarrow CO-\bullet + O-\bullet$$

$$H_2 + 2^{\bullet} \leftrightarrow 2H-\bullet$$

$$H-\bullet + O-\bullet \leftrightarrow HO-\bullet + \bullet$$

$$HO-\bullet + H-\bullet \leftrightarrow H_2O-\bullet + \bullet$$

$$H_2O-\bullet \leftrightarrow H_2O + \bullet$$

$$CO-\bullet \rightleftarrows CO + \bullet$$

S.S. Kim et al., examined the kinetic model based on the associative and redox mechanism for Pt/TiO_2 and Pt/Al_2O_3 [143]. Based on this model, the rate equations were derived and displayed in Table 6. The initial reaction rate from the two mechanisms was consistent with the experimental data under the low and high P_{H2} condition. However, only the initial reaction rate obtained from the surface redox mechanism under the moderate P_{H2} condition was consistent with the experimental results. The rate equation can be determined using the Power rate law expression to compare the reaction order and reaction rate constant k (Eq 12).

$$r_0 = k(P^0_{CO2})^{\alpha}(P^0_{H2})^{\beta} \quad (12)$$

where, r^0 represents the initial reaction rate [mol $CO_2\,h^{-1}\,gcat^{-1}$], k is the reaction rate constant [mol $CO_2\,h^{-1}\,gcat^{-1}\,atm-^{(\alpha+\beta)}$], and α and β represent the order depending on the partial pressure of CO_2 and H_2, respectively. The sum of the alpha and beta values of both Pt/TiO_2 and

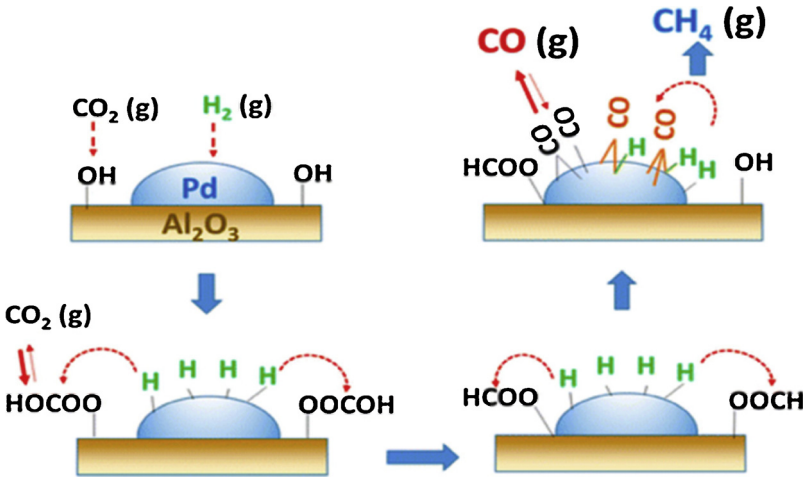

Fig. 7. The proposed reaction mechanism of RWGS reaction over Pd/ Al_2O_3 catalyst [138].

Table 6
Kinetic model/rate equation.

Catalyst	Rate model	Temp. range (°C)	Ref.
Cu/SiO_2	$r = 2^{1/2}k_4K_1^{1/2}K_2^{1/2}K_3P_{H2}^{1/2}P_{CO2}^{1/2}$ ● Rate Determining step: CO_2 dissociation, given as HCOO-2S → CO-S + OH-S ● The rate equation was derived from Langmuir Hinshelwood model	347-502 °C	[124]
$CuO/ZnO/ Al_2O_3$	$r = \frac{k1\,L0\,P0\,CO2\,[P0H2\,(1-X)2 - \frac{P^0_{CO2}}{K}X2]}{P0H2\,(1-X) + \sqrt{K2\,.\,P0H2\,.1.5(1-X)1.5} + P0CO2\,.\,X/K2\,.K3}$ ● Rate limiting step: CO_2 dissociation ● Kinetics is derived based on Langmuir Hinshelwood Model	230 °C	[126]
$Cu/ZrO_2$and $Ga_2O_3/Cu/ZrO_2$	$r = \frac{k1\,.P_{CO_2}\,[.]2Tol\left(1-\frac{P_{CO}P_{H_2O}}{P_{CO_2}P_{H2}K_{RWGS}}\right)}{\left(1+\frac{1}{K2\,.K3\,.K4\,.K5}\frac{P_{H_2O}}{P_{H_2}}\frac{P_{CO}}{K_6}+K_2^{0.5}P_{H_2}^{0.5}+\frac{P_{H_2O}}{K_5}+\frac{1}{K_2^{0.5}K_4K_5}\frac{P_{H_2O}}{P_{H_2}^{0.5}}\right)2}$ ● Rate determining step: Surface reaction between atomic oxygen and hydrogen. ● The kinetic rate expressions were obtained using Langmuir-Hinshelwood-Hougen-Watson formalism.	225 °C	[136]

Pt/Al_2O_3 catalysts was nearly 1, which means that the RWGS reaction for both catalysts was the first order. The reaction rate constant k for the Pt/TiO_2 catalyst was higher than for the Pt/Al_2O_3 catalyst.

According to the study performed for water gas shift reaction [144], the reaction order can differ when the products are not considered because the products act as an inhibitor of the forward reaction. Therefore, it was necessary to identify whether the products acted as an inhibitor in the RWGS reaction. The above Pt/TiO_2 catalyst was analyzed under the same conditions using the following expression.

$$r_0 = k(P^0_{CO2})^{\alpha}(P^0_{H2})^{\beta}\,(P^0_{CO})^{\gamma}\,(P^0_{H2O})^{\delta} \quad (13)$$

For the Pt/TiO_2 catalyst, $k = 0.057$, $\alpha = 0.794$, $\beta = 0.246$, $\gamma = -0.013$, $\delta = -0.014$. The rate constant and the reaction order of CO_2 slightly decreased and the reaction order of H_2O, and CO for the forward reaction had a negative value. These results mean that the products of the RWGS reaction act as an inhibitor. This inhibitor function was thought to be due to the effect of the surface coverage of active sites based on the similar reaction orders observed for the products H_2O and CO. However, these effects were relatively in-significant when compared with the inhibition in the existing reported WGS reaction.

3. CO_2 hydrogenation to methane and methanol

3.1. CO_2 methanation

In recent years, CO_2 hydrogenation to methane (CO_2 methanation) has gained considerable attention as one of the approaches to tackle CO_2-induced climate change and to satisfy high energy demands in today's world. The CO_2 hydrogenation to methane is advantageous over other chemicals in term of an existing distribution network because methane can be directly injected into the existing natural gas pipeline, so as to be promptly distributed or stored [145,146]. Additionally, CO_2 methanation is a simple and fast reaction, which can be operated under atmospheric pressure. Some studies have also reported an important breakthrough in the formation of CH_4 from CO_2 hydrogenation performed at (low) room temperature, in spite of very low conversion [147,148].

The production of CH_4 from CO_2 and renewable H_2, commonly referred as "Power to Gas" (PtG) concept, is a practical and convenient way to utilize excess electricity by converting it into methane as an energy storage intermediate. That is to say, hydrogen generated by water electrolysis, exploiting the excess electricity from renewable wind or solar energy, can react with CO_2 captured from emission sources to produce CH_4. Therefore, this CO_2 methanation reaction (so-called Sabatier reaction) is considered as a feasible process for the long term (chemical) storage of electricity [10,149,150].

CO_2 methanation is the reaction of one mole of carbon dioxide with four moles of hydrogen in which one mole of methane is obtained, represented by following reaction (Eq. 6):

$$CO_2 + 4H_2 \rightarrow CH_4 + 2H_2O \quad (6)$$

where $\Delta H_{298K} = -164\,kJ.mol^{-1}$, $\Delta G_{298K} = -114\,kJ.mol^{-1}$

CO_2 methanation is exothermic and spontaneous at room

Table 7
Summary of catalyst development for CO_2 methanation.

Catalyst	Preparation method	Reaction condition	CO_2 conversion (%)	CH_4 selectivity (%)	Remarks	Ref.
$Ce_{0.95}Ru_{0.05}O_2$	Solution combustion	At 450 °C and 1 bar	55	99	The Ru dopant facilitated the reduction of CeO_2, and the methanation reaction took place on the reduce $Ce_{0.95}Ru_{0.05}O_2$.	[155,184]
3 wt%Ru/Al_2O_3	Commercial catalyst	GHSV = 55,000 h^{-1}, at 400 °C and 1 bar	83	94	To reach full activity, 3%Ru/Al_2O_3 required on stream conditioning associated to impure chlorine cleaning. Conditioned Ru/Al_2O_3 catalyst retained stable and high activity after different cycles.	[185]
5 wt%Ru/CeO_2	Single-step flame spray pyrolysis	GHSV = 7640 h^{-1}, at 300 °C and 1 bar	83	99	CeO_2 showed a moderate Ru-CO coverage, which ensured the presence of H_2 dissociation sites, while the Ru-CO adsorption strength remained sufficiently high.	[186]
1 wt%$Rh/\gamma Al_2O_3$	Wet impregnation	CO_2 = 0.0833 kmol/s, H_2 = 0.0833 kmol/s and He = 0.83 kmol/s, at 25 °C and 1 bar	25	100	The amount of CH_4 produced depended on the temperature, pressure, presence or absence of gas promoters, like CO or O2, in the feed.	[148]
10wt%Ni/CeO_2	Wet impregnation	GHSV = 10,000 h^{-1}, at 350 °C and 1 bar	93	100	The excellent performance was attributed to large amounts of CO_2 adsorption, enhancement of CO_2 reduction to CO because of the oxygen vacancies and prompt conversion of CO to CH_4 over Ni/CeO_2.	[161]
5 wt%Ni/CeO_2-ZrO_2	Pseudo sol-gel	GHSV = 43,000 h^{-1}, at 350 °C and 1 bar	67.9	98.4	CO_2 conversion decreased by ~12% after 90 h.	[162]
10wt%Ni/CeO_2-ZrO_2	Ammonia evaporation (AE)	GHSV = 20,000 ml h^{-1} g^{-1}, at 275 °C and 1 bar	55	99.8	The excellent performance of Ni/CeO_2-ZrO_2 prepared by AE method was due to the ability to be activated at low temperature. It was also stable for nearly 70 h.	[100]
5 wt%Ni/MSN	Wet impregnation	GHSV = 50,000 mL h^{-1} g^{-1}, at 300 °C and 1 bar	64.1	99.9	The existence of both intra- and inter-particle porosity in Ni/MSN led to high concentration of basic sites and large amount of oxygen vacancy. The Ni/MSN catalyst performed with good stability and no deactivation up to 200 h.	[164]
10wt%Ni@MOF-5	Impregnation	GHSV = 2000 h^{-1}, at 320 °C and 1 bar	75.1	100	Ni was uniformly and highly dispersed over MOF-5. This catalyst showed high stability and almost no deactivation in long term stability tests up to 100 h.	[165]
35 wt%Ni-5 wt%Fe-Alumina xerogel	Single-step sol-gel	GHSV = 9600 mL h^{-1} g^{-1}, at 220 °C and 10 bar	63.4	99.5	35Ni5FeAX could provide the most optimal CO dissociation energy and retain the weakest metal-support interaction.	[171]
12wt%Ni-3 wt%Fe/Al_2O_3	Incipient wetness impregnation	GHSV = 50,000 mL h^{-1} g^{-1}, at 420 °C and 1 bar	84.3	100	The additive Fe could offer more suitable electronic environment and increase reducibility of Al_2O_3 supported Ni catalyst. This catalyst showed good stability over 150 h.	[172]
15 wt%Ni-5 wt%Co/ $Ce_{0.25}Zr_{0.75}O_2$	Coprecipitation with 5 wt% PEG-600 addition	GHSV = 10,000 h^{-1}, at 280 °C and 20 bar	85	98	The addition of Co could enhance the reduction capacity and improve the metal dispersion. After used at 320 °C for 12 h, CO_2 conversion of this catalyst slightly decreased (less than 10%).	[173]
Co_3O_4 nanorod	Co-precipitation	GHSV = 18,000 h^{-1}, at 230 °C and 10 bar	70	99	Co nanorods synthesized as Co_3O_4 precursor with preferential [148] facet exhibited considerably enhanced catalytic activity and CH_4 selectivity. Formate spectator species were inhibited via the formation of more active bridge CO as the reactive intermediate for CH_4 production.	[187]
20 wt%Co/KIT-6	Excess impregnation	GHSV = 22,000 mL h^{-1} g^{-1}, at 280 °C and 1 bar	48.9	100	Large surface area and high Co dispersion contributed to the high catalytic activities. The highly ordered, bicontinuous and mesoporous structure of Co/KIT also improved CH_4 selectivity.	[167]
CoNR/TiO_2	Modular synthesis to graft the support onto Co nanorods	GHSV = 18,000 mL h^{-1} g^{-1}, at 250 °C and 10 bar	57	100	CoNR/TiO_2 showed an increase in activity at low reaction temperatures due to the synergistic effect between Co and TiO_2, in which TiO_2 and Co catalyzed RWGS and subsequent CO hydrogenation, respectively.	[166]
$(Co_{0.95}Ru_{0.05})_3O_4$	Modified wet chemistry protocol	GHSV = 21,240 h^{-1}, at 420 °C and 1 bar	34.2	97.4	Doping Ru to cobalt oxide could lower light-off activity temperature and notably enhance CH_4 selectivity due to the formation of Co-Ru ultrathin film in the surface region.	[188]
Co-Al_2O_3 + 0.03 wt%Pt	Double flame spray pyrolysis	GHSV = 36,000 mL h^{-1} g^{-1}, at 400 °C and 1 bar	70	98	Only very low 0.03 wt% Pt content could lead to a significant improvement in Co_3O_4 reducibility and to high catalytic activity for CO_2 methanation.	[189]
3 wt%Ru-30 wt%Ni/ $Ce_{0.9}Zr_{0.1}O_2$		GHSV = 2400 mL h^{-1} g^{-1}, at 230 °C and 1 bar	98.2	100	The addition of Ru could improve Ni dispersion and basicity. Almost no deactivation for this catalyst was observed during 300 h.	[175]
	Deposition precipitation	GHSV = 9000 mL h^{-1} g^{-1}, at 380 °C and 1 bar	85.6	99.8		[179]

(*continued on next page*)

Table 7 (*continued*)

Catalyst	Preparation method	Reaction condition	CO_2 conversion (%)	CH_4 selectivity (%)	Remarks	Ref.
20 wt%Ni-20 wt%CeO_2/MCM-41					Due to synergetic effects, addition of CeO_2 could improve Ni dispersion and increase CO_2 adsorption sites. This catalyst could maintain its high reactivity after 30 h.	
15 wt%Ni-5 wt%La/Mg-Al	Urea hydrolysis	WHSV = 45,000 mL $h^{-1} g^{-1}$, at 250 °C and 1 bar	61	100	Addition of La could improve Ni dispersion, decrease Ni particle size and increase the amount of moderate basic sites. This catalyst exhibited stable activity at 400 °C during 150 h.	[181]
10wt%Ni-1 wt%MgO/SiO_2	Co-impregnation	GHSV = 15,000 mL $h^{-1} g^{-1}$, at 350 °C and 1 bar	> 67	> 98	Addition of MgO could enhance CO_2 adsorption capacity, accelerate CO_2 activation and suppress Ni sintering and oxidation. CO_2 conversion still maintained, while CH_4 selectivity slightly decreased after 50 h.	[182]

temperature, so high equilibrium conversion is predicted at low temperature between 25 °C and 400 °C. Nevertheless, kinetic barrier is still high although it is thermodynamically favorable, which retards the industrial applications [151,152]. Thus, the fundamental studies on the development of highly active and selective catalysts for CO_2 methanation is of great importance. Over the past decade, significant progress has been made on the catalyst support, metal and promoter, along with the attempts to gain good understanding of their roles in catalytic performance and reaction mechanism.

3.1.1. Catalysts for CO_2 methanation

3.1.1.1. Effect of active metal. CO_2 methanation can be catalysed by various metal-based catalysts including noble metals (Ru, Rh, Pt and Pd) and non-noble metals (Ni and Co). The catalytic performances of representative catalysts are summarized in Table 7.

Noble metals, particularly Ru and Rh, are very active even using low metal loading and operating at low temperature. Among noble metals, Ruthenium (Ru) is the most active catalyst for CO_2 methanation, followed by Rh, Pt and Pd, respectively [153]. This trend of the activity performance has been reported in several published literatures [10,152]. Over alumina-supported catalysts, Ru and Rh presented turnover numbers with two orders of magnitude higher than the other noble metals [154]. In the study of CO_2 methanation catalyzed by M-doped ceria (M = Ni, Co, Pd or Ru), best catalytic performance was obtained by $Ce_{0.96}Ru_{0.04}O_2$ and $Ce_{0.95}Ru_{0.05}O_2$ catalysts with 55% CO_2 conversion [155]. Ru as the dopant facilitated the reduction at lower temperature compared to pure CeO_2. It was found that methanation reaction took place on the reduced $Ce_{0.95}Ru_{0.05}O_2$. In term of CH_4 selectivity, the order for various metals may vary remarkably. Ru- and Rh-based catalysts have been found to be more selective to methane than Pt- and Pd-based ones, leading instead to high CO selectivity [156,157]. Similarly, $Ce_{0.95}Ru_{0.05}O_2$ catalyst exhibited maximum CH_4 selectivity of 99%, whereas $Ce_{0.98}Pd_{0.02}O_2$ catalyst predominantly catalyzed reverse water-gas shift (RWGS) and produced no methane [155]. On the contrary, the order of CH_4 selectivity analyzed and summarized from previously published literature is as follows: Pd > Pt > Ir > Rh > Ru [152]. Regarding the resistance to deactivation, noble metals have been reported to be more stable over a wide range of temperatures compared to non-noble metals due to less particle sintering and carbon deposits [145,158].

Albeit noble metal catalysts exhibit superior activity and CH_4 selectivity, their uses have been hindered due to scarce availability and high cost. Considering satisfactory catalytic performance, easy availability and low cost, Ni-based catalysts are thus the most widely used and studied for CO_2 methanation [146,159]. To date, myriad Ni-based catalysts have been developed and proposed as effective catalysts. Nevertheless, their performance in terms of activity, selectivity or stability still cannot outperform that of conventional catalyst when operating under real conditions. Typically, Ni-based catalysts are active at elevated temperature where CO_2 conversion is less thermodynamically favourable. Significant amount of CO may be also produced during CO_2 methanation at that rather high reaction temperature [160]. Additionally, Ni metals are prone to deactivation by sintering during the exothermic methanation reaction and by the formation of very stable Ni-carbonyl species, which block the active sites for CO_2 adsorption [149]. Researchers have devoted their effort to design more promising catalysts, that can be operated under the thermodynamically favorable conditions with good stability. It is well known that the catalytic performance greatly depends on the nature and properties of the support, and the synergy between the primary catalyst and promoter. These factors are further discussed in the next sections.

3.1.1.2. Effect of support. The most common investigated supports for CO_2 methanation are the metal oxides, including Al_2O_3, SiO_2, CeO_2, ZrO_2, TiO_2 and MgO. Tada et al. [161] investigated the effect of support materials (CeO_2, α-Al_2O_3, TiO_2 and MgO) on CO_2 conversion and CH_4

selectivity over Ni-based catalysts. Over the temperature range, Ni/CeO_2 provided highest CO_2 conversion, close to equilibrium value from 300 °C onward. Almost 100% CH_4 selectivity was also obtained by Ni/CeO_2. This excellent performance was attributed to large amounts of CO_2 adsorption, enhancement of CO_2 reduction to CO because of the oxygen vacancies and prompt conversion of CO to CH_4 over Ni/CeO_2. Ceria-zirconia mixed oxides have also become one of the potential supports for CO_2 methanation recently. Their high activity was strongly dependent on oxygen storage capacity and properties to active CO_2 [100,162]. The other set of supports (Al_2O_3, ZrO_2, TiO_2, SiO_2, Nb_2O_5) was also examined for supported Ni-Fe catalysts in CO_2 methanation by Pandey and Deo [163]. It was found that ability of the support to adsorb CO_2 affected the activity of supported catalysts. In this study, Al_2O_3 supported catalyst was the most active due to the maximum amount of CO_2 adsorbed, determined from CO_2-TPD. Aziz et al [164] also studied different types of support such as mesostructured silica nanoparticles (MSN), MCM-41, SiO_2, γ-Al_2O_3 and HY. The activity of CO_2 methanation trailed the following trend: Ni/MSN > Ni/MCM-41 > Ni/HY > Ni/SiO_2 > Ni/HY. The existence of both intra- and inter-particle porosity in Ni/MSN led to high concentration of basic sites and large amount of oxygen vacancy. The high basicity of Ni/MSN contributed to high adsorption of CO_2, while oxygen vacancies in MSN assisted the formation of surface carbon species, which further interacted with atomic hydrogen to form CH_4. Besides ordered porous structure, MSN possesses very high surface area in which Ni particles can disperse well. Likewise, metal-organic framework (MOF) materials with extremely high surface area have attracted significant attention as catalyst supports. At low temperature, notable enhancement of activity in CO_2 methanation could be achieved by highly uniform and well dispersed active metal in the framework of MOF [165]. Apart from Ni-based catalysts, Co nanorod catalysts with preferential [148] facet supported on different metal oxides, namely SiO_2, Al_2O_3 and TiO_2, were developed by Lauterbach [166]. In the kinetically controlled regime (150–250 °C), CoNR/TiO_2 exhibited superior catalytic activity due to the strong metal-support interaction and synergistic effect between Co and Ti, catalyzing RWGS and subsequent CO hydrogenation. In the mass/heat-transfer-controlled region (> 300 °C), CoNR/Al_2O_3 showed an increase in activity as a result of its great thermal conductivity.

Analyzing the effect of support on CO_2 methanation catalytic performance, the nature and properties of the support play a crucial role. In a nutshell, the key characteristics of effective catalysts are (i) ability to adsorb large amounts of CO_2, (ii) high oxygen storage capacity and ability to activate CO_2, (iii) the presence of oxygen vacancies, (iv) basic properties allowing CO_2 to adsorb on the support strongly and (v) porous structure with high surface area allowing active metal to disperse highly and uniformly. In number of studies, structure [167,168] and morphology [169] of the support and metal-support interaction [170] have also been tuned to achieve more active, selective and stable CO_2 methanation catalysts.

3.1.1.3. Effect of second metal / promoter. It has been also reported that the addition of a second metal can enhance the activity and stability of Ni-based catalysts. Hwang et al. [171] investigated the effect of second metal in CO_2 methanation over mesoporous Ni-M-Alumina xerogel (M = Fe, Zr, Y or Mg). An introduction of Fe to this catalytic system could provide the most optimal CO dissociation energy and retain the weakest metal-support interaction, leading to the highest CO_2 conversion and CH_4 yield. In the other study, additive Fe could offer more suitable electronic environment and increase reducibility of Al_2O_3 supported Ni catalyst, thus enhancing CO_2 methanation performance [172]. Co was also used as the second metal in CO_2 methanation. The presence of Co with appropriate amount in $Ce_xZr_{1-x}O_2$ supported Ni-Co bimetallic nano-catalysts could enhance the reduction capacity and improve the metal dispersion [173]. The synergistic effect between Co and Ni in Co-Ni bimetallic ordered mesoporous Al_2O_3 catalyst could also greatly enhance catalytic activity at low temperature by coordinating the activation of CO_2 and H_2, prominently decreasing CO_2 methanation activation energy [174]. Apart from Fe and Co, bimetallic Ni-noble metal catalysts also showed the enhancement in CO_2 methanation activity and stability [175–177].

As previously discussed, typical Ni-based catalysts prone to catalyst deactivation during CO_2 methanation. The addition of promoter has been one of the potential approaches to overcome this issue together with improving the activity. CeO_2 [178,179] and La_2O_3 [180,181] are commonly used rare earth oxides to promote Ni dispersion, strengthen metal-support interaction and restrain the growth of Ni nanoparticles. Among alkaline-earth metal oxides, MgO is frequently utilized as the promoter to intensify the adsorption and activation of CO_2 during CO2 methanation. MgO can also suppress Ni sintering and oxidation, boosting long-term stability [182,183].

3.1.2. Reaction mechanism and kinetics

3.1.2.1. CO_2 methanation mechanism. Although CO_2 methanation mechanism is still under debate, especially the nature of the intermediate species and steps involved, the reaction mechanism can be classified into two main categories in general, CO route and formate route [10,190]. On the first path, the conversion of CO_2 to carbonyl (CO_{ad}) takes place, followed by the reaction of CO_{ad} with H_2 to form CH_4. Throughout the literatures, formation mechanism of CO_{ad} as the intermediate species can be via either the dissociation of CO_2 to CO_{ad} and O_{ad} or the decomposition of formate ($HCOO_{ad}$) species. On the second path, formate species is the main intermediate without formation of CO_{ad} observed during the reaction. The nature of active metal, the typology of the support and the reaction conditions have been found to affect the reaction mechanism strongly. Numerous studies have attempted to get a better insight into CO_2 methanation mechanism through the utilization of the *in-situ* or *operando* IR spectroscopy technique [149,191]. By doing so, the evolution of the surface species can be monitored during the methanation reaction.

Jia et al. [192] performed *operando* diffuse reflectance infrared Fourier transform spectroscopy (DRIFTS) over Ni/ZrO_2 prepared by plasma-assisted impregnation (Ni/ZrO_2-P) and Ni/ZrO_2 prepared by conventional incipient wetness impregnation (Ni/ZrO_2-C) (Fig. 8). The role of Ni active sites on both catalysts is to dissociate gaseous H_2 into H atoms. CO route is proposed for CO_2 methanation on Ni/ZrO_2-P, in which CO_2 is converted to bidentate bicarbonates and monodentate carbonate through the reaction with hydroxyl (OH) groups and adsorbed O^{2-}, respectively. Bidentate bicarbonate and monodentate carbonate are then reacted with H atoms to generate bidentate and monodentate formates. The decomposition of formates leads to the observation of adsorbed CO, which is sequentially hydrogenated to produce CH_4. In contrast, formate route is postulated on Ni/ZrO_2-C due to no carbonyl species observed during DRIFTS experiments. Gaseous CO_2 reacts with OH groups, forming the adsorbed bidentate bicarbonates and subsequent bidentate formates as the main intermediate. Formates are then converted to methoxy prior to the hydrogenation of methoxy (OCH_3) and the formation of CH_4.

As mentioned earlier, carbonyl species can also be formed via CO_2 dissociation. Aziz et al. [193] presented the plausible mechanism of CO_2 methanation on metal-promoted mesostructured silica nanoparticles (MSN). In Fig. 9, adsorbed CO_2 and H_2 on active metal sites dissociate to CO, O and H atoms, which migrate onto the surface of MSN. Carbonyl species are formed through the reaction of CO with oxide surfaces along with the formation of bidentate formate through the interaction with H atom. Concurrently, the reaction between the adsorbed oxygen and H atom forms hydroxyl, becoming H_2O when reacting with another H atom. The bridged carbonyl and bidentate formate are further hydrogenated to produce CH_4.

In other works, the intermediate species and steps involved in the reaction pathway may differ depending on the catalytic system. Wang et al. [194] revealed the formate route for CO_2 methanation over the Ru/CeO_2 catalyst through the steady-state isotope transient kinetic

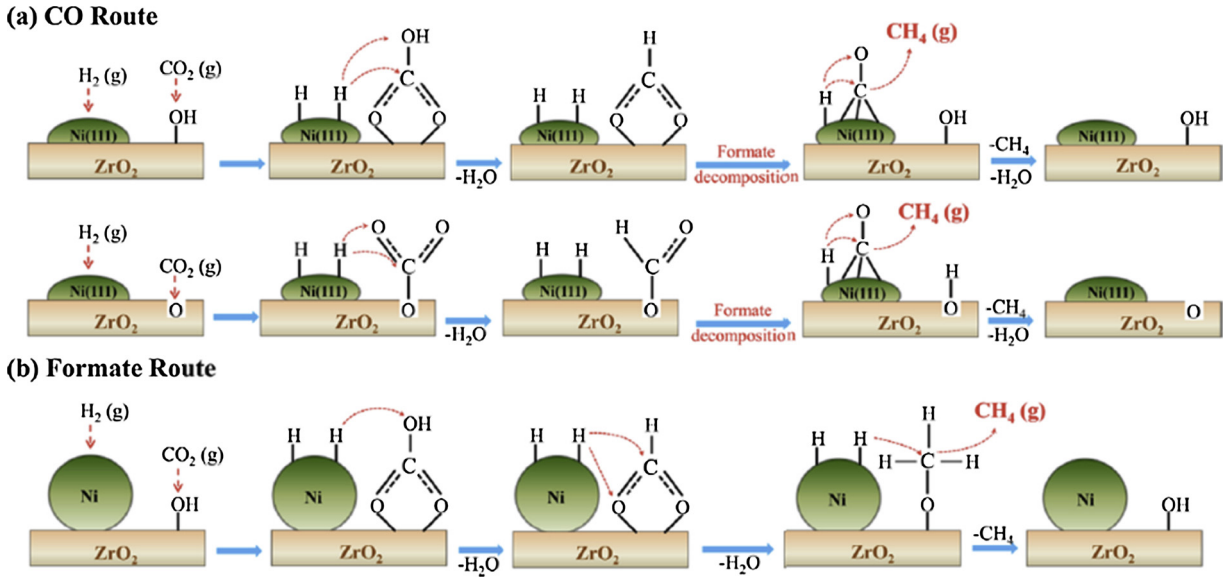

Fig. 8. Proposed pathway for CO_2 methanation over (a) Ni/ZrO_2-P and (b) Ni/ZrO_2-C. [192].

analysis (SSITKA)-type *in-situ* DRIFTS. First, CO_2 is mainly converted to carboxylate ($CO_2^{\delta-}$),likely due to the presence of Ce^{3+} as Lewis base. Formate, as the key intermediate, is then produced from $CO_2^{\delta-}$ hydrogenation assisted by atomic hydrogen in surface OH groups on CeO_2. Oxygen vacancy on CeO_2 surface further catalyzes formate dissociation to methanol, which is easily hydrogenated to CH_4. In the catalytic system of Ru-substituted CeO_2 for CO_2 methanation, Sharma and co-workers [184] observed formation of carbonates and CO intermediates with no role of formate. Based on the results from TPR, *in-situ* DRIFTS and DFT, the following CO_2 methanation pathway over $Ce_{0.95}Ru_{0.05}O_2$ was postulated: $CO_2 \rightarrow CO \rightarrow OCH_2 \rightarrow OCH_3 \rightarrow CH_4$.

3.1.2.2. Kinetic models. Empirical and mechanistic kinetic models have also been developed by conducting the kinetics experiments over a wide range temperatures and concentrations. Considering CO_2 methanation on Ru-based catalysts, literatures mainly reported power-law empirical equations [158,195], although some mechanistic equations are available [196]. The overview of kinetic models on Ru-based catalysts listed by Falbo et al. [158] indicated that the reaction rate has a dependence on H_2 partial pressure (reaction orders (n) in the range 0.3–2.5) stronger than on CO_2 (reaction order 0–1) at low CO_2 conversion values.

The recent study by Miguel et al. well described the reaction mechanism and kinetics of CO_2 methanation over Ni-based catalysts [197]. On one hand, Weatherbee and Bartholomew [198] proposed one of the

Table 8
List of elementary steps in CO_2 methanation mechanism.

CO intermediate mechanism	Formate intermediate mechanism
Dissociation of CO* to C* and O* as RDS	Reaction between CO_2* and H* as RDS
1 $H_2 + 2^* \rightleftharpoons 2H^*$	19. $H_2 + 2^* \rightleftharpoons 2H^*$
2 $CO_2 + 2^* \rightleftharpoons CO^* + O^*$	20. $CO_2 + ^* \rightleftharpoons CO_2^*$
3 $CO^* \rightleftharpoons CO + ^*$	21. $CO_2^* + H^* \rightleftharpoons HCOO^* + ^*$ (RDS)
4 $CO^* + ^* \rightleftharpoons C^* + O^*$ (RDS)	22. $HCOO^* + H^* \rightleftharpoons HCO^* + OH^*$
5 $C^* + 4H^* \rightleftharpoons CH_4^* + 4^*$	23. $HCO^* + H^* \rightleftharpoons CH^* + OH^*$
6 $CH_4^* \rightleftharpoons CH_4 + ^*$	24. $CH^* + 3H^* \rightleftharpoons CH_4 + 4^*$
7 $O^* + H^* \rightleftharpoons OH^* + ^*$	25. $OH^* + H^* \rightleftharpoons H_2O + 2^*$
8 $OH^* + H^* \rightleftharpoons H_2O^* + ^*$	Formation of hydrogen carbonate as RDS
9 $H_2O^* \rightleftharpoons H_2O + ^*$	26. $H_2 + 2^* \rightleftharpoons 2H^*$
Formation of formyl species as RDS	27. $H^* + O^* \rightleftharpoons OH^* + ^*$
10 $H_2 + 2^* \rightleftharpoons 2H^*$	28. $CO_2 + O^* \rightleftharpoons OCO_2^*$
11 $CO_2 + 2^* \rightleftharpoons CO^* + O^*$	29. $OCO_2^* + OH^* \rightleftharpoons OCOOH^* + O^*$ (RDS)
12 $CO^* + H^* \rightleftharpoons CHO^* + ^*$ (RDS)	30. $OCOOH^* + H_2 \rightleftharpoons OCOH^* + H_2O$
13 $CHO^* + ^* \rightleftharpoons CH^* + O^*$	31. $OCOH^* + H_2 \rightleftharpoons OCH_2OH^*$
14 $CH^* + 3H^* \rightleftharpoons CH_4^* + 3^*$	32. $OCH_2OH^* + H_2 \rightleftharpoons OCH_3^* + H_2O$
15 $CH_4^* \rightleftharpoons CH_4 + ^*$	33. $OCH_3^* + H_2 \rightleftharpoons CH_4 + OH^*$
16 $O^* + H^* \rightleftharpoons OH^* + ^*$	
17 $OH^* + H^* \rightleftharpoons H_2O^* + ^*$	
18 $H_2O^* \rightleftharpoons H_2O + ^*$	

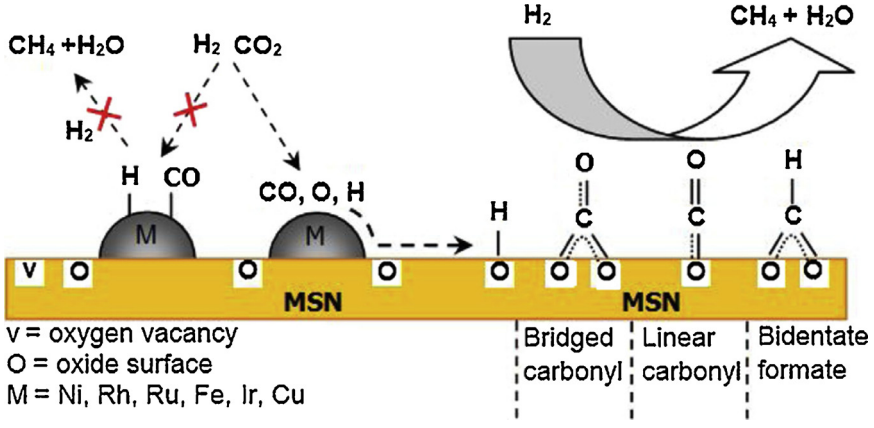

Fig. 9. Plausible mechanism of CO_2 methanation on M/MSN [193].

most comprehensive kinetic studies on the Sabatier process using Ni/SiO_2 catalyst in a single-pass differential fixed-bed reactor at low pressure. Through the CO intermediate mechanism, the elementary steps are presented as steps 1–9, Table 8, assuming dissociation of CO* to C* and O* as the rate determining step (RDS) (step 4, Table 8). Koschany et al. [199] also proposed CO route mechanism, in which adsorbed CO obtained from CO_2 dissociation reacts with atomic hydrogen to form formyl species instead on a co-precipitated $NiAl(O)_X$ (steps 10–18, Table 8). Step 12 in Table 8 is assumed to be the rate determining step. On the other hand, Ibraeva et al. [200] studied the kinetics of CO_2 hydrogenation to CH_4 over NKM-4A nickel-containing catalyst and derived the kinetic equation involving a formate intermediate without preliminary dissociation of CO_2 to CO* and O*. The elementary steps are shown as steps 19–25 in Table 8 with the assumption that the reaction between adsorbed CO_2 and atomic hydrogen is the rate determining step. The reaction mechanism involving the formation of formate intermediate was also proposed with different elementary steps, in which the formation of hydrogen carbonate is assumed to be the rate determining step (steps 26–32 in Table 8) [201].

The form of kinetic rate expressions is typically determined from derivation of Langmuir-Hinshelwood/ Eiley-Rideal based on the reaction mechanism. The derived kinetic rate equation is ultimately fitted to the experimental rate data. These commonly used/ recently reported kinetic expressions from the literatures are listed in Table 9.

3.2. CO_2 hydrogenation to methanol route

The methanol economy concept has been championed by Nobel Laureate, George Olah, as a sustainable and more feasible mean to address the limitations of a full hydrogen economy since a full hydrogen economy requires immense amount of energy to obtain hydrogen through methane steam reforming and electrolysis of water [202]. The means of sustainable hydrogen production are beyond the scope of current discussion in this review, but CO_2 recycling has been proposed as a sustainable mean to convert CO_2 into industrially useful products. Current technology route for methanol production is via syngas conversion whereby CO is hydrogenated to form methanol and water (Eq. 14) at elevated pressure and moderate temperature. The uses of methanol as a valuable chemical product or intermediate are numerous. Methanol can be directly as a solvent and used as an additive product to gasoline though the energy density of methanol is half the volumetric density of gasoline and diesel. Methanol can also be used as a feed to fuel cell to generate electricity by oxidation with air. Methanol can be converted into olefins and gasoline as a chemical intermediate.

$$CO + 2H_2 \leftrightarrow CH_3OH;\ \Delta H_{298K} = -90.6\ kJ/mol \quad (14)$$

For the CO_2 recycling route, CO_2 is hydrogenated into methanol (Eq. 15). CO and H_2O are formed via reverse water gas shift reaction which is considered as a side reaction.

$$CO_2 + 3H_2 \leftrightarrow CH_3OH + H_2O;\ \Delta H_{298K} = -49.5\ kJ/mol \quad (15)$$

From the thermodynamic perspective, Eq. 14. is more exothermic and thermodynamically favoured which is the main reason for widespread industry syngas conversion to methanol. However, it can be noted that Eq. 15 is also thermodynamically favoured as well. It is evident from Eqs. 14 and 15, according to Le Chatelier's principle, the operating conditions for selective methanol production from CO_2 should be conducted at lower temperature and high pressure. Thus, the designed catalyst must be highly active and selective towards methanol production at lower temperature. With a highly active and more selective catalyst, smaller reactor size can be attained. Discussion of reactor design and concept is beyond the scope of this review. The designed catalyst must be stable for long period of time for minimal downtime from replacing depleted catalysts.

3.2.1. Catalysts for CO_2 hydrogenation to methanol

3.2.1.1. Copper-based catalyst for CO2 hydrogenation to methanol. In the early years of commercial methanol synthesis from syngas conversion, $ZnO\text{-}Cr_2O_3$ mixed oxide catalyst were developed for high temperature of 400 °C and high pressure of 300–400 at m by BASF. In the next step to develop highly active catalyst for methanol production at lower temperature and lower pressure, Imperial Chemical Industry (ICI) discovered Cu-Zn-Al catalyst which was prepared using co-precipitation method and found to be active for methanol synthesis

Table 9
Summary of kinetic expressions reported in the literatures for CO_2 methanation.

Kinetic rate equation	Catalyst	Ref.
$r_{CO_2} = k\left\{[P_{CO_2}]^n[P_{H_2}]^{4n} - \frac{[P_{CH_4}]^n[P_{H_2O}]^{2n}}{[Keq]^n}\right\}$	0.5 wt.% Ru/Al_2O_3	[158,195]
$r_{CH_4} = \frac{k\,P_{CO_2}^{0.5}P_{H_2}^{0.5}}{\left(1 + K_1\frac{P_{CO_2}^{0.5}}{P_{H_2}^{0.5}} + K_2P_{CO_2}^{0.5}P_{H_2}^{0.5} + K_3P_{CO}\right)^2}$ when the most abundant surface intermediates are CO* and O*. RDS: CO* + * ⇌ C* + O*	3 wt.% Ni/SiO_2	[198]
$r_{CH_4} = \frac{kP_{CO_2}^{0.5}P_{H_2}^{0.5}\left(1 - \frac{P_{CH_4}P_{H_2O}^2}{P_{CO_2}P_{H_2}^4Keq}\right)}{\left(1 + K_{OH}\frac{P_{H_2O}}{P_{H_2}^{0.5}} + K_{H_2}P_{H_2}^{0.5} + K_{mix}P_{CO_2}^{0.5}\right)^2}$ when the most abundant surface intermediates are CO*, H* and OH*. $r_{CH_4} = \frac{kP_{CO_2}^{0.5}P_{H_2}^{0.5}\left(1 - \frac{P_{CH_4}P_{H_2O}^2}{P_{CO_2}P_{H_2}^4Keq}\right)}{(1 + K_{H_2O}P_{H_2O} + K_{H_2}^{0.5}P_{H_2}^{0.5} + K_{mix}P_{CO_2}^{0.5})^2}$ when H_2O is one of the most abundant surface intermediates instead of OH*. RDS: CO* + H* ⇌ CHO* + *	$NiAl(O)_x$	[199]
$r_{CH_4} = \frac{k\,P_{H_2}^{0.5}P_{CO_2}}{P_{H_2}^{0.5} + KP_{CO_2}}$ RDS: CO_2* + H* ⇌ HCOO* + *	NKM-4A nickel-containing catalyst	[200]
$r_o = \frac{kK_3K_1^{0.5}K_2P_{CO_2}P_{H_2}^{0.5}}{(1 + K_1^{0.5}K_2P_{H_2}^{0.5} + K_2P_{CO_2})^2}\{[O*](1 + K_3P_{CO_2} + K_1^{0.5}K_2P_{H_2}^{0.5})\}^2$ where O* refers to the surface oxygen active site, and when the most abundant surface intermediates are OCO_2* and OH*. RDS: OCO_2* + OH* ⇌ OCOOH* + O*	Ce-Ni catalyst modified with g-C_3N_4	[201]

Table 10
Summary of recent developments for CO_2 hydrogenation to methanol catalysts.

Catalyst	Synthesis method	Reaction conditions	Catalyst performance (CO_2 conversion and methanol yield)	Remarks	Ref.
Cu/Zn/Cr/Al	Gelation method	T = 250 °C P = 50 atm	CO_2 conversion = 10.5% Methanol yield = 176 g/L.h	Gelation method was found to result in better methanol yield and CO_2 conversion than other catalyst	[203]
Cu/Zn/Cr/Al/Pd	Gelation method	T = 250 °C P = 50 atm SV = 4700 h^{-1}	CO_2 conversion = 21.2% Methanol yield = 356 g/L.h	Pd was proposed to induce hydrogen spillover which resulted in higher methanol yield and CO_2 conversion	[203]
$CuO/ZnO/Al_2O_3$	Oxalate gel co-precipitation method	T = 240 °C P = 10 atm SV = 3600 ml/g_{cat}.h		The methanol GC area for the oxalate gel method was more than conventional co-precipitation method	[204]
Cu/ZnO/ Al_2O_3	Oxalate gel co-precipitation method	T = 240 °C P = 20 atm SV = 10,000 h^{-1} CO_2/H_2 = 1/3	CO_2 conversion = 16.8% Methanol yield = 4.35 mmol/ml.h	Copper surface area does not seem to correlate with catalytic activity. The methanol yield for the oxalate method is higher than for conventional co-precipitation method	[204]
$Cu/ZnO/ZrO_2$	Oxalate co-precipitation (ethanol as solvent)	T = 240 °C P = 20 atm SV = 7800 h^{-1} CO_2/H_2 = 1/3	CO_2 conversion = 13.1% Methanol yield = 4.90 mmol/ml.h	Formation of disordered and isomorphous precursors lead to very fine Cu/ZnO/ZrO which lead to optimum catalytic performance.	[206]
$Cu@ZnO_x$	Surface modification precipitation	T = 250 °C P = 30 atm SV = 18,000 h^{-1} CO_2/H_2 = 1/3	CO_2 conversion = 2.3% Methanol yield~4.50 mol/kg.h	Migration of zinc to decorate Cu nanoparticle and increase Cu-ZnO interfacial area is beneficial to methanol formation	[207]
$Cu-ZnO/ZrO_2$	Ultrasound irradiation precipitation	T = 200-240 °C P = 10-30atm GHSV = 4400 L/kg_{cat}.h	CO_2 conversion~2.5% Methanol selectivity~100%	Optimum modification through ZnO loading on Cu nanoparticle can result in higher TOF but too much ZnO loading can bond intermediates too strongly. Al_2O_3 affinity to water is higher than ZrO_2 which results in lower TOF	[208]
$Cu/ZnO/ZrO_2/Al_2O_3$ (promoted with SiO_2)	Conventional co-precipitation	T = 200-240 °C P = 50 atm SV = 10,000 h^{-1} CO_2(6-22%)/CO(3-25%)/H_2(69-75%)	STY~1780gCH_3OH/kg_{cat}.h	Catalytic activity of unpromoted catalyst decreases by 10% in 40 hrs while catalyst promoted with SiO_2 maintained catalytic activity for 500hrs	[209]
Cu/tetragonal ZrO_2 Cu/monoclinic ZrO_2	Citric acid complexation Co-precipitation using ammonia solution	T = 180-260 °C P = 80 atm SV = 3600 h^{-1} CO_2/H_2 = 1/3	CO_2 conversion = 7.8% Methanol selectivity~100%	Tetragonal ZrO_2 contains higher amount of lewis acid sites which contributes to higher methanol yield	[211]
Cu/ZnO(Pd promoted)	One-pot polyol method	T = 230-290 °C P = 45 atm SV = 10,800 h^{-1} CO_2/H_2 = 1/3	CO_2 conversion~9.0% Methanol selectivity~73%	Pd doped catalyst exhibited higher methanol yield by 2.5timesand methanol TOF by 3.5 times as compared to undoped catalyst due to hydrogen spillover	[214]
Pd/ZnO	Sol-immobilization method	T = 250 °C P = 20 atm V = 30 ml/min CO_2/H_2 = 1/3	CO_2 conversion = 10.7% Methanol selectivity = 60% Methanol formation rate = 2420 mmol/kg_{cat}.h	Formation of PdZn alloy is beneficial for methanol formation	[215]
In_2O_3 In_2O_3/ZrO_2	Co-precipitation	T = 300 °C P = 50 atm SV = 16,000 h^{-1} CO_2/H_2 = 1/4	STY~0.33gCH_3OH/g_{cat}.h for 1000 h Methanol selectivity~100%	In_2O_3/ZrO_2 catalyst maintained stable catalytic performance for 1000hrs	[218]

via syngas conversion. However, the same catalyst was found to exhibit poor activity for CO_2 hydrogenation to methanol [203]. Different preparation method for Cu/Zn catalyst were explored to enhance CO_2 conversion and methanol yield [204]. Inui and co-workers utilized gelatine method to prepare Cu/Zn/Cr mixed oxide catalyst which exhibited better CO_2 conversion as compared to the Cu/ZnO catalysts [203] Deng et al. used oxalate co-precipitation method to prepare very small Cu and ZnO nanoparticles which exhibited higher CO_2 conversion and higher methanol yield than the one prepared by co-precipitation method [205]. Solvent, especially one with small surface tension and high viscosity, for the oxalate co-precipitation method was found to enhance isomorphous substitution which resulted in smaller Cu and ZnO nanoparticle size [206].

Cu@ZnO core shell catalysts had been developed in recent years to enhance the synergy between Cu and ZnO [207]. However, the methanol yield and CO_2 conversion suffers when the Cu/ZnO components are on Al_2O_3 support as Al_2O_3 has higher affinity for water adsorption which can decrease methanol yield by driving the equilibrium towards the reactant (CO_2 and H_2) side and greater wetting of the catalyst surface [208]. Furthermore, water had been reported to induce crystallization of ZnO which enhanced metal sintering and hastened catalyst deactivation over time but the addition of Si could suppress crystallization and enhance catalyst stability [209].

Amenomiya demonstrated that Cu/ZrO_2 prepared via co-precipitation method could be potentially better than of Cu/ZnO catalysts. Water affinity for ZrO_2 is lower than that of Al_2O_3 and so water wetting of the zirconia (ZrO_2) surface is lower [210]. In that study, there appeared to be no relationship between copper surface area and methanol yield. Copper on the zirconia surface consists of a mixture of Cu^0, Cu^{2+} cation and Cu hydroxide. The incorporation of Cu^+ or Cu^{2+} into ZrO_2 lattice compensates for the negative charge generated by oxygen vacancies and stabilizes tetragonal ZrO_2 which generates Lewis acidic Zr^{4+} cation to enhance methanol formation [211]. The Lewis acid contribution from Zr^{4+} around the Cu interface are highly likely to be the active sites for methanol synthesis which may enables CO_2 activation and hydrogenation of the surface intermediates [212].

Metallic Cu has been proposed as the metal centre for hydrogen spill-over to occur. Hydrogen spill-over is a catalytic phenomenon whereby adsorbed H_2 is first dissociated on metallic centre and diffuse onto the catalyst support to enhance metal reducibility through the

creation of more active sites. [213]. To further enhance hydrogen spillover effect for higher methanol yield, Pd can be doped to maintain the reduced state of Cu and create strong interaction between Pd and Cu surfaces which reduces the activation energy for CO_2 hydrogenation to methanol [214] If Cu is absent, Pd may form bimetallic alloy with Zn and stabilize reaction intermediate for methanol formation [215]. The presence of chlorine impurities from doping Pd may induce metal sintering during the reaction.

3.2.1.2. Indium-based catalyst for CO_2 hydrogenation to methanol. The emergence of Indium-based catalyst had gained increasing traction in recent years for CO_2 hydrogenation. Lorenz et al. had reported almost 100% CO_2 selectivity in methanol steam reforming using pure indium oxide (In_2O_3) which was attributed to facile replenishment of oxygen vacancies by CO but not CO_2 [216]. Such intriguing redox property leads to more experimental studies which shows that In_2O_3 is highly selective towards CO_2 and less selective towards CO production via RWGS reaction. This made In_2O_3 an attractive material for methanol synthesis via CO_2 hydrogenation. DFT study had predicted that In_2O_3 might be unselective towards RWGS but selective towards methanol synthesis via CO_2 hydrogenation [217]. Based on the prediction made by the DFT study, Oliver et al. prepared a series of In_2O_3 supported on various catalyst support and found that the one supported on ZrO_2 exhibited superior methanol selectivity (100% methanol selectivity) and very stable catalytic performance for over 1000 h under industrial reaction conditions which was better than commercial Cu/ZnO catalyst [218]. The nascent development of In_2O_3 catalyst for methanol synthesis via CO_2 hydrogenation is a positive demonstration of combining experimental studies with computational simulation to achieve quantum leap in methanol yield and highly stable catalytic performance. Table 10 shows some representative catalysts reported in recent years and their performance in CO_2 hydrogenation to methanol.

3.2.2. Reaction mechanism and kinetics

The concept of adsorption kinetic in heterogeneous catalysis introduced by Irwin Langmuir and applied by Sir Cyril Hinshelwood, Sir Eric Rideal and Michel Boudart had been extremely useful in describing reaction mechanism and enhancing mechanistic understanding for many decades. Clear mechanistic understanding had enabled many researchers to develop new and improved catalyst with higher reaction rate and higher product selectivity. In conjunction with clear mechanistic understanding, an awareness of the state of the catalyst surface under working condition had to be developed. In the past decades, the reaction mechanism behind CO_2 hydrogenation to methanol and the working of the metal components were relatively unclear. However, with the emergence of DFT for *ab-initio* modelling and practical application of *in-situ* and *operando* spectroscopy techniques, FTIR, XAS and NMR, for experimental evaluation of the reaction intermediates on the catalyst surface, clearer picture of the working state of the catalyst surface and reaction mechanism begin to emerge [219–223].

In the formate route, CO_2 and H_2 is predicted to adsorb and dissociate on the catalyst surface. Bifunctional Langmuir-Hinshelwood reaction mechanism is generally well-accepted for the initial adsorption of CO_2 and H_2 (Table. 11) [224,225]. In Figs. 10 and 11, the adsorbed species combine to form carbonate and bicarbonate species which will be hydrogenated to form formate specie (HCOO*). The presence of these carbonate and bicarbonate intermediates are detected using *in-situ* infra-red (IR) spectroscopy [224,226]. Hydrogenation of HCOO* will lead to the formation of methoxy specie (CH_3O*). CH_3O* will be subsequently hydrogenated to form methanol [226,227]. Hydrogenation of methoxy (CH_3O*) is predicted to be the rate-limiting step by microkinetic modelling and DFT simulation while formation of HCOO* and H* species are fast [227–229]. Isotopic exchange experiments between H_2 and D_2 with $H^{13}COO$* specie present on Cu/ZrO_2 catalyst surface reveals the formation of methoxy specie is slower than the H/D exchange of formate specie which provide strong evidence for

Table 11
Kinetic models for CO_2 hydrogenation to methanol via formate route.

Catalyst	Kinetic model	Ref.
Cu/ZnO/ Al_2O_3/ ZrO_2	$r_c = \frac{k_c K_{CO_2} K_{H_2} K_{CHCO_2} \left(P_{CO_2} P_{H_2}^{3} - \frac{P_{CH_3OH} P_{H_2O}}{K_{PC}}\right) / P_{H_2}^{2}}{(1 + K_{H_2}^{0.5} P_{H_2}^{0.5} + K_{H_2O} P_{H_2O})(1 + K_{CO_2} P_{CO_2})}$ Rate-limiting step: Formate hydrogenation (HCO_2.s_3 + H.s_2→ H_2CO_2.s_3 + s_2) Formate species as the reactive intermediate where s_2 is the active site for hydrogen adsorption and s_3 is Cu^0	[228]
Cu/ZnO/ Al_2O_3	$r_{MeOH} = \frac{k'_{5a} K'_2 K_3 K_4 K_{H_2} P_{CO_2} P_{H_2} \left[1 - \left(\frac{1}{K^*}\right)\left(\frac{P_{H_2O} P_{CH_3OH}}{P_{H_2}^{3} P_{CO_2}}\right)\right]}{\left(1 + \left(\frac{K_{H_2O}}{K_8 K_9 K_{H_2}}\right)\left(\frac{P_{H_2O}}{P_{H_2}}\right) + \sqrt{K_{H_2} P_{H_2}} + K_{H_2O} P_{H_2O}\right)^{3}}$ Rate-limiting step: Formate hydrogenation (HCO_2.s + H.s→ H_2CO_2.s + s) Formate species as the reactive intermediate	[237]
Cu/ZnO/ Al_2O_3& Cu/ ZnO/ ZrO_2	$r_3 = k_3 b_{CO_2} \left\{ \frac{P_{CO_2} P_{H_2}^{\frac{3}{2}} - \frac{P_{CH_3OH} P_{H_2O}}{P_{H_2}^{\frac{3}{2}} K_3}}{(1 + b_{CO} P_{CO} + b_{CO_2} P_{CO_2}) \left[P_{H_2}^{\frac{1}{2}} + \left(\frac{b_{H_2O}}{b_{H_2}^{\frac{1}{2}}}\right) P_{H_2O}\right]} \right\}$	[238]

hydrogenation of methoxy specie as the rate-limiting step [226,227]. HCOO* intermediate is probably located on the Cu/Zr interface [212,224,226]. However, there are other conflicting evidence in the form of kinetic isotopic effect (KIE) studies over Cu/ZnO catalyst that also strongly suggest that hydrogenation of formate is the rate-limiting step instead [229,230]. The differing evidence may be due to the difference in catalyst surface for the mechanistic investigation as well as different reaction conditions which might be worthy of further investigation.

The role of Cu was found to be a centre for adsorptive of dissociation of H_2 for enhanced hydrogenation of HCOO* and CH_3O* through *in-situ* IR spectroscopy [224]. Larger Cu nanoparticle size is found to be beneficial for methanol synthesis activity to a certain extent and the Cu/ZnO catalyst perform better than pure Cu and Cu silicate catalysts due to strong metal-support interaction by ZnO [232]. Fujitani et al. observed that the methanol TOF increased with the Zn content which was attributed to the formation of Cu-Zn alloy and interface that encouraged the hydrogenation of formate species [230]. However, further increase of Zn content corresponds to decreasing methanol yield which suggests that CO_2 hydrogenation to methanol can be a structurally sensitive reaction. Increased Zn content also correspond to increased formate coverage which may “poison” the active site and lead to lower methanol production [230,233]. Such finding provides further credence to the theory that formate is the reactive intermediate in this reaction. There are several speculations on the role of Zn in the reaction: first possibility is that Zn can be a hydrogen reservoir, structural modifier or direct promoter for bond activation. The other possibility is that CuZn alloy or decoration of Cu with metallic Zn can occur. Recent HRTEM evidence and DFT prediction reveal that thin layer of ZnO overlayer is decorated onto Cu nanoparticle to create defects which can stabilize HCOOH* intermediate and enable facile hydrogenation of HCOO* through strong metal support interaction effect [233–236].

To improve legibility, H* was omitted from the labels after the adsorption of six H atoms in the first step. The black line indicates the lowest-energy pathway through the HCOO*, HCOOH*, CH_3O_2*, CH_2O*, and CH_3O* intermediates. The main intermediates along the red path are HCOO*, H_2CO_2*, CH_2O* and CH_2O*. The two dashed horizontal lines indicate the desorption barriers of HCOOH and CH_2O (Fig. 11) [227].

Isotopic tracer studies, using ^{14}CO and $^{14}CO_2$ and performed at 50 bars and 250 °C, had shown that most of the produced methanol

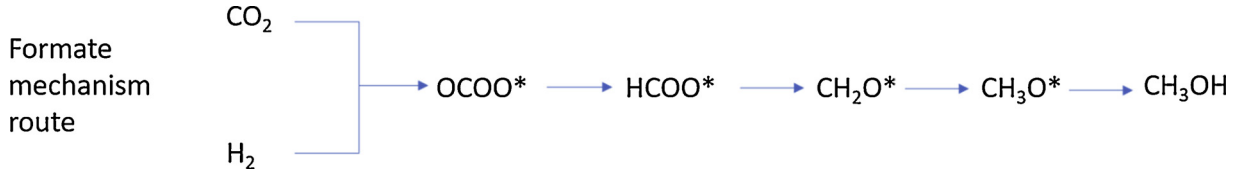

Fig. 10. Proposed reaction pathway via formate (HCOO*) mechanism route for CO_2 hydrogenation to methanol from various references [212,224,226,227,229,231].

originates from CO_2 hydrogenation instead of CO hydrogenation. Yang et al. added CO to D_2/CO_2 mixture and reported that the symmetric stretch for formate in the steady-state IR spectra became absent after some time. The absence of the symmetric stretch was attributed to lateral interaction of absorbate by water which may probably encourage formate decomposition into methanol [231]. However, there are other reports on the inhibitive effects of water on methanol yield and catalyst stability which appear to contradict the findings by Yang et al [226,229,239]. Thus, the effect of water and effect of lateral interactions between co-absorbates on methanol yield and catalytic activity should be studied in greater detail to reconcile the conflicting evidences and come to a common consensus on the role of water on methanol synthesis.

4. Future outlook and conclusion

The rapid increase in CO_2 emission due to human-made causes such as the burning of fossil fuels, vehicles, and industrial processes led to global climate change caused by greenhouse gases is a significant challenge of the 21st century. Three ways can reduce the increase in CO_2 concentration in the atmosphere: (1) control of CO_2 emissions, (2) CO_2 capture and storage, and (3) chemical conversion and utilization of CO_2. Therefore, this review covered the various process for the direct conversion of CO_2 to useful chemicals such as syngas, methane, and methanol via synthetic routes including reforming, reverse water gas shift, methanation and hydrogenation. In this review paper, several technological developments have been underlined to understand the processes involving conversion of CO_2 to various C_1 chemicals. This is highlighted by elucidating the development of heterogeneous catalysts, kinetics and mechanism of the reaction. After extensively reviewing the reactions, it can be concluded that the catalysts play crucial role for the process to be economically feasible.

For dry reforming of methane where CO_2 acts as an oxidant play important role in the reaction. It is an avenue to develop efficient system to convert CO_2 into syngas. Over the last few decades a substantial progress was made in developing highly efficient catalysts to allow long term stability during the reaction and prevent challenges related to metal sintering and coke deposition eventually leading to catalyst deactivation. Development core shell catalyst with dual functionality such as simultaneous removal of coke and CO_2 adsorption as is the case with mixed oxides with high oxygen carriers are few of the future class of catalyst to be considered. Yet, additional work is required to scale-up the process to industrial scale form lab scale. As of 2015, the Linde Group officially opened a dry-reforming based pilot facility at Pullach near Munich. With more research both on key catalyst development and on addressing the practical challenges of scale-up, DRM may be at the cusp of commercialization shortly.

Another process which converts CO_2 to syngas is reverse water gas shift (RWGS) reaction RWGS is the most straightforward way for large-scale production of value-added chemical when combined with CO_2-FT synthesis units. A few of the possible reasons for catalyst deactivation are large amount of water formation, metal sintering and coke deposition which decreases the selectivity towards CO formation. Controlling the selectivity of RWGS requires a deep understanding of thermodynamics, reaction kinetics, and mechanism which becomes easier by the utilization of advanced techniques such as transient quantitative temporal analysis, *in-situ* DRIFTS, and few more. In parallel with the experimental study simulation method involving DFT calculations, the structures of well -performing catalysts can be designed. With the recent development in use of transition metal based carbide catalyst, there is a potential to overcome the challenges of this reaction. Therefore, a focus is required to improve the transition metal carbide catalyst by studying the mechanism over metal carbides and performing the simulation study to predict the suitable combination of active metal and carbide support to enhance the CO selectivity at lower temperature.

Considering the current uses of renewable energy sources which are limited availability and require scalable means of storage. Thus, the production of synthetic natural gas or liquid fuels is the most viable pathway to store large amounts of energy produced from renewable sources for long periods. The most prominent process called as Power to Gas (PtG) has gained tremendous attention for the production of synthetic natural gas (SNG). The current development in the catalysts for

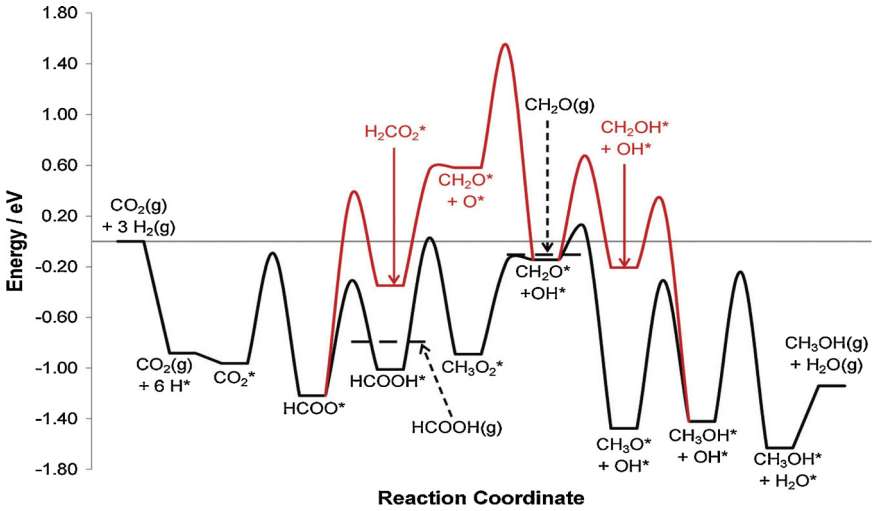

Fig. 11. Potential energy surface of CO_2 hydrogenation to methanol.

CO_2 methanation reaction focused on low temperature active catalysts to overcome the thermodynamic limitations. Nanosized nickel particles appear to be the most suitable non-precious to achieve high conversion at low temperatures. Additionally, development of the catalyst is based on improving the selectivity of methane by avoiding the formation route of carbonyls and carbides which causes deactivation. Apart from active catalytic sites, designing support and addition of promoters play a crucial role in improving the performance by H_2 and CO_2 activation, metal dispersion and improve metal support interaction. Apart from the development of efficient catalytic systems, it is also necessary to design an appropriate reactor to remove additional heat being an exothermic process. The fixed-bed reactors are the most widely used systems for the CO_2 methanation. Fluidized-bed reactors have proven highly reliable for the CO methanation, and other types of reactor are still under development.

To make methanol economy concept more widely adopted globally, a quantum leap in methanol yield must be achieved through a more rational understanding of the reaction mechanism to develop highly active and highly methanol selective to achieve this aim. Core-shell catalyst preparation technique should be refined to introduce greater synergy to improve methanol yield and activity. To improve catalytic performance and product selectivity in a more practical manner, the catalyst preparation method can be further developed and refined to prepare high surface area catalyst for higher methanol yield and CO_2 conversion. A more rational understanding of the reaction mechanism is required. This can be achieved through a combination of experimental and computational studies. *In-situ* and *operando* spectroscopic techniques, combined with computational techniques such as DFT and kinetic monte carlo methods, will be synergistically used to unravel new scientific insights for quantum improvement in methanol yield and catalytic activity. Kinetic monte carlo method can be used to elucidate the effect of lateral interactions between reaction intermediates on methanol selectivity. More DFT studies can include the metal center and catalyst support to better account for metal-support interface effect. For more in-depth elucidation of the reaction intermediates, isotopic labelling techniques and steady state transient kinetic analysis (SSTIKA) can be utilized to determine if one specie is actively involved in the reaction or a “spectator” specie and on which catalytic sites.

In brief, the conversion of CO_2 to synthesize valuable chemicals has a tremendous potential to be commercialized on a large scale. These processes require a practical design of the catalyst system and an energy efficient reactor design to improve the performance regarding activity, selectivity, and stability.

Acknowledgement

The authors gratefully thank the financial support from National University of Singapore, National Research Foundation, Prime Minister's Office, Singapore, the National Environment Agency under the Waste-to-Energy Competitive Research Program (WTE CRP 1501 103, WBS No. R-279-000-491-279), Agency for Science, Technology and Research (AME-IRG A1783c0016, WBS No.R-279-000-509-305) and Ministry of Education (MOE2017-T2-2-130, WBS No. R-279-000-544-112).

References

[1] I. Dincer, C. Acar, Review and evaluation of hydrogen production methods for better sustainability, Int. J. Hydrogen Energy 40 (2015) 11094–11111.
[2] Z.G. Wang, N. Dewangan, S. Das, M.H. Wai, S. Kawi, High oxygen permeable and CO2-tolerant SrCoxFe0.9-xNb0.1O3-delta (x = 0.1-0.8) perovskite membranes: behavior and mechanism, Sep. Purif. Technol. 201 (2018) 30–40.
[3] Z.G. Wang, J. Ashok, Z.W. Pu, S. Kawi, Low temperature partial oxidation of methane via BaBi0.05Co0.8Nb0.15O3_(delta)-Ni phyllosilicate catalytic hollow fiber membrane reactor, Chem. Eng. J. 315 (2017) 315–323.
[4] J. Ashok, S. Das, T.Y. Yeo, N. Dewangan, S. Kawi, Incinerator bottom ash derived from municipal solid waste as a potential catalytic support for biomass tar reforming, Waste Manag. 82 (2018) 249–257.
[5] J. Ashok, M.H. Wai, S. Kawi, Nickel-based catalysts for high-temperature water gas shift reaction-methane suppression, ChemCatChem 10 (2018) 3927–3942.
[6] S. Pati, A. Jangam, Z.G. Wang, N. Dewangan, W.M. Hui, S. Kawi, Catalytic Pd0.77Ag0.23 alloy membrane reactor for high temperature water-gas shift reaction: methane suppression, Chem. Eng. J. 362 (2019) 116–125.
[7] A. Álvarez, A. Bansode, A. Urakawa, A.V. Bavykina, T.A. Wezendonk, M. Makkee, J. Gascon, F. Kapteijn, Challenges in the greener production of formates/formic acid, methanol, and DME by heterogeneously catalyzed CO2 hydrogenation processes, Chem. Rev. 117 (2017) 9804–9838.
[8] S. Kawi, Y. Kathiraser, CO2 as an oxidant for high-temperature reactions, Front. Energy Res. (2015).
[9] R.W. Dorner, D.R. Hardy, F.W. Williams, H.D. Willauer, Heterogeneous catalytic CO 2 conversion to value-added hydrocarbons, Energy Environ. Sci. 3 (2010) 884–890.
[10] W. Li, H. Wang, X. Jiang, J. Zhu, Z. Liu, X. Guo, C. Song, A short review of recent advances in CO2 hydrogenation to hydrocarbons over heterogeneous catalysts, RSC Adv. 8 (2018) 7651–7669.
[11] F. Wang, M. Wei, D.G. Evans, X. Duan, CeO2-based heterogeneous catalysts toward catalytic conversion of CO2, J. Mater. Chem. A 4 (2016) 5773–5783.
[12] J. Artz, T.E. Müller, K. Thenert, J. Kleinekorte, R. Meys, A. Sternberg, A. Bardow, W. Leitner, Sustainable conversion of carbon dioxide: an integrated review of catalysis and life cycle assessment, Chem. Rev. 118 (2018) 434–504.
[13] E.V. Kondratenko, G. Mul, J. Baltrusaitis, G.O. Larrazábal, J. Pérez-Ramírez, Status and perspectives of CO2 conversion into fuels and chemicals by catalytic, photocatalytic and electrocatalytic processes, Energy Environ. Sci. 6 (2013) 3112–3135.
[14] W. Wang, S. Wang, X. Ma, J. Gong, Recent advances in catalytic hydrogenation of carbon dioxide, Chem. Soc. Rev. 40 (2011) 3703–3727.
[15] X. Hu, M. Gholizadeh, Biomass pyrolysis: a review of the process development and challenges from initial researches up to the commercialisation stage, J. Energy Chem. 39 (2019) 109–143.
[16] G. Zhang, J. Liu, Y. Xu, Y. Sun, A review of CH4CO2 reforming to synthesis gas over Ni-based catalysts in recent years (2010–2017), Int. J. Hydrogen Energy 43 (2018) 15030–15054.
[17] T. Yabe, Y. Sekine, Methane conversion using carbon dioxide as an oxidizing agent: a review, Fuel Process. Technol. 181 (2018) 187–198.
[18] Z.F. Bian, S. Das, M.H. Wai, P. Hongmanorom, S. Kawi, A review on bimetallic nickel-based catalysts for CO2 reforming of methane, ChemPhysChem 18 (2017) 3117–3134.
[19] M. García-Diéguez, I.S. Pieta, M.C. Herrera, M.A. Larrubia, L.J. Alemany, Improved Pt-Ni nanocatalysts for dry reforming of methane, Appl. Catal. A Gen. 377 (2010) 191–199.
[20] N.H. Elsayed, N.R.M. Roberts, B. Joseph, J.N. Kuhn, Low temperature dry reforming of methane over Pt–Ni–Mg/ceria–zirconia catalysts, Appl. Catal. B 179 (2015) 213–219.
[21] U. Oemar, Z. Bian, K. Hidajat, S. Kawi, Sulfur resistant LaxCe1-xNi0.5Cu0.5O3 catalysts for an ultra-high temperature water gas shift reaction, Catal. Sci. Technol. 6 (2016) 6569–6580.
[22] L. Li, L. Zhou, S. Ould-Chikh, D.H. Anjum, M.B. Kanoun, J. Scaranto, M.N. Hedhili, S. Khalid, P.V. Laveille, L. D'Souza, A. Clo, J.-M. Basset, Controlled surface segregation leads to efficient coke-resistant Nickel/Platinum bimetallic catalysts for the dry reforming of methane, ChemCatChem 7 (2015) 819–829.
[23] B. Li, S. Kado, Y. Mukainakano, T. Miyazawa, T. Miyao, S. Naito, K. Okumura, K. Kunimori, K. Tomishige, Surface modification of Ni catalysts with trace Pt for oxidative steam reforming of methane, J. Catal. 245 (2007) 144–155.
[24] X. Gao, Z. Tan, K. Hidajat, S. Kawi, Highly reactive Ni-Co/SiO2 bimetallic catalyst via complexation with oleylamine/oleic acid organic pair for dry reforming of methane, Catal. Today 281 (2017) 250–258.
[25] Z. Bian, S. Kawi, Highly carbon-resistant Ni–Co/SiO2 catalysts derived from phyllosilicates for dry reforming of methane, J. Co2 Util. 18 (2017) 345–352.
[26] J.-H. Kim, D.J. Suh, T.-J. Park, K.-L. Kim, Effect of metal particle size on coking during CO2 reforming of CH4 over Ni–alumina aerogel catalysts, Appl. Catal. A Gen. 197 (2000) 191–200.
[27] L.Y. Mo, K.K.M. Leong, S. Kawi, A highly dispersed and anti-coking Ni-La2O3/SiO2 catalyst for syngas production from dry carbon dioxide reforming of methane, Catal. Sci. Technol. 4 (2014) 2107–2114.
[28] J. Ni, L.W. Chen, J.Y. Lin, M.K. Schreyer, Z. Wang, S. Kawi, High performance of Mg-La mixed oxides supported Ni catalysts for dry reforming of methane: the effect of crystal structure, Int. J. Hydrogen Energy 38 (2013) 13631–13642.
[29] J. Ashok, Z. Bian, Z. Wang, S. Kawi, Ni-phyllosilicate structure derived Ni–SiO2–MgO catalysts for bi-reforming applications: acidity, basicity and thermal stability, Catal. Sci. Technol. 8 (2018) 1730–1742.
[30] S. Kawi, Y. Kathiraser, J. Ni, U. Oemar, Z.W. Li, E.T. Saw, Progress in synthesis of highly active and stable nickel-based catalysts for carbon dioxide reforming of methane, ChemSusChem 8 (2015) 3556–3575.
[31] M. Li, A.C. van Veen, Tuning the catalytic performance of Ni-catalysed dry reforming of methane and carbon deposition via Ni-CeO2-x interaction, Appl. Catal. B 237 (2018) 641–648.
[32] K. Sutthiumporn, S. Kawi, Promotional effect of alkaline earth over Ni–La2O3 catalyst for CO2 reforming of CH4: Role of surface oxygen species on H2 production and carbon suppression, Int. J. Hydrogen Energy 36 (2011) 14435–14446.
[33] S. Zhang, S. Muratsugu, N. Ishiguro, M. Tada, Ceria-doped Ni/SBA-16 catalysts for dry reforming of methane, ACS Catal. 3 (2013) 1855–1864.
[34] Z. Li, S. Das, P. Hongmanorom, N. Dewangan, M.H. Wai, S. Kawi, Silica-based micro- and mesoporous catalysts for dry reforming of methane, Catal. Sci. Technol. 8 (2018) 2763–2778.
[35] W. Yang, D. He, Role of poly(N-vinyl-2-pyrrolidone) in Ni dispersion for highly-

dispersed Ni/SBA-15 catalyst and its catalytic performance in carbon dioxide reforming of methane, Appl. Catal. A Gen. 524 (2016) 94–104.
[36] X.Y. Gao, J. Ashok, S. Widjaja, K. Hidajat, S. Kawi, Ni/SiO2 catalyst prepared via Ni-aliphatic amine complexation for dry reforming of methane: effect of carbon chain number and amine concentration, Appl. Catal. A Gen. 503 (2015) 34–42.
[37] X. Gao, H. Liu, K. Hidajat, S. Kawi, Anti-coking Ni/SiO2 catalyst for dry reforming of methane: role of oleylamine/oleic acid organic pair, ChemCatChem 7 (2015) 4188–4196.
[38] L. Mo, S. Kawi, An in situ self-assembled core–shell precursor route to prepare ultrasmall copper nanoparticles on silica catalysts, J. Mater. Chem. A 2 (2014) 7837–7844.
[39] X.Y. Gao, K. Hidajat, S. Kawi, Facile synthesis of Ni/SiO2 catalyst by sequential hydrogen/air treatment: a superior anti-coking catalyst for dry reforming of methane, J. Co2 Util. 15 (2016) 146–153.
[40] L.Y. Mo, E.T. Saw, Y. Kathiraser, M.L. Ang, S. Kawi, Preparation of highly dispersed Cu/SiO2 doped with CeO2 and its application for high temperature water gas shift reaction, Int. J. Hydrogen Energy 43 (2018) 15891–15897.
[41] L.Y. Mo, E.T. Saw, Y.H. Du, A. Borgna, M.L. Ang, Y. Kathiraser, Z.W. Li, W. Thitsartarn, M. Lin, S. Kawi, Highly dispersed supported metal catalysts prepared via in-situ self-assembled core-shell precursor route, Int. J. Hydrogen Energy 40 (2015) 13388–13398.
[42] K. Sutthiumporn, T. Maneerung, Y. Kathiraser, S. Kawi, CO2 dry-reforming of methane over La0.8Sr0.2Ni0.8M0.2O3 perovskite (M = Bi, Co, Cr, Cu, Fe): roles of lattice oxygen on C–H activation and carbon suppression, Int. J. Hydrogen Energy 37 (2012) 11195–11207.
[43] R. Dębek, M. Motak, D. Duraczyska, F. Launay, M.E. Galvez, T. Grzybek, P. Da Costa, Methane dry reforming over hydrotalcite-derived Ni–Mg–Al mixed oxides: the influence of Ni content on catalytic activity, selectivity and stability, Catal. Sci. Technol. 6 (2016) 6705–6715.
[44] Z. Li, M. Li, Z. Bian, Y. Kathiraser, S. Kawi, Design of highly stable and selective core/yolk–shell nanocatalysts—a review, Appl. Catal. B 188 (2016) 324–341.
[45] Z.W. Li, L.Y. Mo, Y. Kathiraser, S. Kawi, Yolk-satellite-Shell structured Ni-Yolk@Ni@SiO2 nanocomposite: superb catalyst toward methane CO2 reforming reaction, ACS Catal. 4 (2014) 1526–1536.
[46] Z. Li, L. Mo, Y. Kathiraser, S. Kawi, Yolk–satellite–shell structured Ni–Yolk@Ni@SiO2 nanocomposite: superb catalyst toward methane CO2 reforming reaction, ACS Catal. 4 (2014) 1526–1536.
[47] Z. Li, S. Kawi, Multi-Ni@Ni phyllosilicate hollow sphere for CO2 reforming of CH4: influence of Ni precursors on structure, sintering, and carbon resistance, Catal. Sci. Technol. 8 (2018) 1915–1922.
[48] S. Das, J. Ashok, Z. Bian, N. Dewangan, M.H. Wai, Y. Du, A. Borgna, K. Hidajat, S. Kawi, Silica–ceria sandwiched Ni core–shell catalyst for low temperature dry reforming of biogas: coke resistance and mechanistic insights, Appl. Catal. B 230 (2018) 220–236.
[49] Y. Zhao, H. Li, H. Li, NiCo@SiO2 core-shell catalyst with high activity and long lifetime for CO2 conversion through DRM reaction, Nano Energy 45 (2018) 101–108.
[50] J.W. Han, C. Kim, J.S. Park, H. Lee, Highly coke-resistant Ni nanoparticle catalysts with minimal sintering in dry reforming of methane, ChemSusChem 7 (2014) 451–456.
[51] Z. Li, B. Jiang, Z. Wang, S. Kawi, High carbon resistant Ni@Ni phyllosilicate@SiO2 core shell hollow sphere catalysts for low temperature CH4 dry reforming, J. Co2 Util. 27 (2018) 238–246.
[52] B. Jiang, L. Li, Z.F. Bian, Z.W. Li, M. Othman, Z.H. Sun, D.W. Tang, S. Kawi, B.L. Dou, Hydrogen generation from chemical looping reforming of glycerol by Ce-doped nickel phyllosilicate nanotube oxygen carriers, Fuel 222 (2018) 185–192.
[53] Z. Li, Z. Wang, B. Jiang, S. Kawi, Sintering resistant Ni nanoparticles exclusively confined within SiO2 nanotubes for CH4 dry reforming, Catal. Sci. Technol. 8 (2018) 3363–3371.
[54] Z. Li, Y. Kathiraser, J. Ashok, U. Oemar, S. Kawi, Simultaneous Tuning Porosity and Basicity of Nickel@Nickel–Magnesium Phyllosilicate Core–Shell Catalysts for CO2 Reforming of CH4, Langmuir 30 (2014) 14694–14705.
[55] Z. Li, Y. Kathiraser, S. Kawi, Facile Synthesis of High Surface Area Yolk–Shell Ni@Ni Embedded SiO2 via Ni Phyllosilicate with Enhanced Performance for CO2 Reforming of CH4, ChemCatChem 7 (2015) 160–168.
[56] Z.F. Bian, I.Y. Suryawinata, S. Kawi, Highly carbon resistant multicore-shell catalyst derived from Ni-Mg phyllosilicate nanotubes@silica for dry reforming of methane, Applied Catalysis B-Environmental 195 (2016) 1–8.
[57] Z. Li, K. Sibudjing, Facile Synthesis of Multi-Ni-Core@Ni Phyllosilicate@CeO2 Shell Hollow Spheres with High Oxygen Vacancy Concentration for Dry Reforming of CH4, ChemCatChem 10 (2018) 2994–3001.
[58] Z.-Y. Lim, C. Wu, W.G. Wang, K.-L. Choy, H. Yin, Porosity effect on ZrO2 hollow shells and hydrothermal stability for catalytic steam reforming of methane, J. Mater. Chem. A 4 (2016) 153–159.
[59] X. Zhang, L. Zhang, H. Peng, X. You, C. Peng, X. Xu, W. Liu, X. Fang, Z. Wang, N. Zhang, X. Wang, Nickel nanoparticles embedded in mesopores of AlSBA-15 with a perfect peasecod-like structure: a catalyst with superior sintering resistance and hydrothermal stability for methane dry reforming, Appl. Catal. B 224 (2018) 488–499.
[60] X. Zhang, Q. Zhang, N. Tsubaki, Y. Tan, Y. Han, Carbon dioxide reforming of methane over Ni nanoparticles incorporated into mesoporous amorphous ZrO2 matrix, Fuel 147 (2015) 243–252.
[61] J.C.S. Araújo, A.L.G. Pinheiro, A.C. Oliveira, M.G.A. Cruz, J.M.C. Bueno, R.S. Araujo, R. Lang, Catalytic assessment of nanostructured Pt/xLa2O3-Al2O3 oxides for hydrogen production by dry reforming of methane: effects of the lanthana content on the catalytic activity, Catal. Today (2018).
[62] C. Ruocco, B. de Caprariis, V. Palma, A. Petrullo, A. Ricca, M. Scarsella, P. De Filippis, Methane dry reforming on Ru perovskites, AZrRuO3: influence of preparation method and substitution of A cation with alkaline earth metals, J. Co2 Util. 30 (2019) 222–231.
[63] S.A. Singh, G. Madras, Sonochemical synthesis of Pt, Ru doped TiO2 for methane reforming, Appl. Catal. A Gen. 518 (2016) 102–114.
[64] S. Pavlova, L. Kapokova, R. Bunina, G. Alikina, N. Sazonova, T. Krieger, A. Ishchenko, V. Rogov, R. Gulyaev, V. Sadykov, C. Mirodatos, Syngas production by CO2 reforming of methane using LnFeNi(Ru)O3 perovskites as precursors of robust catalysts, Catal. Sci. Technol. 2 (2012) 2099–2108.
[65] D. Pakhare, J. Spivey, A review of dry (CO2) reforming of methane over noble metal catalysts, Chem. Soc. Rev. 43 (2014) 7813–7837.
[66] Y. Kathiraser, U. Oemar, E.T. Saw, Z. Li, S. Kawi, Kinetic and mechanistic aspects for CO2 reforming of methane over Ni based catalysts, Chem. Eng. J. 278 (2015) 62–78.
[67] J.H. Bitter, K. Seshan, J.A. Lercher, Mono and Bifunctional Pathways of CO2/CH4Reforming over Pt and Rh Based Catalysts, J. Catal. 176 (1998) 93–101.
[68] U. Oemar, Y. Kathiraser, L. Mo, X.K. Ho, S. Kawi, CO2 reforming of methane over highly active La-promoted Ni supported on SBA-15 catalysts: mechanism and kinetic modelling, Catal. Sci. Technol. 6 (2016) 1173–1186.
[69] B. Bachiller-Baeza, C. Mateos-Pedrero, M.A. Soria, A. Guerrero-Ruiz, U. Rodemerck, I. Rodríguez-Ramos, Transient studies of low-temperature dry reforming of methane over Ni-CaO/ZrO2-La2O3, Appl. Catal. B 129 (2013) 450–459.
[70] Z.L. Zhang, X.E. Verykios, Carbon dioxide reforming of methane to synthesis gas over supported Ni catalysts, Catal. Today 21 (1994) 589–595.
[71] X. Li, D. Li, H. Tian, L. Zeng, Z.-J. Zhao, J. Gong, Dry reforming of methane over Ni/La2O3 nanorod catalysts with stabilized Ni nanoparticles, Appl. Catal. B 202 (2017) 683–694.
[72] O.U. Osazuwa, H.D. Setiabudi, S. Abdullah, C.K. Cheng, Syngas production from methane dry reforming over SmCoO3 perovskite catalyst: kinetics and mechanistic studies, Int. J. Hydrogen Energy 42 (2017) 9707–9721.
[73] N. Almana, S.P. Phivilay, P. Laveille, M.N. Hedhili, P. Fornasiero, K. Takanabe, J.-M. Basset, Design of a core–shell Pt–SiO2 catalyst in a reverse microemulsion system: distinctive kinetics on CO oxidation at low temperature, J. Catal. 340 (2016) 368–375.
[74] Z. Xie, B. Yan, S. Kattel, J.H. Lee, S. Yao, Q. Wu, N. Rui, E. Gomez, Z. Liu, W. Xu, L. Zhang, J.G. Chen, Dry reforming of methane over CeO2-supported Pt-Co catalysts with enhanced activity, Appl. Catal. B 236 (2018) 280–293.
[75] D. Pakhare, J. Spivey, A review of dry (CO2) reforming of methane over noble metal catalysts, Chem. Soc. Rev. 43 (2014) 7813–7837.
[76] J. Wei, E. Iglesia, Isotopic and kinetic assessment of the mechanism of reactions of CH4 with CO2 or H2O to form synthesis gas and carbon on nickel catalysts, J. Catal. 224 (2004) 370–383.
[77] B. AlSabban, L. Falivene, S.M. Kozlov, A. Aguilar-Tapia, S. Ould-Chikh, J.-L. Hazemann, L. Cavallo, J.-M. Basset, K. Takanabe, In-operando elucidation of bimetallic CoNi nanoparticles during high-temperature CH4/CO2 reaction, Appl. Catal. B 213 (2017) 177–189.
[78] L.N. Bobrova, A.S. Bobin, N.V. Mezentseva, V.A. Sadykov, J.W. Thybaut, G.B. Marin, Kinetic assessment of dry reforming of methane on Pt + Ni containing composite of fluorite-like structure, Appl. Catal. B 182 (2016) 513–524.
[79] E. Akpan, Y. Sun, P. Kumar, H. Ibrahim, A. Aboudheir, R. Idem, Kinetics, experimental and reactor modeling studies of the carbon dioxide reforming of methane (CDRM) over a new Ni/CeO2–ZrO2 catalyst in a packed bed tubular reactor, Chem. Eng. Sci. 62 (2007) 4012–4024.
[80] Y. Cui, H. Zhang, H. Xu, W. Li, Kinetic study of the catalytic reforming of CH4 with CO2 to syngas over Ni/α-Al2O3 catalyst: The effect of temperature on the reforming mechanism, Appl. Catal. A Gen. 318 (2007) 79–88.
[81] S. Kawi, Y. Kathiraser, J. Ni, U. Oemar, Z. Li, E.T. Saw, Progress in synthesis of highly active and stable nickel-based catalysts for carbon dioxide reforming of methane, ChemSusChem 8 (2015) 3556–3575.
[82] A. Yamaguchi, E. Iglesia, Catalytic activation and reforming of methane on supported palladium clusters, J. Catal. 274 (2010) 52–63.
[83] J. Wei, E. Iglesia, Structural requirements and reaction pathways in methane activation and chemical conversion catalyzed by rhodium, J. Catal. 225 (2004) 116–127.
[84] S.Y. Foo, C.K. Cheng, T.-H. Nguyen, A.A. Adesina, Kinetic study of methane CO2 reforming on Co–Ni/Al2O3 and Ce–Co–Ni/Al2O3 catalysts, Catal. Today 164 (2011) 221–226.
[85] B.V. Ayodele, S.B. Abdullah, C.K. Cheng, Kinetics and mechanistic studies of CO-rich hydrogen production by CH4/CO2 reforming over Praseodymia supported cobalt catalysts, Int. J. Hydrogen Energy 42 (2017) 28408–28424.
[86] M.-S. Fan, A.Z. Abdullah, S. Bhatia, Utilization of greenhouse gases through dry reforming: screening of nickel-based bimetallic catalysts and kinetic studies, ChemSusChem 4 (2011) 1643–1653.
[87] M.M. Barroso Quiroga, A.E. Castro Luna, Kinetic analysis of rate data for dry reforming of methane, Ind. Eng. Chem. Res. 46 (2007) 5265–5270.
[88] J. Zhang, H. Wang, A.K. Dalai, Kinetic studies of carbon dioxide reforming of methane over Ni − Co/Al − Mg − O bimetallic catalyst, Ind. Eng. Chem. Res. 48 (2009) 677–684.
[89] S.-W. Park, O.-S. Joo, K.-D. Jung, H. Kim, S.-H. Han, Development of ZnO/Al2O3 catalyst for reverse-water-gas-shift reaction of CAMERE (carbon dioxide hydrogenation to form methanol via a reverse-water-gas-shift reaction) process, Appl. Catal. A Gen. 211 (2001) 81–90.
[90] L. Yang, L. Pastor-Pérez, S. Gu, A. Sepúlveda-Escribano, T.R. Reina, Highly efficient Ni/CeO2-Al2O3 catalysts for CO2 upgrading via reverse water-gas shift:

effect of selected transition metal promoters, Appl. Catal. B 232 (2018) 464–471.
[91] F. Lin, R. Delmelle, T. Vinodkumar, B.M. Reddy, A. Wokaun, I. Alxneit, Correlation between the structural characteristics, oxygen storage capacities and catalytic activities of dual-phase Zn-modified ceria nanocrystals, Catal. Sci. Technol. 5 (2015) 3556–3567.
[92] L. Silva-Calpa, P.C. Zonetti, C.P. Rodrigues, O.C. Alves, L.G. Appel, R.R. de Avillez, The ZnxZr1 − xO2 − y solid solution on m-ZrO2: creating O vacancies and improving the m-ZrO2 redox properties, J. Mol. Catal. A Chem. 425 (2016) 166–173.
[93] P.C. Zonetti, S. Letichevsky, A.B. Gaspar, E.F. Sousa-Aguiar, L.G. Appel, The NixCe0.75Zr0.25 − xO2 solid solution and the RWGS, Appl. Catal. A Gen. 475 (2014) 48–54.
[94] B.J. Hare, D. Maiti, S. Ramani, A.E. Ramos, V.R. Bhethanabotla, J.N. Kuhn, Thermochemical conversion of carbon dioxide by reverse water-gas shift chemical looping using supported perovskite oxides, Catal. Today (2018).
[95] Y.A. Daza, D. Maiti, R.A. Kent, V.R. Bhethanabotla, J.N. Kuhn, Isothermal reverse water gas shift chemical looping on La0.75Sr0.25Co(1 − Y)FeYO3 perovskite-type oxides, Catal. Today 258 (2015) 691–698.
[96] H.D.A.L. Viana, J.T.S. Irvine, Catalytic properties of the proton conductor materials: Sr3CaZr0.5Ta1.5O8.75, BaCe0.9Y0.1O2.95 and Ba3Ca1.18Nb1.82O8.73 for reverse water gas shift, Solid State Ion. 178 (2007) 717–722.
[97] N. Zakowsky, S. Williamson, J.T.S. Irvine, Elaboration of CO2 tolerance limits of BaCe0.9Y0.1O3–δ electrolytes for fuel cells and other applications, Solid State Ion. 176 (2005) 3019–3026.
[98] J. Wambach, A. Baiker, A. Wokaun, CO2 hydrogenation over metal/zirconia catalysts, J. Chem. Soc. Faraday Trans. 1 (1999) 5071–5080.
[99] Y. Yu, Y.M. Chan, Z.F. Bian, F.J. Song, J. Wang, Q. Zhong, S. Kawi, Enhanced performance and selectivity of CO2 methanation over g-C3N4 assisted synthesis of Ni-CeO2 catalyst: kinetics and DRIFTS studies, Int. J. Hydrogen Energy 43 (2018) 15191–15204.
[100] J. Ashok, M.L. Ang, S. Kawi, Enhanced activity of CO2 methanation over Ni/CeO2-ZrO2 catalysts: influence of preparation methods, Catal. Today 281 (2017) 304–311.
[101] E.T. Saw, U. Oemar, M.L. Ang, H. Kus, S. Kawi, High-temperature water gas shift reaction on Ni-Cu/CeO2 catalysts: effect of ceria nanocrystal size on carboxylate formation, Catal. Sci. Technol. 6 (2016) 5336–5349.
[102] M.L. Ang, J.T. Miller, Y. Cui, L. Mo, S. Kawi, Bimetallic Ni-Cu alloy nanoparticles supported on silica for the water-gas shift reaction: activating surface hydroxyls via enhanced CO adsorption, Catal. Sci. Technol. 6 (2016) 3394–3409.
[103] E.T. Saw, U. Oemar, X.R. Tan, Y. Du, A. Borgna, K. Hidajat, S. Kawi, Bimetallic Ni-Cu catalyst supported on CeO2 for high-temperature water-gas shift reaction: methane suppression via enhanced CO adsorption, J. Catal. 314 (2014) 32–46.
[104] M.L. Ang, U. Oemar, Y. Kathiraser, E.T. Saw, C.H.K. Lew, Y. Du, A. Borgna, S. Kawi, High-temperature water-gas shift reaction over Ni/xK/CeO2 catalysts: suppression of methanation via formation of bridging carbonyls, J. Catal. 329 (2015) 130–143.
[105] M.L. Ang, U. Oemar, E.T. Saw, L. Mo, Y. Kathiraser, B.H. Chia, S. Kawi, Highly active Ni/xNa/CeO2 catalyst for the water gas shift reaction: effect of sodium on methane suppression, ACS Catal. 4 (2014) 3237–3248.
[106] Z.F. Bian, Z.W. Li, J. Ashok, S. Kawi, A highly active and stable Ni-Mg phyllosilicate nanotubular catalyst for ultrahigh temperature water-gas shift reaction, Chem. Commun. 51 (2015) 16324–16326.
[107] J.R. Wagner Jr, E.M. Mount Iii, H.F. Giles Jr, 46 - Blown Film, Extrusion, second edition, William Andrew Publishing, Oxford, 2014, pp. 539–549.
[108] S. Pati, A. Jangam, W. Zhigang, N. Dewangan, W. Ming Hui, S. Kawi, Catalytic Pd0.77Ag0.23 alloy membrane reactor for high temperature water-gas shift reaction: methane suppression, Chem. Eng. J. (2018).
[109] B. Dai, G. Zhou, S. Ge, H. Xie, Z. Jiao, G. Zhang, K. Xiong, CO2 reverse water-gas shift reaction on mesoporous M-CeO2 catalysts, Can. J. Chem. Eng. 95 (2017) 634–642.
[110] H.C. Wu, Y.C. Chang, J.H. Wu, J.H. Lin, I.K. Lin, C.S. Chen, Methanation of CO2 and reverse water gas shift reactions on Ni/SiO2 catalysts: the influence of particle size on selectivity and reaction pathway, Catal. Sci. Technol. 5 (2015) 4154–4163.
[111] S. Choi, B.-I. Sang, J. Hong, K.J. Yoon, J.-W. Son, J.-H. Lee, B.-K. Kim, H. Kim, Catalytic behavior of metal catalysts in high-temperature RWGS reaction: In-situ FT-IR experiments and first-principles calculations, Sci. Rep. 7 (2017) 41207.
[112] S.S. Kim, H.H. Lee, S.C. Hong, The effect of the morphological characteristics of TiO2 supports on the reverse water–gas shift reaction over Pt/TiO2 catalysts, Appl. Catal. B 119–120 (2012) 100–108.
[113] W. Yu, M.D. Porosoff, J.G. Chen, Review of Pt-Based bimetallic catalysis: from model surfaces to supported catalysts, Chem. Rev. 112 (2012) 5780–5817.
[114] P. Zhang, M. Chi, S. Sharma, E. McFarland, Silica encapsulated heterostructure catalyst of Pt nanoclusters on hematite nanocubes: synthesis and reactivity, J. Mater. Chem. 20 (2010) 2013–2017.
[115] I. Ro, C. Sener, T.M. Stadelman, M.R. Ball, J.M. Venegas, S.P. Burt, I. Hermans, J.A. Dumesic, G.W. Huber, Measurement of intrinsic catalytic activity of Pt monometallic and Pt-MoOx interfacial sites over visible light enhanced PtMoOx/SiO2 catalyst in reverse water gas shift reaction, J. Catal. 344 (2016) 784–794.
[116] L.C. Wang, M. Tahvildar Khazaneh, D. Widmann, R.J. Behm, TAP reactor studies of the oxidizing capability of CO2 on a Au/CeO2 catalyst – a first step toward identifying a redox mechanism in the Reverse Water–gas Shift reaction, J. Catal. 302 (2013) 20–30.
[117] X. Yang, X. Su, X. Chen, H. Duan, B. Liang, Q. Liu, X. Liu, Y. Ren, Y. Huang, T. Zhang, Promotion effects of potassium on the activity and selectivity of Pt/zeolite catalysts for reverse water gas shift reaction, Appl. Catal. B 216 (2017) 95–105.
[118] B. Liang, H. Duan, X. Su, X. Chen, Y. Huang, X. Chen, J.J. Delgado, T. Zhang, Promoting role of potassium in the reverse water gas shift reaction on Pt/mullite catalyst, Catal. Today 281 (2017) 319–326.
[119] J.C. Matsubu, V.N. Yang, P. Christopher, Isolated metal active site concentration and stability control catalytic CO2 reduction selectivity, J. Am. Chem. Soc. 137 (2015) 3076–3084.
[120] J.H. Kwak, L. Kovarik, J. Szanyi, CO2 reduction on supported Ru/Al2O3 catalysts: cluster size dependence of product selectivity, ACS Catal. 3 (2013) 2449–2455.
[121] R.B. Levy, M. Boudart, Platinum-like behavior of tungsten carbide in surface catalysis, Science 181 (1973) 547.
[122] U. Burghaus, Surface chemistry of CO2 – adsorption of carbon dioxide on clean surfaces at ultrahigh vacuum, Prog. Surf. Sci. 89 (2014) 161–217.
[123] H.J. Freund, M.W. Roberts, Surface chemistry of carbon dioxide, Surf. Sci. Rep. 25 (1996) 225–273.
[124] M.D. Porosoff, X. Yang, J.A. Boscoboinik, J.G. Chen, Molybdenum carbide as alternative catalysts to precious metals for highly selective reduction of CO2 to CO, Angew. Chem. Int. Ed. 53 (2014) 6705–6709.
[125] S. Posada-Pérez, P.J. Ramírez, J. Evans, F. Viñes, P. Liu, F. Illas, J.A. Rodriguez, Highly Active Au/δ-MoC and Cu/δ-MoC Catalysts for the Conversion of CO2: The Metal/C Ratio as a Key Factor Defining Activity, Selectivity, and Stability, J. Am. Chem. Soc. 138 (2016) 8269–8278.
[126] X. Zhang, X. Zhu, L. Lin, S. Yao, M. Zhang, X. Liu, X. Wang, Y.-W. Li, C. Shi, D. Ma, Highly dispersed copper over β-Mo2C as an efficient and stable catalyst for the reverse water gas shift (RWGS) reaction, ACS Catal. 7 (2017) 912–918.
[127] Q. Zhang, L. Pastor-Pérez, W. Jin, S. Gu, T.R. Reina, Understanding the promoter effect of Cu and Cs over highly effective β-Mo2C catalysts for the reverse water-gas shift reaction, Appl. Catal. B 244 (2019) 889–898.
[128] L.F. Bobadilla, J.L. Santos, S. Ivanova, J.A. Odriozola, A. Urakawa, Unravelling the role of oxygen vacancies in the mechanism of the reverse water–Gas shift reaction by operando DRIFTS and ultraviolet–Visible spectroscopy, ACS Catal. 8 (2018) 7455–7467.
[129] S. Sharma, S. Hilaire, J.M. Vohs, R.J. Gorte, H.W. Jen, Evidence for oxidation of Ceria by CO2, J. Catal. 190 (2000) 199–204.
[130] C.S. Chen, J.H. Wu, T.W. Lai, Carbon dioxide hydrogenation on Cu nanoparticles, J. Phys. Chem. C 114 (2010) 15021–15028.
[131] Q. Zhang, L. Guo, Mechanism of the reverse water-gas shift reaction catalyzed by Cu12TM bimetallic nanocluster: a density functional theory study, J. Clust. Sci. 29 (2018) 867–877.
[132] M.J.L. Ginés, A.J. Marchi, C.R. Apesteguía, Kinetic study of the reverse water-gas shift reaction over CuO/ZnO/Al2O3 catalysts, Appl. Catal. A Gen. 154 (1997) 155–171.
[133] S.-I. Fujita, M. Usui, N. Takezawa, Mechanism of the reverse water gas shift reaction over Cu/ZnO catalyst, J. Catal. 134 (1992) 220–225.
[134] G.-C. Wang, J. Nakamura, Structure sensitivity for forward and reverse water-gas shift reactions on copper surfaces: a DFT study, J. Phys. Chem. Lett. 1 (2010) 3053–3057.
[135] A. Goguet, F.C. Meunier, D. Tibiletti, J.P. Breen, R. Burch, Spectrokinetic investigation of reverse water-gas-Shift reaction intermediates over a Pt/CeO2 catalyst, J. Phys. Chem. B 108 (2004) 20240–20246.
[136] V. Arunajatesan, B. Subramaniam, K.W. Hutchenson, F.E. Herkes, In situ FTIR investigations of reverse water gas shift reaction activity at supercritical conditions, Chem. Eng. Sci. 62 (2007) 5062–5069.
[137] N. Ishito, K. Hara, K. Nakajima, A. Fukuoka, Selective synthesis of carbon monoxide via formates in reverse water–gas shift reaction over alumina-supported gold catalyst, J. Energy Chem. 25 (2016) 306–310.
[138] X. Wang, H. Shi, J.H. Kwak, J. Szanyi, Mechanism of CO2 hydrogenation on Pd/Al2O3 catalysts: kinetics and transient DRIFTS-MS studies, ACS Catal. 5 (2015) 6337–6349.
[139] T. Reichenbach, K. Mondal, M. Jäger, T. Vent-Schmidt, D. Himmel, V. Dybbert, A. Bruix, I. Krossing, M. Walter, M. Moseler, Ab initio study of CO2 hydrogenation mechanisms on inverse ZnO/Cu catalysts, J. Catal. 360 (2018) 168–174.
[140] M. Kiyomiya, N. Momma, I. Yasumori, The kinetics and mechanism of hydrogen adsorption and hydrogen–Deuterium equilibration on the copper surface, Bull. Chem. Soc. Jpn. 47 (1974) 1852–1857.
[141] K.-H. Ernst, C.T. Campbell, G. Moretti, Kinetics of the reverse water-gas shift reaction over Cu(110), J. Catal. 134 (1992) 66–74.
[142] E.L. Fornero, D.L. Chiavassa, A.L. Bonivardi, M.A. Baltanás, Transient analysis of the reverse water gas shift reaction on Cu/ZrO2 and Ga2O3/Cu/ZrO2 catalysts, J. Co2 Util. 22 (2017) 289–298.
[143] S.S. Kim, H.H. Lee, S.C. Hong, A study on the effect of support's reducibility on the reverse water-gas shift reaction over Pt catalysts, Appl. Catal. A Gen. 423–424 (2012) 100–107.
[144] A.A. Phatak, N. Koryabkina, S. Rai, J.L. Ratts, W. Ruettinger, R.J. Farrauto, G.E. Blau, W.N. Delgass, F.H. Ribeiro, Kinetics of the water–gas shift reaction on Pt catalysts supported on alumina and ceria, Catal. Today 123 (2007) 224–234.
[145] M.A.A. Aziz, A.A. Jalil, S. Triwahyono, A. Ahmad, CO2 methanation over heterogeneous catalysts: recent progress and future prospects, Green Chem. 17 (2015) 2647–2663.
[146] P. Frontera, A. Macario, M. Ferraro, P. Antonucci, Supported catalysts for CO2 methanation: a review, Catalysts 7 (2017) 59.
[147] M. Jacquemin, A. Beuls, P. Ruiz, Catalytic production of methane from CO2 and H2 at low temperature: insight on the reaction mechanism, Catal. Today 157 (2010) 462–466.
[148] A. Beuls, C. Swalus, M. Jacquemin, G. Heyen, A. Karelovic, P. Ruiz, Methanation of CO2: further insight into the mechanism over Rh/γ-Al2O3 catalyst, Appl. Catal. B 113–114 (2012) 2–10.
[149] B. Miao, S.S.K. Ma, X. Wang, H. Su, S.H. Chan, Catalysis mechanisms of CO2 and

CO methanation, Catal. Sci. Technol. 6 (2016) 4048–4058.
[150] M. Götz, J. Lefebvre, F. Mörs, A. McDaniel Koch, F. Graf, S. Bajohr, R. Reimert, T. Kolb, Renewable Power-to-Gas: A technological and economic review, Renew. Energy 85 (2016) 1371–1390.
[151] E. Baraj, S. Vagaský, T. Hlinčik, K. Ciahotný, V. Tekáč, Reaction Mechanisms of Carbon Dioxide Methanation, Chemical Papers, (2016), p. 395.
[152] M. Younas, L. Loong Kong, M.J.K. Bashir, H. Nadeem, A. Shehzad, S. Sethupathi, R. Advancements, Fundamental challenges, and opportunities in catalytic methanation of CO2, Energy Fuels 30 (2016) 8815–8831.
[153] I. Kuznecova, J. Gusca, Property based ranking of CO and CO2 methanation catalysts, Energy Procedia 128 (2017) 255–260.
[154] F. Solymosi, A. Erdöhelyi, Hydrogenation of CO2 to CH4 over alumina-supported noble metals, J. Mol. Catal. 8 (1980) 471–474.
[155] S. Sharma, Z. Hu, P. Zhang, E.W. McFarland, H. Metiu, CO2 methanation on Ru-doped ceria, J. Catal. 278 (2011) 297–309.
[156] G.A. Mills, F.W. Steffgen, Catalytic methanation, Catal. Rev. 8 (1974) 159–210.
[157] S. Rönsch, J. Schneider, S. Matthischke, M. Schlüter, M. Götz, J. Lefebvre, P. Prabhakaran, S. Bajohr, Review on methanation – from fundamentals to current projects, Fuel 166 (2016) 276–296.
[158] L. Falbo, M. Martinelli, C.G. Visconti, L. Lietti, C. Bassano, P. Deiana, Kinetics of CO2 methanation on a Ru-based catalyst at process conditions relevant for Power-to-Gas applications, Appl. Catal. B 225 (2018) 354–363.
[159] W. Wei, G. Jinlong, Methanation of carbon dioxide: an overview, Front. Chem. Sci. Eng. 5 (2011) 2–10.
[160] X. Su, J. Xu, B. Liang, H. Duan, B. Hou, Y. Huang, Catalytic carbon dioxide hydrogenation to methane: a review of recent studies, J. Energy Chem. 25 (2016) 553–565.
[161] S. Tada, T. Shimizu, H. Kameyama, T. Haneda, R. Kikuchi, Ni/CeO2 catalysts with high CO2 methanation activity and high CH4 selectivity at low temperatures, Int. J. Hydrogen Energy 37 (2012) 5527–5531.
[162] P.A.U. Aldana, F. Ocampo, K. Kobl, B. Louis, F. Thibault-Starzyk, M. Daturi, P. Bazin, S. Thomas, A.C. Roger, Catalytic CO2 valorization into CH4 on Ni-based ceria-zirconia. Reaction mechanism by operando IR spectroscopy, Catal. Today 215 (2013) 201–207.
[163] D. Pandey, G. Deo, Effect of support on the catalytic activity of supported Ni–Fe catalysts for the CO2 methanation reaction, J. Ind. Eng. Chem. 33 (2016) 99–107.
[164] M.A.A. Aziz, A.A. Jalil, S. Triwahyono, R.R. Mukti, Y.H. Taufiq-Yap, M.R. Sazegar, Highly active Ni-promoted mesostructured silica nanoparticles for CO2 methanation, Appl. Catal. B 147 (2014) 359–368.
[165] W. Zhen, B. Li, G. Lu, J. Ma, Enhancing catalytic activity and stability for CO2 methanation on Ni@MOF-5 via control of active species dispersion, Chem. Commun. 51 (2015) 1728–1731.
[166] J. Jimenez, A. Bird, M. Santos Santiago, C. Wen, J. Lauterbach, Supported cobalt nanorod catalysts for carbon dioxide hydrogenation, Energy Technol. 5 (2017) 884–891.
[167] G. Zhou, T. Wu, H. Xie, X. Zheng, Effects of structure on the carbon dioxide methanation performance of Co-based catalysts, Int. J. Hydrogen Energy 38 (2013) 10012–10018.
[168] G. Zhou, H. Liu, K. Cui, H. Xie, Z. Jiao, G. Zhang, K. Xiong, X. Zheng, Methanation of carbon dioxide over Ni/CeO2 catalysts: effects of support CeO2 structure, Int. J. Hydrogen Energy 42 (2017) 16108–16117.
[169] Z. Bian, Y.M. Chan, Y. Yu, S. Kawi, Morphology dependence of catalytic properties of Ni/CeO2 for CO2 methanation: a kinetic and mechanism study, Catal. Today (2018).
[170] A.M. Abdel-Mageed, D. Widmann, S.E. Olesen, I. Chorkendorff, J. Biskupek, R.J. Behm, Selective CO methanation on Ru/TiO2 catalysts: role and influence of metal–support interactions, ACS Catal. 5 (2015) 6753–6763.
[171] S. Hwang, U.G. Hong, J. Lee, J.H. Baik, D.J. Koh, H. Lim, I.K. Song, Methanation of carbon dioxide over mesoporous nickel–m–alumina (M = Fe, Zr, Ni, Y, and Mg) xerogel catalysts: effect of second metal, Catal. Lett. 142 (2012) 860–868.
[172] Z. Li, T. Zhao, L. Zhang, Promotion effect of additive Fe on Al2O3 supported Ni catalyst for CO2 methanation, Appl. Organomet. Chem. 32 (2018) e4328.
[173] H. Zhu, R. Razzaq, C. Li, Y. Muhmmad, S. Zhang, Catalytic Methanation of Carbon Dioxide by Active Oxygen Material CexZr1−xO2 Supported Ni–Co Bimetallic Nanocatalysts, Aiche J. 59 (2013) 2567–2576.
[174] L. Xu, X. Lian, M. Chen, Y. Cui, F. Wang, W. Li, B. Huang, CO2 methanation over CoNi bimetal-doped ordered mesoporous Al2O3 catalysts with enhanced low-temperature activities, Int. J. Hydrogen Energy 43 (2018) 17172–17184.
[175] X. Shang, D. Deng, X. Wang, W. Xuan, X. Zou, W. Ding, X. Lu, Enhanced low-temperature activity for CO2 methanation over Ru doped the Ni/CexZr(1−x)O2 catalysts prepared by one-pot hydrolysis method, Int. J. Hydrogen Energy 43 (2018) 7179–7189.
[176] Q. Liu, S. Wang, G. Zhao, H. Yang, M. Yuan, X. An, H. Zhou, Y. Qiao, Y. Tian, CO2 methanation over ordered mesoporous NiRu-doped CaO-Al2O3 nanocomposites with enhanced catalytic performance, Int. J. Hydrogen Energy 43 (2018) 239–250.
[177] M. Mihet, M.D. Lazar, Methanation of CO2 on Ni/γ-Al2O3: influence of Pt, Pd or Rh promotion, Catal. Today 306 (2018) 294–299.
[178] H. Liu, X. Zou, X. Wang, X. Lu, W. Ding, Effect of CeO2 addition on Ni/Al2O3 catalysts for methanation of carbon dioxide with hydrogen, J. Nat. Gas Chem. 21 (2012) 703–707.
[179] X. Wang, L. Zhu, Y. Liu, S. Wang, CO2 methanation on the catalyst of Ni/MCM-41 promoted with CeO2, Sci. Total Environ. 625 (2018) 686–695.
[180] G. Zhi, X. Guo, Y. Wang, G. Jin, X. Guo, Effect of La2O3 modification on the catalytic performance of Ni/SiC for methanation of carbon dioxide, Catal. Commun. 16 (2011) 56–59.
[181] L. Zhang, L. Bian, Z. Zhu, Z. Li, La-promoted Ni/Mg-Al catalysts with highly enhanced low-temperature CO2 methanation performance, Int. J. Hydrogen Energy 43 (2018) 2197–2206.
[182] M. Guo, G. Lu, The effect of impregnation strategy on structural characters and CO2 methanation properties over MgO modified Ni/SiO2 catalysts, Catal. Commun. 54 (2014) 55–60.
[183] L. Xu, F. Wang, M. Chen, H. Yang, D. Nie, L. Qi, X. Lian, Alkaline-promoted Ni based ordered mesoporous catalysts with enhanced low-temperature catalytic activity toward CO2 methanation, RSC Adv. 7 (2017) 18199–18210.
[184] S. Sharma, K.B. Sravan Kumar, Y.M. Chandnani, V.S. Phani Kumar, B.P. Gangwar, A. Singhal, P.A. Deshpande, Mechanistic insights into CO2 methanation over Ru-Substituted CeO2, J. Phys. Chem. C 120 (2016) 14101–14112.
[185] G. Garbarino, D. Bellotti, P. Riani, L. Magistri, G. Busca, Methanation of carbon dioxide on Ru/Al2O3 and Ni/Al2O3 catalysts at atmospheric pressure: catalysts activation, behaviour and stability, Int. J. Hydrogen Energy 40 (2015) 9171–9182.
[186] J.A.H. Dreyer, P. Li, L. Zhang, G.K. Beh, R. Zhang, P.H.L. Sit, W.Y. Teoh, Influence of the oxide support reducibility on the CO2 methanation over Ru-based catalysts, Appl. Catal. B 219 (2017) 715–726.
[187] J.D. Jimenez, C. Wen, J. Lauterbach, Design of highly active cobalt catalysts for CO2 hydrogenation via the tailoring of surface orientation of nanostructures, Catal. Sci. Technol. 9 (2019) 1970–1978.
[188] Y. Zhu, S. Zhang, Y. Ye, X. Zhang, L. Wang, W. Zhu, F. Cheng, F. Tao, Catalytic conversion of carbon dioxide to methane on ruthenium–cobalt bimetallic nanocatalysts and correlation between surface chemistry of catalysts under reaction conditions and catalytic performances, ACS Catal. 2 (2012) 2403–2408.
[189] M. Schubert, S. Pokhrel, A. Thomé, V. Zielasek, T.M. Gesing, F. Roessner, L. Mädler, M. Bäumer, Highly active Co–Al2O3-based catalysts for CO2 methanation with very low platinum promotion prepared by double flame spray pyrolysis, Catal. Sci. Technol. 6 (2016) 7449–7460.
[190] E. Baraj, S. Vagaský, T. Hlinčík, K. Ciahotný, V. Tekáč, Reaction mechanisms of carbon dioxide methanation, Chem. Pap. 70 (2016) 395–403.
[191] A. Solis-Garcia, J.F. Louvier-Hernandez, A. Almendarez-Camarillo, J.C. Fierro-Gonzalez, Participation of surface bicarbonate, formate and methoxy species in the carbon dioxide methanation catalyzed by ZrO2-supported Ni, Appl. Catal. B 218 (2017) 611–620.
[192] X. Jia, X. Zhang, N. Rui, X. Hu, C. Liu, Structural effect of Ni/ZrO2 catalyst on CO2 methanation with enhanced activity, Appl. Catal. B 244 (2019) 159–169.
[193] M.A.A. Aziz, A.A. Jalil, S. Triwahyono, S.M. Sidik, Methanation of carbon dioxide on metal-promoted mesostructured silica nanoparticles, Appl. Catal. A Gen. 486 (2014) 115–122.
[194] F. Wang, S. He, H. Chen, B. Wang, L. Zheng, M. Wei, D.G. Evans, X. Duan, Active site dependent reaction mechanism over Ru/CeO2 catalyst toward CO2 methanation, J. Am. Chem. Soc. 138 (2016) 6298–6305.
[195] P.J. Lunde, F.L. Kester, Rates of methane formation from carbon dioxide and hydrogen over a ruthenium catalyst, J. Catal. 30 (1973) 423–429.
[196] X. Wang, Y. Hong, H. Shi, J. Szanyi, Kinetic modeling and transient DRIFTS–MS studies of CO2 methanation over Ru/Al2O3 catalysts, J. Catal. 343 (2016) 185–195.
[197] C.V. Miguel, A. Mendes, L.M. Madeira, Intrinsic kinetics of CO2 methanation over an industrial nickel-based catalyst, J. Co2 Util. 25 (2018) 128–136.
[198] G.D. Weatherbee, C.H. Bartholomew, Hydrogenation of CO2 on group VIII metals: II. Kinetics and mechanism of CO2 hydrogenation on nickel, J. Catal. 77 (1982) 460–472.
[199] F. Koschany, D. Schlereth, O. Hinrichsen, On the kinetics of the methanation of carbon dioxide on coprecipitated NiAl(O)x, Appl. Catal. B 181 (2016) 504–516.
[200] Z.A. Ibraeva, N.V. Nekrasov, B.S. Gudkov, V.I. Yakerson, Z.T. Beisembaeva, E.Z. Golosman, S.L. Kiperman, Kinetics of methanation of carbon dioxide on a nickel catalyst, Theor. Exp. Chem. 26 (1991) 584–588.
[201] Y. Yu, Y.M. Chan, Z. Bian, F. Song, J. Wang, Q. Zhong, S. Kawi, Enhanced performance and selectivity of CO2 methanation over g-C3N4 assisted synthesis of NiCeO2 catalyst: kinetics and DRIFTS studies, Int. J. Hydrogen Energy 43 (2018) 15191–15204.
[202] G.A. Olah, Beyond oil and gas: the methanol economy, Angew. Chem. Int. Ed. 44 (2005) 2636–2639.
[203] T. Inui, T. Takeguchi, Effective conversion of carbon dioxide and hydrogen to hydrocarbons, Catal. Today 10 (1991) 95–106.
[204] W. Ning, H. Shen, H. Liu, Study of the effect of preparation method on CuO-ZnO-Al2O3catalyst, Appl. Catal. A Gen. 211 (2001) 153–157.
[205] D. Jingfa, S. Qi, Z. Yulong, C. Songying, W. Dong, A novel process for preparation of a Cu/ZnO/Al2O3 ultrafine catalyst for methanol synthesis from CO2 + H2: comparison of various preparation methods, Appl. Catal. A Gen. 139 (1996) 75–85.
[206] Y. Ma, Q. Sun, D. Wu, W.H. Fan, Y.L. Zhang, J.F. Deng, A practical approach for the preparation of high activity Cu/ZnO/ZrO2 catalyst for methanol synthesis from CO2 hydrogenation, Appl. Catal. A Gen. 171 (1998) 45–55.
[207] C. Tisseraud, C. Comminges, S. Pronier, Y. Pouilloux, A.L. Valant, The Cu – ZnO synergy in methanol synthesis Part 3 : impact of the composition of a selective Cu @ ZnO x core – shell catalyst on methanol rate explained by experimental studies and a concentric spheres model, J. Catal. 343 (2016) 106–114.
[208] F. Arena, K. Barbera, G. Italiano, G. Bonura, L. Spadaro, F. Frusteri, Synthesis, characterization and activity pattern of Cu-ZnO/ZrO2 catalysts in the hydrogenation of carbon dioxide to methanol, J. Catal. 249 (2007) 185–194.
[209] J. Wu, M. Saito, M. Takeuchi, T. Watanabe, The stability of Cu / ZnO-based catalysts in methanol synthesis from a CO 2 -rich feed and from a CO-rich feed, Appl. Catal. A Gen. 218 (2001) 235–240.
[210] Y. Amenomiya, Methanol synthesis from CO2 + H2 II. Copper-based binary and ternary catalysts, Appl. Catal. 30 (1987) 57–68.

[211] R.P. Socha, J.-F. Paul, M. Ruggiero-Mikołajczyk, J. Słoczyński, D. Rutkowska-Zbik, R. Grabowski, D. Mucha, K. Samson, M. Śliwa, K. Góra-Marek, Influence of ZrO 2 structure and copper electronic state on activity of Cu/ZrO 2 catalysts in methanol synthesis from CO 2, ACS Catal. 4 (2014) 3730–3741.
[212] E. Lam, K. Larmier, P. Wolf, S. Tada, O. Safonova, C. Copéret, Isolated Zr Surface Sites on Silica Promotes Hydrogenation of CO2-to-CH3OH in Supported Cu Catalysts, J. Am. Chem. Soc. (2018).
[213] Z. Bian, S. Das, M.H. Wai, P. Hongmanorom, S. Kawi, A review on bimetallic nickel-based catalysts for CO2Reforming of methane, ChemPhysChem 18 (2017) 3117–3134.
[214] B. Hu, Y. Yin, G. Liu, S. Chen, X. Hong, S. Chi, E. Tsang, Hydrogen spillover enabled active Cu sites for methanol synthesis from CO 2 hydrogenation over Pd doped CuZn catalysts, J. Catal. 359 (2018) 17–26.
[215] H. Bahruji, M. Bowker, G. Hutchings, N. Dimitratos, P. Wells, E. Gibson, W. Jones, C. Brookes, D. Morgan, G. Lalev, Pd/ZnO catalysts for direct CO2 hydrogenation to methanol, J. Catal. 343 (2016) 133–146.
[216] H. Lorenz, W. Jochum, B. Klötzer, M. Stöger-Pollach, S. Schwarz, K. Pfaller, S. Penner, Novel methanol steam reforming activity and selectivity of pure In2O3, Appl. Catal. A Gen. 347 (2008) 34–42.
[217] J. Ye, C. Liu, D. Mei, Q. Ge, Active oxygen vacancy site for methanol synthesis from CO2 hydrogenation on In2O3(110): a DFT study, ACS Catal. 3 (2013) 1296–1306.
[218] O. Martin, A.J. Martin, C. Mondelli, S. Mitchell, T.F. Segawa, R. Hauert, C. Drouilly, D. Curulla-Ferre, J. Perez-Ramirez, Indium oxide as a superior catalyst for methanol synthesis by CO2 hydrogenation, Angew. Chem. Int. Ed. 55 (2016) 6261–6265.
[219] A. Rodriguez, J.C. Hanson, W. Wen, X. Wang, M. Ferna, In-situ characterization of water – gas shift catalysts using time-resolved X-ray diffraction, Catal. Today 145 (2009) 188–194.
[220] F. Zaera, New advances in the use of infrared absorption spectroscopy for the characterization of heterogeneous catalytic reactions, Chem. Soc. Rev. 43 (2014) 7624–7663.
[221] A.J. Foster, R.F. Lobo, Identifying reaction intermediates and catalytic active sites through in situ characterization techniques, Chem. Soc. Rev. 39 (2010) 4783.
[222] G. Paul, C. Bisio, I. Braschi, M. Cossi, G. Gatti, E. Gianotti, L. Marchese, Combined solid-state NMR, FT-IR and computational studies on layered and porous materials, Chem. Soc. Rev. 47 (2018) 5684–5739.
[223] J.K. Norskov, F. Abild-Pedersen, F. Studt, T. Bligaard, Density functional theory in surface chemistry and catalysis, Proc. Natl. Acad. Sci. 108 (2011) 937–943.
[224] I.A. Fisher, A.T. Bell, In-situ infrared study of methanol synthesis from H2/CO2, J. Catal. 172 (1997) 222–237.
[225] X.-M. Liu, G.Q. Lu, Z.-F. Yan, J. Beltramini, Recent advances in catalysts for methanol synthesis via hydrogenation of CO and CO 2, Ind. Eng. Chem. Res. 42 (2003) 6518–6530.
[226] K. Larmier, W.C. Liao, S. Tada, E. Lam, R. Verel, A. Bansode, A. Urakawa, A. Comas-Vives, C. Copéret, CO2-to-Methanol hydrogenation on zirconia-supported copper nanoparticles: reaction intermediates and the role of the metal–support interface, Angew. Chem. Int. Ed. 56 (2017) 2318–2323.
[227] L.C. Grabow, M. Mavrikakis, Mechanism of methanol synthesis on cu through CO2 and CO hydrogenation, ACS Catal. 1 (2011) 365–384.
[228] H.W. Lim, M.J. Park, S.H. Kang, H.J. Chae, J.W. Bae, K.W. Jun, Modeling of the kinetics for methanol synthesis using Cu/ZnO/Al2O3/ZrO2 catalyst: influence of carbon dioxide during hydrogenation, Ind. Eng. Chem. Res. 48 (2009) 10448–10455.
[229] R. Schlögl, F. Studt, M. Behrens, E.L. Kunkes, F. Abild-Pedersen, Hydrogenation of CO2 to methanol and CO on Cu/ZnO/Al2O3: Is there a common intermediate or not? J. Catal. 328 (2015) 43–48.
[230] T. Fujitani, I. Nakamura, T. Uchijima, J. Nakamura, The kinetics and mechanism of methanol synthesis by hydrogenation of CO2 over a Zn-deposited Cu(111) surface, Surf. Sci. 383 (1997) 285–298.
[231] Y. Yang, C.A. Mims, D.H. Mei, C.H.F. Peden, C.T. Campbell, Mechanistic studies of methanol synthesis over Cu from CO/CO 2/H2/H2O mixtures: the source of C in methanol and the role of water, J. Catal. 298 (2013) 10–17.
[232] R. Van den Berg, G. Prieto, G. Korpershoek, L.I. Van der Wal, A.J. Van Bunningen, S. Lægsgaard-Jørgensen, P.E. De Jongh, K.P. De Jong, Structure sensitivity of Cu and CuZn catalysts relevant to industrial methanol synthesis, Nat. Commun. 7 (2016) 1–7.
[233] S. Kattel, P.J. Ramírez, J.G. Chen, J.A. Rodriguez, P. Liu, Active sites for CO_2 hydrogenation to methanol on Cu/ZnO catalysts, Science 355 (2017) 1296–1299.
[234] M. Behrens, F. Studt, I. Kasatkin, S. Kühl, M. Hävecker, F. Abild-pedersen, S. Zander, F. Girgsdies, P. Kurr, B. Kniep, M. Tovar, R.W. Fischer, J.K. Nørskov, R. Schlögl, The active site of methanol synthesis over Cu/ZnO/Al2O3, Ind. Catal. 759 (2012) 893–898.
[235] J. Ge, W. Zheng, S.C. Tsang, Y. Huang, X. Hong, F. Liao, K. Tedsree, P. Collier, Morphology-Dependent Interactions of ZnO with Cu Nanoparticles at the Materials' Interface in Selective Hydrogenation of CO2 to CH3OH, Angew. Chem. Int. Ed. 50 (2011) 2162–2165.
[236] T. Lunkenbein, J. Schumann, M. Behrens, R. Schlögl, M.G. Willinger, Formation of a ZnO overlayer in industrial Cu/ZnO/Al2O3Catalysts induced by strong metal-support interactions, Angew. Chem. Int. Ed. 54 (2015) 4544–4548.
[237] K.M.V. Bussche, G.F. Froment, A steady-state kinetic model for methanol synthesis and the water gas shift reaction on a commercial Cu/ZnO/Al2O3Catalyst, J. Catal. 161 (1996) 1–10.
[238] J.F. Portha, K. Parkhomenko, K. Kobl, A.C. Roger, S. Arab, J.M. Commenge, L. Falk, Kinetics of methanol synthesis from carbon dioxide hydrogenation over copper-zinc oxide catalysts, Ind. Eng. Chem. Res. 56 (2017) 13133–13145.
[239] M. Saito, T. Fujitani, M. Takeuchi, T. Watanabe, Development of copper/zinc oxide-based multicomponent catalysts for methanol synthesis from carbon dioxide and hydrogen, Appl. Catal. A-Gen. 138 (1996) 311–318.